The Astrophysical Journal, 783:135 (31pp), 2014 March 10 doi:10.1088/0004-637X/783/2/135

STAR FORMATION BIMODALITY IN EARLY-TYPE GALAXIES

A. Amblard[1,2], L. Riguccini[1,2], P. Temi[1], S. Im[1,2], M. Fanelli[1,2], and P. Serra[3]
[1] NASA Ames Research Center, Moffett Field, CA, USA
[2] BAER Institute, Sonoma, CA, USA
[3] IAS, CNRS (UMR8617), Université Paris-Sud 11, Bâtiment 121, F-91400 Orsay, France
Received 2013 September 20; accepted 2014 January 18; published 2014 February 24

ABSTRACT

We compute the properties of a sample of 221 local, early-type galaxies with a spectral energy distribution (SED) modeling software, CIGALEMC. Concentrating on the star-forming (SF) activity and dust contents, we derive parameters such as the specific star formation rate (sSFR), the dust luminosity, dust mass, and temperature. In our sample, 52% is composed of elliptical (E) galaxies and 48% of lenticular (S0) galaxies. We find a larger proportion of S0 galaxies among galaxies with a large sSFR and large specific dust emission. The stronger activity of S0 galaxies is confirmed by larger dust masses. We investigate the relative proportion of active galactic nuclei (AGNs) and SF galaxies in our sample using spectroscopic Sloan Digital Sky Survey data and near-infrared selection techniques, and find a larger proportion of AGN-dominated galaxies in the S0 sample than the E one. This could corroborate a scenario where blue galaxies evolve into red ellipticals by passing through an S0 AGN active period while quenching its star formation. Finally, we find a good agreement comparing our estimates with color indicators.

Key words: galaxies: elliptical and lenticular, cD – galaxies: ISM – infrared: galaxies – infrared: ISM

Online-only material: color figures

1. INTRODUCTION

Elliptical (E) and lenticular (S0) galaxies, early-type galaxies (ETGs), are among the most massive galaxies today. Their poorly known formation is subject to much debate.

The two main scenarios of ETG formation are the monolithic and hierarchical models. In the monolithic view, ETGs assembled most of their mass quite early on ($z > 2$–3) as they merge with smaller substructures. They are characterized by a strong early star formation and then evolve passively into galaxies we see today. In the hierarchical view, ETGs are formed by mergers of galaxies either rich ("wet" merger) or poor ("dry" merger) in gas. In this picture, it is not clear which merging path(s) ETGs follow.

ETGs constitute the majority of the red galaxies (∼75% Driver et al. 2006) in the bimodal color distribution of galaxies, their stellar population already transitioned from blue to red as their star formation ceased (Faber et al. 2007; Hughes & Cortese 2009). Indeed the most massive ($>10^{10}$ $M_{\odot}$) ETGs are red and with little star formation (Temi et al. 2009b); their stellar content formed at an early epoch (Trager et al. 2000; Cimatti et al. 2004; Thomas et al. 2005; Temi et al. 2005a, 2005b) and passively evolved to their present form.

However, multi-frequency observations in recent years have revealed that on closer inspection many E galaxies and even more S0 galaxies do in fact contain dust and cold gas in amounts that cannot be ignored (Young et al. 2011; Temi et al. 2007a, 2007b), sufficient to generate appreciable star formation at rates as large as several $M_{\odot}$ yr^{-1} (Temi et al. 2009a, 2009b).

Recent ultraviolet (UV) observations of large samples of ETGs present clear evidence of current star formation (Yi et al. 2005; Schawinski et al. 2007a; Kaviraj et al. 2007, 2008; Kaviraj 2010; Salim et al. 2012; Fang et al. 2012; Barway et al. 2013). Using UV–optical colors, Kaviraj et al. (2007) show that at least ∼30% of UV-selected ETGs at $z < 0.11$ have evidence of recent star formation within the last 1 Gyr. The contribution from old stars to the UV flux is, however, uncertain.

The remarkable diversity of nearby ETG galaxies is most clearly expressed in infrared (IR) emission where many S0 galaxies exhibit a range of unusual properties not often found in ellipticals. Temi et al. (2009a, 2009b) showed a banana-shaped mid (24 μm) and far (70 μm) correlation containing only ETGs. While S0 galaxies are spread along the entire correlation, most elliptical galaxies, for which star formation is negligible, occupy an extended region with a nearly flat $\log(L_{24}/L_K) \approx 30.2$. S0 galaxies have a star-forming (SF) diversity that mimics IR colors of galaxies of any type. The SAURON survey (Bacon et al. 2001; de Zeeuw et al. 2002) found that E and S0 can be separated into slow and fast rotators, the slow rotator group being composed mostly of ellipticals (Cappellari et al. 2007; Emsellem et al. 2007). Building in part on this finding, the ATLAS^{3D} project (Cappellari et al. 2011a) observed a sample of 260 local, ETGs (complete within 42 Mpc at −21.5 K band magnitude) in a large number of wavelengths, including optical integral-field spectroscopy. Emsellem et al. (2011) showed that most ETGs are fast rotators (86% ± 2%) and Cappellari et al. (2011b) showed that slow rotators are, in general, round ellipticals (E4 or rounder). They also showed that the slow/fast rotators classification improves the kinematic morphology–density T–Σ relation over the E/S0 classification and argue that the kinematic classification may be more accurate than the morphologic classification which is plagued by projection effects.

Lenticular S0 galaxies differ morphologically from E galaxies having stellar distributions in bulges and rotating disks that are somewhat less concentrated than E galaxies. In this paper, we investigate differences between Elliptical and Lenticular local galaxy populations. Although the distinction between E and S0 morphologies is not always easy, many local S0 galaxies are quite distinct from ellipticals, having attributes consistent with recent star formation: significantly larger mid-IR (MIR) and far-IR (FIR) luminosities, large masses of molecular gas, and younger stellar ages as inferred from optical absorption line spectra. Since S0 galaxies at higher redshifts are difficult to distinguish from E galaxies, particularly if the S0s are face-on,

the two types of galaxies are often combined. Therefore, results from large surveys of "early-type" galaxies that combine S0 and E galaxies will be misleading if applied only to E. However, the distribution of old population starlight in low-redshift S0s, which are of interest here, define a unique and rather large fraction of ETGs.

As our main tool, we use a spectral energy distribution (SED) fitter, CIGALEMC (Serra et al. 2011), capable of modeling our galaxy SED from a UV to a millimeter wavelength, which allows us to determine the stellar mass, dust luminosity, stellar population age, bolometric luminosity, and star formation rate (SFR) of our galaxies in a less ambiguous manner than single-band photometric indicators.

In the second part of the paper, we concentrate on the FIR emission and estimate the dust mass and temperature of our sample. We compare these quantities with the ones estimated from the full SED and distinguish the two sub-populations. In the third part, we investigate the proportion of active galactic nuclei (AGNs) in both the E and S0 populations using Sloan Digital Sky Survey (SDSS) spectroscopic and near-IR (NIR) selection criteria. In the last part, we compare our analysis with optical, UV, and FIR colors.

2. THE DATA

We base our work on a sample of 225 ETGs from Temi et al. (2009b). As pointed out in their work, a few sources present an uncertain morphological classification, in particular galaxies NGC 3656 and NGC 5666. We use the morphological type T from the HyperLeda database[4] (Paturel et al. 2003) and exclude the two following sources: NGC 3656 and NGC 5666 because of the positive value of their T parameter, indicating that they are not ETGs, as expected. Our sample is composed of 116 ellipticals (52% of the sample), 35 E-S0 (16%), 48 S0 (22%), and 22 S0-a (10%), which is roughly the same distribution as in Temi et al. (2009b). In order to perform a reliable SED-fitting for each source, we need to have access to a large fraction of their SED from the UV to the FIR (Tables 1–4). To facilitate the data analysis, we concentrate primarily on six instruments which span these wavelengths and have extensive sky coverage: *Galaxy Evolution Explorer* (*GALEX*) for the UV part, SDSS for the optical, Two Micron All Sky Survey (2MASS) and IRAC-*Spitzer* for the NIR and MIR, and MIPS-*Spitzer* and *IRAS* for the mid and FIR. We also use public data from *Herschel*-SPIRE (Griffin et al. 2010) when available.

We address the representativeness of our sample using the wide (2 deg^2) equatorial COSMOS field (Scoville et al. 2007). With a large statistic and multi wavelength data sets, and in particular an optical catalog with morphological indexes and a 24 μm sources catalog, it is a good source to answer this question. We select 4605 "local" sources ($z < 0.09$, about $D <$ 400 Mpc) in the COSMOS optical catalog (Ilbert et al. 2009). 3 873 of these sources are in the morphological catalog of Tasca et al. (2009) (i.e., 84%), and 994 are classified as ETGs (i.e., 26%)). In the 24 μm catalog (Le Floc'h et al. 2009), 236 sources are lying at $D < 400$ Mpc, 206 are in the morphological catalog (i.e., 87%), and 64 sources are classified as ETGs (i.e., 31%). The percentage of 24 μm selected ETGs is slightly larger than the optical selected one, but it is not statistically significant, a 24 μm selection does not bias an ETG sample much.

We also compared the absolute B magnitude distribution of these three ETGs samples (COSMOS optical, COSMOS 24 μm, and our sample). The comparison between the distribution of our sample of ETGs in absolute B magnitude with the one from the optically selected ETGs in COSMOS shows that they cover the same range of M_B but the COSMOS distribution is slightly shifted towards brightest sources than the distribution of our sources, similar to the COSMOS 24 μm sample. We conclude that our ETGs sample is quite representative of the overall distribution of ETGs in the local universe.

2.1. UV Observations

To cover the UV part of the spectrum, we use *GALEX* GR6 data release,[5] since it covers 25,000 deg^2 of the sky with a sensitivity down to $m_{\rm AB} = 21$ for the All Sky Imaging Survey and $m_{\rm AB} = 25$ for the Deep Imaging Survey (Morrissey et al. 2007). *GALEX* is a NASA satellite, equipped with two microchannel plate detectors imaging in the near-UV (NUV) at 2316 Å and far-UV (FUV) at 1539 Å (Morrissey et al. 2007), and a grism to disperse light for low-resolution spectroscopy. The source position accuracy is about 0.″34 and the angular resolution of FUV and NUV is 4.″3 and 5.″3, respectively. We find matches in the *GALEX* catalog for 199 sources of our sample in the FUV band and 198 sources in the NUV band. We apply a galactic dust extinction correction, $A({\rm FUV})/E(B-V) = 8.376$ $A({\rm NUV})/E(B-V) = 8.741$, to *GALEX* data, assuming Milky Way dust with $R_v = 3.1$ (Cardelli et al. 1989; Marino et al. 2011), and using NASA/IPAC Extragalactic Database (NED) $E(B-V)$ values. The UV emission is a good indicator of the dust content and SFR of galaxies in our sample when compared with the optical data.

2.2. Optical and NIR Observations

We chose SDSS data to cover the optical range of the SED of our galaxies, given the large part of the sky covered by SDSS (14,555 deg^2). The SDSS data have an angular resolution of about 1.″5. We retrieve SDSS data through the Imaging Query Form interface.[6] 147 sources from our sample have an optical counterpart in the five bands of the SDSS, u, g, r, i, and z (respectively 0.335 μm, 0.469 μm, 0.616 μm, 0.748 μm, and 0.893 μm). At NIR wavelengths, we use the extended source catalog of the 2MASS data, which contains 1,647,599 sources. 2MASS resolution is about 2″ and its source position accuracy is about 0.″5. The 10σ limit magnitude in the three filters J, H, K_s is about 14.7, 13.9, 13.1.[7] 220 Galaxies in our sample have counterparts in the three different filters, J, H, and K_s bands, at 1.24 μm, 1.66 μm, and 2.16 μm, respectively.

2.3. Infrared Observations

The *Spitzer Space Telescope* provides data in the NIR and MIR with the IRAC camera with four channels imaging at 3.6, 4.5, 5.6, and 8 μm with about 2″ angular resolution and in the MIR and FIR with the MIPS instrument observing at 24, 70, and 160 μm at an angular resolution of 6″, 18″, and 40″ (Rieke et al. 2004). We download data for our galaxies from the NASA/IPAC Infrared Science Archive.[8] Reduction of the data follows Temi et al. (2009b) for MIPS and a similar treatment is applied on IRAC data to produce maps.

[4] http://leda.univ-lyon1.fr/

[5] http://galex.stsci.edu/GR6/

[6] http://skyserver.sdss3.org/dr9/en/tools/search/IQS.asp

[7] http://www.ipac.caltech.edu/2mass/releases/allsky/doc/sec4_5.html

[8] http://sha.ipac.caltech.edu/applications/Spitzer/SHA

Table 1
Fluxes (FUV to z Band, from *GALEX* and SDSS Data) and Redshifts Used in This Study; Data Were Collected According to Section 2

Name	Redshift[a]	FUV (μJy)	NUV (μJy)	u (mJy)	g (mJy)	r (mJy)	i (mJy)	z (mJy)
Eso103-35	0.0133	...	...	...	...	...	...	...
Eso428-14	0.0057	...	...	...	...	...	...	...
Eso462-15	0.0191	76.33 ± 8.11	351.30 ± 17.22	...	...	...	...	...
Eso483-13	0.0030	1541.00 ± 10.35	2364.00 ± 10.02	...	...	...	...	...
IC0798	0.0047	16.75 ± 2.97	133.10 ± 4.56	1.24 ± 0.02	4.71 ± 0.01	8.58 ± 0.02	11.97 ± 0.03	14.31 ± 0.10
IC1144	0.0403	1.58 ± 0.46	184.20 ± 3.95	1.50 ± 0.02	6.99 ± 0.08	13.24 ± 0.15	17.94 ± 0.21	22.13 ± 0.24
IC1459	0.0060	781.10 ± 8.39	3327.00 ± 15.47	...	...	...	...	...
IC1639	0.0179	33.79 ± 1.23	189.70 ± 2.34	2.03 ± 0.01	8.81 ± 0.02	16.26 ± 0.03	22.03 ± 0.05	26.80 ± 0.07
IC3032	0.0040	...	7.90 ± 3.67	0.91 ± 0.02	3.56 ± 0.01	6.18 ± 0.02	7.36 ± 0.03	9.59 ± 0.12
IC3101	0.0048	...	42.70 ± 7.75	0.61 ± 0.03	2.24 ± 0.01	4.14 ± 0.02	5.91 ± 0.03	6.72 ± 0.08
IC3328	0.0034	0.79 ± 0.28	240.00 ± 4.81	1.70 ± 0.04	6.92 ± 0.02	12.36 ± 0.03	16.21 ± 0.04	17.02 ± 0.15
IC3370	0.0098	...	...	...	...	...	...	...
IC3381	0.0023	8.04 ± 1.41	231.30 ± 3.72	1.54 ± 0.02	7.50 ± 0.02	13.96 ± 0.03	19.40 ± 0.03	23.28 ± 0.07
IC3383	0.0062	5.95 ± 3.35	20.37 ± 7.97	0.71 ± 0.09	6.41 ± 0.04	9.82 ± 0.05	10.75 ± 0.09	10.86 ± 0.30
IC3461	0.0034	24.48 ± 2.86	126.80 ± 2.64	0.95 ± 0.03	3.83 ± 0.02	6.75 ± 0.02	9.28 ± 0.04	9.19 ± 0.12
IC3468	0.0043	...	259.40 ± 18.57	2.30 ± 0.05	11.15 ± 0.02	19.82 ± 0.06	26.72 ± 0.12	28.60 ± 0.27
IC3470	0.0050	32.21 ± 3.21	183.40 ± 2.94	1.68 ± 0.03	6.89 ± 0.01	13.77 ± 0.02	19.90 ± 0.03	23.61 ± 0.10
IC3487	0.0036	2.03 ± 0.69	268.80 ± 3.19	1.14 ± 0.03	4.39 ± 0.04	5.69 ± 0.03	7.84 ± 0.07	7.72 ± 0.10
IC3501	0.0055	1.02 ± 0.94	178.30 ± 3.71	1.64 ± 0.03	6.10 ± 0.02	11.52 ± 0.03	14.89 ± 0.04	18.86 ± 0.11
IC3586	0.0052	8.03 ± 1.96	307.70 ± 5.56	1.87 ± 0.06	7.06 ± 0.03	11.89 ± 0.04	14.44 ± 0.07	17.39 ± 0.26
IC3602	0.0043	3.33 ± 0.97	75.50 ± 3.27	0.44 ± 0.03	2.09 ± 0.02	3.83 ± 0.02	4.79 ± 0.06	4.21 ± 0.17
IC3633	0.0068	2.84 ± 0.70	84.31 ± 3.05	0.66 ± 0.02	2.33 ± 0.01	4.12 ± 0.02	5.50 ± 0.02	6.24 ± 0.08
IC3652	0.0021	10.78 ± 2.03	204.30 ± 6.13	1.82 ± 0.05	7.25 ± 0.02	12.97 ± 0.03	17.49 ± 0.05	22.12 ± 0.16
IC3653	0.0020	13.84 ± 1.50	113.10 ± 3.40	1.54 ± 0.02	7.60 ± 0.01	16.08 ± 0.02	23.01 ± 0.03	27.82 ± 0.08
IC3735	0.0063	...	...	2.05 ± 0.04	6.26 ± 0.02	10.98 ± 0.03	15.32 ± 0.05	15.88 ± 0.20
IC3773	0.0036	23.38 ± 2.76	315.60 ± 5.65	2.43 ± 0.06	9.70 ± 0.33	18.77 ± 0.56	25.52 ± 0.73	30.42 ± 0.84
IC3779	0.0039	2.56 ± 0.34	94.16 ± 2.84	1.04 ± 0.04	3.14 ± 0.01	5.77 ± 0.02	7.90 ± 0.03	8.71 ± 0.13
IC4296	0.0125	288.00 ± 7.30	1952.00 ± 13.86	...	...	...	...	...
IC4329	0.0151	256.30 ± 6.19	623.60 ± 3.08	...	...	...	...	...
IC5063	0.0113	385.90 ± 7.07	1151.00 ± 9.06	...	...	...	...	...
NGC 0221	0.0002	1839.00 ± 20.46	...	...	...	...	...	...
NGC 0315	0.0165	220.50 ± 5.98	816.20 ± 11.22	5.61 ± 0.10	49.91 ± 0.36	113.00 ± 0.79	172.10 ± 1.15	224.20 ± 1.15
NGC 0404	0.0009	861.90 ± 2.73	5439.00 ± 5.36	...	...	...	...	...
NGC 0410	0.0177	154.80 ± 4.30	902.00 ± 15.42	6.50 ± 0.14	39.52 ± 0.48	93.68 ± 1.14	144.50 ± 1.57	179.40 ± 1.31
NGC 0474	0.0078	102.50 ± 3.38	1231.00 ± 11.50	8.36 ± 0.07	39.77 ± 0.10	82.31 ± 0.18	120.60 ± 0.25	143.10 ± 0.32
NGC 0507	0.0165	192.10 ± 5.92	1394.00 ± 14.05	6.29 ± 0.03	25.33 ± 0.04	100.20 ± 0.14	150.90 ± 0.21	192.20 ± 0.31
NGC 0516	0.0082	1.91 ± 0.89	206.20 ± 3.95	1.92 ± 0.05	9.49 ± 0.18	18.88 ± 0.28	26.72 ± 0.22	34.63 ± 0.60
NGC 0526	0.0192	207.40 ± 4.78	361.70 ± 4.40	...	...	...	...	...
NGC 0533	0.0185	181.80 ± 11.55	527.70 ± 18.88	6.30 ± 0.10	32.15 ± 0.17	73.34 ± 0.48	109.30 ± 0.71	138.70 ± 0.57
NGC 0584	0.0048	230.10 ± 6.21	1660.00 ± 11.69	17.02 ± 0.10	103.50 ± 1.71	215.60 ± 3.55	193.20 ± 1.14	411.90 ± 5.92
NGC 0596	0.0051	146.10 ± 5.08	1418.00 ± 10.83	13.61 ± 0.10	72.51 ± 0.38	143.20 ± 0.71	205.60 ± 1.00	229.90 ± 0.66
NGC 0636	0.0062	90.51 ± 9.36	760.90 ± 16.83	9.18 ± 0.09	49.13 ± 0.25	100.70 ± 0.54	150.80 ± 0.73	178.00 ± 0.57
NGC 0720	0.0058	642.90 ± 1.09	1840.00 ± 1.51	...	...	...	...	...
NGC 0777	0.0167	242.80 ± 4.19	716.00 ± 10.60	5.39 ± 0.06	32.40 ± 0.12	75.04 ± 0.32	115.30 ± 0.44	149.30 ± 0.53
NGC 0807	0.0159	227.10 ± 13.97	609.00 ± 18.61	2.53 ± 0.40	7.30 ± 1.62	14.33 ± 1.29	36.44 ± 2.67	60.20 ± 3.39
NGC 0814	0.0054	336.30 ± 6.47	663.80 ± 4.84	...	...	...	...	...
NGC 0821	0.0058	12.92 ± 2.76	...	...	...	...	...	...
NGC 0855	0.0020	1327.00 ± 12.37	3314.00 ± 17.30	8.19 ± 0.20	23.35 ± 0.40	39.83 ± 0.66	51.71 ± 0.60	60.00 ± 0.78
NGC 1016	0.0222	78.17 ± 12.93	333.50 ± 20.61	5.24 ± 0.06	28.36 ± 0.04	68.29 ± 0.12	104.00 ± 0.15	122.00 ± 0.25
NGC 1023	0.0028	759.70 ± 15.34	3848.00 ± 21.64	...	...	...	...	...
NGC 1199	0.0086	126.30 ± 5.02	735.10 ± 7.85	6.65 ± 0.07	46.67 ± 0.32	101.20 ± 0.47	154.90 ± 0.78	188.60 ± 0.81
NGC 1266	0.0073	22.95 ± 4.31	372.90 ± 10.46	...	...	...	...	...
NGC 1316	0.0059	1730.00 ± 16.08	13110.00 ± 29.48	...	...	...	...	...
NGC 1374	0.0043	234.60 ± 1.12	1007.00 ± 1.59	...	...	...	...	...
NGC 1377	0.0060	...	...	...	...	...	...	...
NGC 1386	0.0029	606.20 ± 1.32	1965.00 ± 1.62	...	...	...	...	...
NGC 1395	0.0057	739.20 ± 20.96	2447.00 ± 30.25	...	...	...	...	...
NGC 1399	0.0048	2572.00 ± 2.77	3494.00 ± 1.86	...	...	...	...	...
NGC 1404	0.0065	858.70 ± 4.33	3510.00 ± 8.35	...	...	...	...	...
NGC 1407	0.0059	1276.00 ± 14.15	3580.00 ± 24.28	...	...	...	...	...
NGC 1426	0.0048	108.90 ± 3.75	904.50 ± 8.74	...	...	...	...	...
NGC 1427	0.0046	313.40 ± 4.18	1917.00 ± 7.62	...	...	...	...	...
NGC 1439	0.0056	111.60 ± 5.20	958.50 ± 9.14	...	...	...	...	...
NGC 1510	0.0030	4617.00 ± 15.37	4707.00 ± 10.98	...	...	...	...	...
NGC 1522	0.0030	2751.00 ± 15.51	3611.00 ± 8.31	...	...	...	...	...

Table 1
(Continued)

Name	Redshift[a]	FUV (μJy)	NUV (μJy)	u (mJy)	g (mJy)	r (mJy)	i (mJy)	z (mJy)
NGC 1533	0.0026	682.40 ± 12.32	1922.00 ± 9.28	...	...	...	...	...
NGC 1543	0.0039	202.30 ± 11.90	1363.00 ± 26.77	...	...	...	...	...
NGC 1553	0.0036	828.20 ± 8.75	5241.00 ± 17.34	...	...	...	...	...
NGC 1700	0.0130	...	...	8.33 ± 0.04	52.68 ± 0.40	110.50 ± 0.85	162.10 ± 1.10	215.50 ± 1.49
NGC 2110	0.0078	...	...	...	...	...	...	...
NGC 2300	0.0064	349.30 ± 9.11	1284.00 ± 18.69	...	...	...	...	...
NGC 2325	0.0073	...	...	...	...	...	...	...
NGC 2434	0.0046	475.70 ± 28.16	3738.00 ± 41.46	...	...	...	...	...
NGC 2685	0.0029	2103.00 ± 10.52	3655.00 ± 13.79	11.69 ± 0.33	57.18 ± 1.29	116.10 ± 1.94	169.60 ± 2.17	212.90 ± 3.41
NGC 2768	0.0046	382.00 ± 9.09	2994.00 ± 25.65	14.68 ± 0.04	86.16 ± 0.12	203.40 ± 0.27	306.60 ± 0.41	422.10 ± 0.61
NGC 2778	0.0068	47.42 ± 7.88	276.90 ± 15.79	3.98 ± 0.03	21.27 ± 0.05	43.62 ± 0.09	63.88 ± 0.14	76.47 ± 0.18
NGC 2787	0.0023	269.60 ± 24.63	1598.00 ± 42.67	...	...	...	...	...
NGC 2832	0.0232	43.16 ± 2.27	150.00 ± 2.71	3.69 ± 0.04	23.77 ± 0.23	52.70 ± 0.58	79.49 ± 0.83	100.80 ± 0.90
NGC 2970	0.0054	51.05 ± 2.21	285.90 ± 4.99	2.25 ± 0.03	7.59 ± 0.02	13.21 ± 0.04	17.80 ± 0.06	20.82 ± 0.11
NGC 2974	0.0064	394.80 ± 7.32	1882.00 ± 12.86	...	...	...	...	...
NGC 2986	0.0077	364.50 ± 25.92	1284.00 ± 27.34	...	...	...	...	...
NGC 3011	0.0051	754.00 ± 6.09	1064.00 ± 6.39	1.78 ± 0.03	7.54 ± 0.05	13.98 ± 0.09	18.57 ± 0.13	21.40 ± 0.13
NGC 3032	0.0051	1144.00 ± 6.81	2543.00 ± 6.93	7.24 ± 0.06	28.22 ± 0.10	48.49 ± 0.22	33.62 ± 0.05	73.67 ± 0.27
NGC 3073	0.0039	311.30 ± 1.33	743.50 ± 1.55	2.90 ± 0.02	10.10 ± 0.02	15.85 ± 0.03	20.57 ± 0.04	23.29 ± 0.09
NGC 3115	0.0022	1364.00 ± 14.98	7402.00 ± 26.46	...	...	...	...	...
NGC 3125	0.0037	5554.00 ± 16.48	9416.00 ± 12.27	...	...	...	...	...
NGC 3156	0.0044	149.60 ± 1.70	990.00 ± 4.69	6.93 ± 0.08	28.30 ± 0.23	48.67 ± 0.36	59.66 ± 0.29	77.63 ± 0.75
NGC 3226	0.0038	...	...	7.54 ± 0.07	41.75 ± 0.07	90.76 ± 0.09	139.10 ± 0.11	177.70 ± 0.27
NGC 3265	0.0044	521.30 ± 6.97	1067.00 ± 6.77	3.27 ± 0.02	10.76 ± 0.04	19.93 ± 0.07	27.41 ± 0.10	33.49 ± 0.12
NGC 3377	0.0022	289.50 ± 6.88	3547.00 ± 17.73	27.49 ± 0.05	139.80 ± 0.19	277.00 ± 0.37	210.20 ± 1.54	514.70 ± 0.73
NGC 3379	0.0030	932.80 ± 6.67	3455.00 ± 4.23	29.04 ± 0.08	167.80 ± 0.35	352.30 ± 0.74	300.20 ± 0.20	663.40 ± 1.30
NGC 3384	0.0023	416.00 ± 4.76	2253.00 ± 3.33	24.90 ± 0.14	148.30 ± 0.95	301.20 ± 1.96	233.00 ± 0.22	537.80 ± 3.32
NGC 3412	0.0028	234.80 ± 2.99	1829.00 ± 3.55	19.95 ± 0.06	117.80 ± 0.47	219.90 ± 0.39	314.40 ± 1.01	362.20 ± 0.87
NGC 3489	0.0023	639.60 ± 14.00	3976.00 ± 14.28	25.57 ± 0.13	118.40 ± 0.55	172.10 ± 0.17	258.80 ± 0.66	373.00 ± 1.61
NGC 3516	0.0088	1888.00 ± 13.33	3951.00 ± 12.47	...	...	...	...	...
NGC 3522	0.0041	42.20 ± 2.18	404.90 ± 6.43	3.40 ± 0.10	14.16 ± 0.20	26.27 ± 0.31	35.94 ± 0.37	39.21 ± 0.17
NGC 3557	0.0103	17.44 ± 8.06	1132.00 ± 48.36	...	...	...	...	...
NGC 3585	0.0048	494.70 ± 22.99	2980.00 ± 42.40	...	...	...	...	...
NGC 3593	0.0021	508.40 ± 7.92	2834.00 ± 13.60	9.80 ± 0.09	50.58 ± 0.09	116.00 ± 0.68	183.20 ± 0.19	254.40 ± 0.34
NGC 3607	0.0032	720.00 ± 5.46	3221.00 ± 12.30	34.17 ± 0.08	184.20 ± 0.25	403.30 ± 0.52	618.40 ± 0.80	819.30 ± 1.12
NGC 3608	0.0042	255.00 ± 3.38	1384.00 ± 9.22	...	...	...	...	...
NGC 3610	0.0057	141.00 ± 2.70	1548.00 ± 7.33	21.35 ± 0.32	99.37 ± 1.65	187.20 ± 2.88	258.40 ± 3.74	304.00 ± 3.33
NGC 3640	0.0042	187.90 ± 4.66	2242.00 ± 15.11	19.72 ± 0.09	109.30 ± 0.62	235.70 ± 1.37	360.00 ± 2.16	435.90 ± 2.31
NGC 3706	0.0099	142.50 ± 21.31	860.70 ± 42.62	...	...	...	...	...
NGC 3773	0.0033	3660.00 ± 49.27	4822.00 ± 32.17	7.07 ± 0.04	15.79 ± 0.03	23.18 ± 0.07	26.75 ± 0.09	27.84 ± 0.14
NGC 3870	0.0025	3161.00 ± 16.77	4213.00 ± 11.48	7.43 ± 0.07	15.56 ± 0.15	20.71 ± 0.17	23.79 ± 0.22	25.86 ± 0.15
NGC 3923	0.0058	843.00 ± 11.73	5879.00 ± 27.05	...	...	...	...	...
NGC 3941	0.0031	12.76 ± 6.03	1276.00 ± 40.19	29.75 ± 0.25	152.50 ± 0.90	300.80 ± 1.50	426.30 ± 1.82	511.70 ± 1.78
NGC 3945	0.0042	165.60 ± 20.86	965.90 ± 31.22	9.74 ± 0.05	59.87 ± 0.32	119.40 ± 0.03	196.00 ± 1.13	240.80 ± 1.31
NGC 3962	0.0061	275.30 ± 5.41	2190.00 ± 16.29	...	...	...	...	...
NGC 4026	0.0031	139.90 ± 9.22	1252.00 ± 19.46	15.96 ± 0.59	90.50 ± 3.65	185.80 ± 7.11	220.30 ± 6.36	340.40 ± 12.87
NGC 4073	0.0196	238.40 ± 4.92	593.60 ± 7.20	3.92 ± 0.07	28.90 ± 0.13	71.50 ± 0.58	106.80 ± 0.80	140.70 ± 1.36
NGC 4117	0.0031	179.60 ± 3.63	439.20 ± 4.36	3.29 ± 0.10	13.57 ± 0.24	27.20 ± 0.44	39.06 ± 0.63	46.62 ± 0.68
NGC 4125	0.0045	242.70 ± 19.46	1929.00 ± 37.41	20.76 ± 0.11	130.50 ± 0.75	288.90 ± 1.91	434.90 ± 3.02	553.30 ± 3.70
NGC 4138	0.0030	2309.00 ± 11.31	3726.00 ± 8.56	11.60 ± 0.11	72.73 ± 0.33	140.60 ± 0.52	199.80 ± 0.61	260.40 ± 1.67
NGC 4150	0.0034	111.70 ± 2.46	449.20 ± 3.53	9.96 ± 0.04	43.69 ± 0.05	82.15 ± 0.07	118.30 ± 0.11	131.50 ± 0.23
NGC 4168	0.0074	175.80 ± 6.73	1636.00 ± 9.66	9.88 ± 0.07	48.61 ± 0.07	101.90 ± 0.16	147.60 ± 0.26	191.50 ± 0.52
NGC 4203	0.0036	554.90 ± 12.79	1928.00 ± 18.89	10.92 ± 0.11	61.72 ± 0.59	128.20 ± 0.22	198.80 ± 1.97	249.80 ± 2.29
NGC 4251	0.0036	108.80 ± 11.43	1534.00 ± 33.06	16.52 ± 0.34	76.60 ± 0.91	131.50 ± 1.85	216.30 ± 2.50	276.60 ± 4.62
NGC 4261	0.0075	599.50 ± 5.27	2069.00 ± 12.97	18.12 ± 0.08	106.60 ± 0.34	231.80 ± 0.75	350.30 ± 1.11	444.20 ± 1.27
NGC 4267	0.0034	152.60 ± 6.16	1141.00 ± 13.82	11.38 ± 0.07	61.83 ± 0.16	128.20 ± 0.31	191.70 ± 0.34	236.40 ± 0.34
NGC 4278	0.0022	943.10 ± 12.01	3155.00 ± 16.59	23.24 ± 0.07	133.90 ± 0.16	285.70 ± 0.41	424.50 ± 0.58	522.70 ± 0.57
NGC 4291	0.0059	...	...	...	...	...	...	...
NGC 4308	0.0020	23.60 ± 2.16	198.00 ± 2.89	2.19 ± 0.02	9.30 ± 0.01	17.61 ± 0.02	24.70 ± 0.03	30.03 ± 0.13
NGC 4344	0.0038	449.80 ± 6.48	1134.00 ± 7.60	5.80 ± 0.06	19.08 ± 0.09	35.17 ± 0.21	46.93 ± 0.14	54.30 ± 1.06
NGC 4350	0.0040	276.80 ± 19.95	1086.00 ± 29.70	12.63 ± 0.08	82.83 ± 3.52	180.70 ± 9.49	268.70 ± 12.75	335.40 ± 16.02
NGC 4352	0.0069	30.51 ± 3.25	399.50 ± 4.13	5.76 ± 0.15	21.32 ± 0.26	40.38 ± 0.43	58.77 ± 0.80	71.90 ± 0.94
NGC 4365	0.0041	988.40 ± 7.66	4419.00 ± 13.28	28.54 ± 0.07	169.80 ± 0.23	365.60 ± 0.48	537.70 ± 0.71	730.80 ± 1.02
NGC 4371	0.0031	254.40 ± 6.57	1413.00 ± 7.76	14.48 ± 0.08	88.37 ± 0.28	187.40 ± 0.54	288.20 ± 0.90	364.10 ± 1.32
NGC 4374	0.0035	1311.00 ± 14.20	6867.00 ± 19.68	...	...	...	...	...

Table 1
(Continued)

Name	Redshift[a]	FUV (μJy)	NUV (μJy)	u (mJy)	g (mJy)	r (mJy)	i (mJy)	z (mJy)
NGC 4377	0.0046	74.57 ± 13.39	361.60 ± 16.24	7.28 ± 0.04	38.82 ± 0.11	78.56 ± 0.21	114.20 ± 0.29	141.30 ± 0.37
NGC 4379	0.0036	135.00 ± 5.93	289.20 ± 5.02	9.13 ± 0.05	45.31 ± 0.13	90.23 ± 0.21	135.30 ± 0.37	165.20 ± 0.40
NGC 4382	0.0024	572.40 ± 33.07	5630.00 ± 65.97	23.85 ± 0.64	121.70 ± 1.30	244.30 ± 0.64	334.20 ± 2.16	427.70 ± 2.57
NGC 4386	0.0056	...	...	...	...	...	...	...
NGC 4406	0.0039	1315.00 ± 16.06	8308.00 ± 23.69	33.49 ± 0.07	216.20 ± 0.28	430.90 ± 0.55	641.20 ± 0.82	861.50 ± 1.15
NGC 4417	0.0028	183.20 ± 3.43	1177.00 ± 8.69	12.32 ± 0.29	64.95 ± 1.15	129.60 ± 2.36	190.20 ± 3.47	226.60 ± 4.12
NGC 4421	0.0053	48.03 ± 2.74	1079.00 ± 10.75	5.32 ± 0.07	46.04 ± 0.16	84.11 ± 0.25	124.10 ± 0.39	128.40 ± 0.83
NGC 4434	0.0036	78.18 ± 2.49	469.50 ± 4.12	6.14 ± 0.04	30.45 ± 0.03	60.98 ± 0.06	87.97 ± 0.08	105.40 ± 0.14
NGC 4435	0.0027	187.50 ± 5.12	1780.00 ± 7.10	44.68 ± 0.17	203.80 ± 0.08	421.30 ± 0.12	644.80 ± 0.19	749.70 ± 0.64
NGC 4442	0.0018	378.50 ± 4.90	1791.00 ± 9.19	18.56 ± 0.22	119.80 ± 1.54	256.00 ± 3.51	371.40 ± 4.60	481.00 ± 7.19
NGC 4458	0.0021	48.66 ± 2.62	596.20 ± 5.26	5.49 ± 0.05	29.21 ± 0.04	57.16 ± 0.07	82.33 ± 0.10	102.30 ± 0.18
NGC 4459	0.0040	429.60 ± 7.06	2240.00 ± 12.53	...	...	...	...	...
NGC 4460	0.0016	2130.00 ± 13.41	4495.00 ± 8.57	13.10 ± 0.13	42.01 ± 0.13	70.98 ± 1.57	93.35 ± 0.24	100.50 ± 1.88
NGC 4464	0.0041	63.19 ± 1.73	252.50 ± 3.01	4.17 ± 0.04	20.36 ± 0.12	40.96 ± 0.24	60.32 ± 0.38	72.86 ± 0.38
NGC 4472	0.0033	2605.00 ± 17.86	8820.00 ± 28.03	37.65 ± 0.09	253.40 ± 0.35	557.70 ± 0.76	858.50 ± 1.17	1071.00 ± 1.50
NGC 4473	0.0075	434.10 ± 7.14	2366.00 ± 8.47	19.63 ± 0.07	111.20 ± 0.35	228.70 ± 0.72	342.20 ± 1.08	424.90 ± 1.15
NGC 4474	0.0053	69.82 ± 4.00	890.90 ± 9.03	7.59 ± 0.05	44.90 ± 0.40	96.14 ± 1.44	134.60 ± 1.34	157.00 ± 1.26
NGC 4476	0.0066	155.70 ± 3.17	977.00 ± 4.37	7.46 ± 0.15	28.68 ± 0.45	53.15 ± 0.72	73.84 ± 0.96	88.18 ± 1.14
NGC 4477	0.0045	353.20 ± 7.70	1768.00 ± 7.59	18.62 ± 0.12	115.70 ± 0.61	239.80 ± 0.79	350.30 ± 0.90	467.40 ± 2.15
NGC 4478	0.0045	215.30 ± 3.87	1050.00 ± 3.89	6.59 ± 0.21	42.97 ± 0.33	91.45 ± 0.51	142.00 ± 0.64	183.10 ± 0.70
NGC 4479	0.0029	67.48 ± 4.15	370.50 ± 3.84	3.77 ± 0.05	18.91 ± 0.08	37.12 ± 0.11	51.58 ± 0.10	63.48 ± 0.25
NGC 4482	0.0062	14.31 ± 5.26	374.60 ± 21.34	3.29 ± 0.06	13.97 ± 0.07	26.12 ± 0.14	33.67 ± 0.12	36.67 ± 0.20
NGC 4483	0.0029	67.64 ± 1.56	408.60 ± 4.39	5.46 ± 0.06	26.44 ± 0.12	53.40 ± 0.26	77.34 ± 0.36	94.69 ± 0.47
NGC 4486	0.0044	4771.00 ± 17.30	12200.00 ± 15.87	...	...	...	...	...
NGC 4489	0.0032	55.09 ± 2.40	591.20 ± 5.20	5.12 ± 0.08	26.62 ± 0.21	48.96 ± 0.32	70.47 ± 0.47	81.28 ± 0.48
NGC 4494	0.0045	...	...	...	...	...	...	...
NGC 4515	0.0032	56.97 ± 3.85	449.20 ± 6.92	5.02 ± 0.04	20.24 ± 0.06	38.43 ± 0.11	54.90 ± 0.17	61.56 ± 0.17
NGC 4526	0.0015	667.50 ± 7.11	3613.00 ± 16.00	30.95 ± 0.23	186.30 ± 2.26	400.10 ± 4.92	331.90 ± 0.34	799.40 ± 11.30
NGC 4528	0.0045	75.13 ± 3.81	529.10 ± 3.58	7.46 ± 0.08	33.79 ± 0.28	67.40 ± 0.54	98.55 ± 0.84	121.60 ± 1.03
NGC 4552	0.0037	1193.00 ± 12.74	4166.00 ± 12.78	31.92 ± 0.06	190.90 ± 0.25	405.60 ± 0.51	390.40 ± 2.57	840.10 ± 1.12
NGC 4564	0.0038	267.40 ± 4.46	1221.00 ± 5.22	13.12 ± 0.22	68.49 ± 0.17	145.80 ± 0.78	215.30 ± 0.76	259.90 ± 0.92
NGC 4570	0.0058	285.70 ± 5.10	1350.00 ± 9.57	16.51 ± 1.19	88.74 ± 5.89	183.40 ± 12.37	270.70 ± 18.07	333.70 ± 20.83
NGC 4578	0.0076	11.69 ± 1.12	1089.00 ± 9.91	8.06 ± 0.05	41.12 ± 0.06	84.27 ± 0.15	118.40 ± 0.12	143.30 ± 0.24
NGC 4589	0.0066	178.20 ± 3.62	1831.00 ± 11.23	...	...	...	...	...
NGC 4612	0.0059	85.07 ± 7.28	1052.00 ± 17.58	10.69 ± 1.11	56.35 ± 0.69	106.80 ± 0.86	149.70 ± 1.25	173.10 ± 3.76
NGC 4621	0.0037	701.90 ± 9.00	3069.00 ± 14.66	32.67 ± 0.07	219.50 ± 0.28	449.50 ± 0.57	682.40 ± 0.86	889.00 ± 1.16
NGC 4623	0.0063	47.77 ± 5.34	525.60 ± 16.32	4.40 ± 0.05	19.81 ± 0.03	38.71 ± 0.07	55.67 ± 0.10	65.78 ± 0.17
NGC 4636	0.0031	750.60 ± 31.02	3341.00 ± 58.03	24.78 ± 0.07	126.20 ± 0.18	268.30 ± 0.37	395.50 ± 0.55	568.30 ± 0.87
NGC 4638	0.0039	130.90 ± 4.68	1004.00 ± 5.79	11.67 ± 0.40	63.26 ± 2.50	127.50 ± 5.01	184.20 ± 7.45	220.60 ± 6.50
NGC 4649	0.0037	3149.00 ± 19.62	7900.00 ± 16.28	...	...	...	...	...
NGC 4660	0.0036	212.20 ± 5.05	1466.00 ± 8.90	12.80 ± 0.30	67.10 ± 1.30	134.90 ± 2.58	202.30 ± 3.79	243.50 ± 4.05
NGC 4694	0.0039	794.10 ± 8.84	3710.00 ± 14.88	10.93 ± 0.06	44.24 ± 0.63	67.59 ± 0.32	84.17 ± 0.18	94.77 ± 0.20
NGC 4696	0.0099	161.70 ± 26.86	1262.00 ± 78.20	...	...	...	...	...
NGC 4697	0.0041	756.40 ± 10.49	6516.00 ± 25.32	...	...	...	...	...
NGC 4709	0.0156	132.50 ± 23.48	606.00 ± 48.87	...	...	...	...	...
NGC 4754	0.0045	240.10 ± 16.93	1088.00 ± 28.32	15.66 ± 0.15	91.35 ± 0.86	208.10 ± 2.94	309.20 ± 4.29	376.30 ± 5.08
NGC 4762	0.0033	203.00 ± 21.87	2556.00 ± 26.90	20.68 ± 0.12	106.50 ± 0.75	209.00 ± 1.15	300.70 ± 1.93	362.40 ± 1.28
NGC 4786	0.0155	83.90 ± 10.85	382.70 ± 19.56	...	...	...	...	...
NGC 4915	0.0101	47.69 ± 10.07	420.10 ± 12.08	...	...	...	...	...
NGC 4936	0.0104	134.50 ± 17.83	1246.00 ± 39.13	...	...	...	...	...
NGC 5018	0.0094	171.20 ± 18.23	1949.00 ± 35.43	...	...	...	...	...
NGC 5044	0.0093	514.10 ± 11.95	2116.00 ± 21.83	...	...	...	...	...
NGC 5061	0.0069	264.80 ± 14.17	2955.00 ± 40.88	...	...	...	...	...
NGC 5077	0.0094	...	...	...	...	...	...	...
NGC 5173	0.0081	535.90 ± 7.16	1022.00 ± 5.81	3.36 ± 0.03	15.85 ± 0.08	30.15 ± 0.20	42.13 ± 0.36	48.29 ± 0.35
NGC 5273	0.0035	163.40 ± 3.55	1045.00 ± 8.34	10.46 ± 0.06	48.17 ± 0.05	90.45 ± 0.08	122.00 ± 0.10	142.20 ± 0.29
NGC 5322	0.0059	300.00 ± 7.14	2172.00 ± 11.86	19.85 ± 0.21	101.90 ± 1.09	207.20 ± 1.98	299.00 ± 2.81	378.00 ± 3.06
NGC 5338	0.0027	258.50 ± 4.89	872.60 ± 7.54	2.75 ± 0.08	13.43 ± 0.33	23.39 ± 0.58	31.25 ± 0.73	34.83 ± 0.65
NGC 5353	0.0078	272.60 ± 19.73	890.60 ± 22.04	12.01 ± 0.33	72.57 ± 1.48	156.20 ± 3.08	242.30 ± 5.29	296.30 ± 3.79
NGC 5419	0.0138	307.10 ± 27.32	782.60 ± 33.38	...	...	...	...	...
NGC 5481	0.0071	...	...	3.79 ± 0.04	18.13 ± 0.04	39.97 ± 0.09	65.93 ± 0.31	63.21 ± 0.16
NGC 5557	0.0107	12.74 ± 1.14	1001.00 ± 6.98	9.64 ± 0.06	52.65 ± 0.46	99.23 ± 0.99	185.50 ± 1.92	184.30 ± 1.81
NGC 5576	0.0050	181.00 ± 3.51	2064.00 ± 10.88	13.68 ± 0.07	70.77 ± 0.47	139.40 ± 0.79	200.90 ± 1.19	247.00 ± 1.49
NGC 5596	0.0104	176.70 ± 2.33	314.70 ± 2.84	2.21 ± 0.02	9.24 ± 0.02	18.79 ± 0.03	27.03 ± 0.05	33.18 ± 0.11
NGC 5813	0.0066	391.60 ± 7.09	2638.00 ± 19.84	10.23 ± 0.08	59.72 ± 4.10	133.10 ± 0.83	199.60 ± 1.16	256.50 ± 5.64

Table 1
(Continued)

Name	Redshift[a]	FUV (μJy)	NUV (μJy)	u (mJy)	g (mJy)	r (mJy)	i (mJy)	z (mJy)
NGC 5831	0.0055	116.00 ± 4.06	1078.00 ± 8.34	6.36 ± 0.04	33.00 ± 0.13	69.19 ± 0.30	102.70 ± 0.37	131.10 ± 0.38
NGC 5845	0.0048	85.48 ± 2.39	275.60 ± 3.63	3.43 ± 0.02	19.94 ± 0.08	43.14 ± 0.19	64.77 ± 0.30	84.54 ± 0.35
NGC 5846	0.0057	844.60 ± 8.43	2751.00 ± 15.17	16.80 ± 0.05	96.80 ± 0.14	210.60 ± 0.29	316.00 ± 0.43	462.20 ± 0.70
NGC 5866	0.0022	501.60 ± 7.90	4212.00 ± 16.53	40.00 ± 0.44	168.60 ± 1.13	336.00 ± 2.42	481.70 ± 3.06	615.10 ± 2.54
NGC 5982	0.0101	214.50 ± 5.62	1434.00 ± 9.97	10.21 ± 0.09	59.32 ± 0.42	124.20 ± 0.96	182.90 ± 1.24	220.50 ± 1.49
NGC 6482	0.0131	98.41 ± 4.30	36.19 ± 1.20	...	...	...	...	...
NGC 6684	0.0029	...	...	...	...	...	...	...
NGC 6703	0.0082	4.25 ± 1.79	...	...	...	...	...	...
NGC 6776	0.0183	49.83 ± 8.86	342.10 ± 18.64	...	...	...	...	...
NGC 6849	0.0201	21.12 ± 4.59	...	...	...	...	...	...
NGC 7077	0.0032	1310.00 ± 8.56	1849.00 ± 7.49	2.52 ± 0.02	9.27 ± 0.02	14.27 ± 0.03	18.39 ± 0.05	22.48 ± 0.09
NGC 7176	0.0084	...	...	...	...	...	...	...
NGC 7360	0.0156	284.70 ± 3.39	518.30 ± 5.19	1.69 ± 0.04	6.92 ± 0.06	14.18 ± 0.11	20.43 ± 0.13	27.52 ± 0.43
NGC 7457	0.0027	90.41 ± 4.55	1686.00 ± 10.25	9.90 ± 0.03	53.61 ± 0.08	103.70 ± 0.14	147.50 ± 0.21	195.10 ± 0.31
NGC 7619	0.0125	179.30 ± 6.24	1013.00 ± 16.85	7.39 ± 0.08	57.18 ± 0.14	131.60 ± 0.43	208.50 ± 0.83	255.50 ± 0.59
NGC 7626	0.0114	203.60 ± 6.79	851.80 ± 12.51	8.24 ± 0.03	55.52 ± 0.08	129.30 ± 0.17	202.20 ± 0.26	265.70 ± 0.39
NGC 7785	0.0127	...	...	8.05 ± 0.24	41.58 ± 0.80	92.26 ± 1.61	139.30 ± 2.12	184.70 ± 3.32
UGC01503	0.0170	...	...	1.76 ± 0.02	5.51 ± 0.06	9.90 ± 0.10	15.49 ± 0.29	19.45 ± 0.45
UGC06570	0.0053	203.70 ± 3.85	613.40 ± 4.89	2.55 ± 0.06	9.11 ± 0.18	16.17 ± 0.33	21.33 ± 0.43	24.93 ± 0.48
UGC06637	0.0061	777.00 ± 7.91	1186.00 ± 6.52	2.36 ± 0.02	6.01 ± 0.03	8.91 ± 0.06	11.00 ± 0.09	12.25 ± 0.11
UGC06655	0.0025	903.90 ± 6.82	1257.00 ± 5.61	2.29 ± 0.02	5.40 ± 0.02	8.19 ± 0.03	9.98 ± 0.04	11.02 ± 0.07
UGC06805	0.0039	483.50 ± 6.45	879.80 ± 5.75	2.15 ± 0.02	5.77 ± 0.02	9.11 ± 0.04	11.02 ± 0.06	12.56 ± 0.10
UGC07436	0.0033	14.87 ± 2.52	205.50 ± 5.57	1.70 ± 0.05	6.81 ± 0.02	12.49 ± 0.03	16.91 ± 0.06	20.82 ± 0.25
UGC07580	0.0021	27.84 ± 1.41	45.86 ± 1.28	1.43 ± 0.03	4.66 ± 0.02	7.79 ± 0.06	10.31 ± 0.12	11.64 ± 0.09
UGC07854	0.0034	...	...	1.04 ± 0.04	3.96 ± 0.01	7.05 ± 0.04	9.65 ± 0.06	11.06 ± 0.13
UGC08876	0.0069	28.18 ± 1.83	141.90 ± 3.03	2.26 ± 0.12	10.63 ± 0.43	21.03 ± 0.83	30.78 ± 1.24	37.89 ± 1.39

Note. [a] For a few galaxies (mainly very nearby galaxies), the redshift was calculated using the distance from NED.

The Mosaicing and Pointsource Extraction (MOPEX)[9] is used to process BCD data into corrected images and to co-add them into a mosaic. To compute IRAC fluxes, a number of packages in the Image Reduction and Analysis Facility (IRAF)[10] are used for unit conversion, to remove artifacts, and to perform aperture photometry. We use the centroid sky fitting algorithm of the PHOT function (part of the APPHOT IRAF package) with an appropriate annulus and dannulu value, and a constant photometric weighting scheme for wphot. For MIPS, flux densities are extracted from apertures that cover the entire optical disk (R25). Sky subtraction is performed by averaging values from multiple apertures placed around the target, avoiding any overlap with the faint extended emission from the galaxy. Foreground stars and background galaxies present in the original mosaiced images are deleted before flux extraction is performed. These are identified by eye and cross-checked using surveys at other wavelengths (Digital Sky Survey and 2MASS). Fluxes of each IRAC and MIPS channel are obtained in mJy units. We obtain a flux measurement for 165, 173, 164, 171, 204, 121, and 93 of our galaxies at 3.6, 4.5, 5.6, 8, 24, 70, and 160 μm, respectively.

In order to have better constraints on the peak of the SED in the IR, to derive, for example, the dust temperature of our sources, we also include the observations from the *Infrared Astronomical Satellite* (*IRAS*). We obtain the *IRAS* data set for our sample using the Scan Processing and Integration tool (Scanpi) which gives us the fluxes and errors in the four *IRAS* bands: 12, 25, 60, and 100 μm. The larger errors and the poor angular resolution (4′ at 100 μm) of the *IRAS* observations compared with the rest of the available data encouraged us to check if the *IRAS* data agree well with the other data points. After removing the *IRAS* observations in case of conflict, we finally have a detection in the 12 μm band for 154 sources, in the 25 μm band for 124 sources, in the 60 μm band for 135 sources, and in the 100 μm band for 141 sources.

The launch of the *Herschel*[11] telescope allows unprecedented precisions at FIR wavelengths. We use public level2 data, which are maps of Astronomical Observation Requests (AORs), from the SPIRE instrument, downloaded from the Herschel Science Archive.[12] The SPIRE instrument observes at 250, 350, and 500 μm with an angular resolution of about 18″, 25″, and 36″ (Griffin et al. 2010). Level2 maps are combined into a single map for each object using a simple pixel co-addition technique (several AORs were requested for most objects). We subtract a background level from each image; the background is estimated by taking a median at 3′around the source. We compute the size of each galaxy on our 250 μm map by grouping neighboring pixels with a signal-to-noise ratio (S/N) greater than 2 around the source location using a friend-of-friend algorithm. We then perform an aperture photometry of this angular size at each wavelength. The size of the galaxies, which surface brightness is too low to perform this measurement (no pixels with a S/N larger than 2), is taken to be the major axis diameter from

[9] http://irsa.ipac.caltech.edu/data/SPITZER/docs/dataanalysistools/tools/mopex/mopexusersguide/
[10] http://iraf.noao.edu

[11] *Herschel* is an ESA space observatory with science instruments provided by European-led Principal Investigator consortia and with important participation from NASA.
[12] http://herschel.esac.esa.int/Science_Archive.shtml

Table 2
Fluxes (2MASS J to K Band and *Spitzer* IRAC 3.6 to 8 μm) Used in This Study; Data Were Collected According to Section 2

Name	J (mJy)	H (mJy)	Ks (mJy)	$i3.6$ (mJy)	$i4.5$ (mJy)	$i5.8$ (mJy)	$i8.0$ (mJy)
Eso103-35	46.14 ± 1.02	58.98 ± 1.58	50.70 ± 1.64	...	...	...	...
Eso428-14	197.20 ± 2.36	252.50 ± 3.02	213.30 ± 4.52	121.60 ± 6.08	81.35 ± 4.07	119.10 ± 5.96	249.40 ± 12.47
Eso462-15	197.60 ± 2.37	242.50 ± 3.80	205.20 ± 3.78	138.20 ± 6.91	73.53 ± 3.68	54.14 ± 2.71	22.39 ± 1.12
Eso483-13	35.33 ± 1.53	36.47 ± 2.39	31.67 ± 2.86	13.53 ± 0.68	8.80 ± 0.44	7.26 ± 0.36	10.22 ± 0.51
IC0798	17.54 ± 0.63	21.24 ± 1.12	15.21 ± 1.05	...	...	...	...
IC1144	33.96 ± 0.88	43.21 ± 1.43	37.20 ± 1.27	20.56 ± 1.03	11.88 ± 0.59	7.67 ± 0.38	5.87 ± 0.29
IC1459	1373.00 ± 24.03	1573.00 ± 30.43	1301.00 ± 29.95	591.90 ± 29.60	290.40 ± 14.52	156.00 ± 7.80	140.10 ± 7.01
IC1639	38.35 ± 0.60	46.17 ± 0.94	38.42 ± 1.03	19.10 ± 0.96	11.38 ± 0.57	8.12 ± 0.41	5.48 ± 0.27
IC3032	12.24 ± 0.73	12.22 ± 0.89	9.29 ± 0.83	...	...	...	...
IC3101	4.82 ± 0.52	5.25 ± 0.71	4.67 ± 0.89	...	...	...	...
IC3328	26.63 ± 1.40	27.14 ± 1.98	20.65 ± 2.35	...	5.92 ± 0.30	...	1.36 ± 0.07
IC3370	482.70 ± 5.78	599.70 ± 7.73	493.20 ± 9.54	266.90 ± 13.35	158.70 ± 7.94	123.90 ± 6.20	91.30 ± 4.57
IC3381	35.30 ± 1.69	43.33 ± 2.48	26.12 ± 2.87	...	8.47 ± 0.42	...	1.90 ± 0.09
IC3383	9.57 ± 0.63	10.59 ± 0.91	5.10 ± 1.07	...	...	...	...
IC3461	11.59 ± 0.61	13.10 ± 0.93	7.42 ± 1.04	...	...	...	...
IC3468	45.76 ± 2.62	52.52 ± 4.02	42.83 ± 4.47	...	9.26 ± 0.46	...	2.46 ± 0.12
IC3470	27.63 ± 1.07	29.95 ± 1.35	23.19 ± 1.50	...	...	...	...
IC3487	9.27 ± 0.67	15.56 ± 1.00	8.84 ± 1.15	...	...	...	...
IC3501	24.42 ± 0.70	25.02 ± 1.22	21.87 ± 1.15	...	...	...	...
IC3586	10.20 ± 0.44	10.94 ± 0.77	9.63 ± 0.72	...	...	...	...
IC3602	10.00 ± 0.53	12.27 ± 0.77	12.62 ± 0.91	...	...	...	...
IC3633	3.53 ± 0.30	4.53 ± 0.45	2.74 ± 0.52	...	...	...	...
IC3652	29.85 ± 1.76	33.76 ± 2.40	26.12 ± 3.06	...	...	...	...
IC3653	42.63 ± 1.06	51.14 ± 1.46	40.34 ± 1.86	...	...	...	...
IC3735	17.84 ± 0.94	20.21 ± 1.68	19.27 ± 1.48	...	...	...	...
IC3773	34.30 ± 1.11	36.07 ± 1.46	29.17 ± 1.88	...	...	...	...
IC3779	4.76 ± 0.37	9.36 ± 0.67	5.16 ± 0.60	...	...	...	...
IC4296	663.30 ± 7.94	826.30 ± 9.89	684.50 ± 13.24	271.60 ± 13.58	132.70 ± 6.63	58.72 ± 2.94	47.60 ± 2.38
IC4329	433.00 ± 6.78	483.40 ± 10.69	411.30 ± 9.85	161.70 ± 8.09	103.20 ± 5.16	69.40 ± 3.47	38.04 ± 1.90
IC5063	215.20 ± 2.77	259.40 ± 3.82	216.90 ± 4.00	155.10 ± 7.75	145.00 ± 7.25	302.50 ± 15.12	451.10 ± 22.55
NGC 0221	5060.00 ± 74.56	7536.00 ± 111.10	6283.00 ± 98.39	2460.00 ± 123.00	1440.00 ± 72.00	1230.00 ± 61.52	879.70 ± 43.98
NGC 0315	431.80 ± 4.77	550.50 ± 8.11	451.00 ± 6.65	249.80 ± 12.49	120.70 ± 6.03	68.89 ± 3.44	47.28 ± 2.36
NGC 0404	713.40 ± 11.83	830.10 ± 15.29	665.90 ± 14.72	442.80 ± 22.14	209.00 ± 10.45	152.10 ± 7.60	105.30 ± 5.27
NGC 0410	290.60 ± 3.48	363.00 ± 5.35	304.90 ± 5.90	182.00 ± 9.10	83.59 ± 4.18	41.71 ± 2.08	20.37 ± 1.02
NGC 0474	263.10 ± 6.30	317.90 ± 9.96	259.50 ± 9.32	...	70.93 ± 3.55	44.25 ± 2.21	22.99 ± 1.15
NGC 0507	335.50 ± 4.95	353.50 ± 7.49	327.60 ± 6.94	196.40 ± 9.82	126.90 ± 6.35	104.10 ± 5.21	32.46 ± 1.62
NGC 0516	46.44 ± 1.07	53.06 ± 1.42	42.56 ± 1.73	22.04 ± 1.10	13.91 ± 0.70	8.45 ± 0.42	5.81 ± 0.29
NGC 0526	...	...	...	...	...	...	...
NGC 0533	278.30 ± 4.10	345.40 ± 6.04	287.50 ± 7.15	...	...	...	...
NGC 0584	827.40 ± 14.48	1071.00 ± 20.72	821.50 ± 18.92	353.30 ± 17.67	186.70 ± 9.34	159.20 ± 7.96	102.60 ± 5.13
NGC 0596	466.10 ± 5.15	560.70 ± 8.78	442.80 ± 9.38	209.90 ± 10.50	120.90 ± 6.04	84.68 ± 4.23	42.63 ± 2.13
NGC 0636	307.40 ± 4.25	358.40 ± 5.61	289.30 ± 6.66	157.10 ± 7.85	76.97 ± 3.85	60.52 ± 3.03	27.02 ± 1.35
NGC 0720	873.60 ± 14.48	1046.00 ± 19.27	846.80 ± 18.72	...	...	...	...
NGC 0777	288.00 ± 3.18	360.00 ± 4.97	308.90 ± 5.12	157.90 ± 7.89	82.38 ± 4.12	53.71 ± 2.69	27.71 ± 1.39
NGC 0807	118.00 ± 1.85	145.30 ± 2.94	123.60 ± 2.62	...	...	...	...
NGC 0814	24.44 ± 0.68	30.36 ± 1.09	23.11 ± 1.11	13.54 ± 0.68	11.13 ± 0.56	38.07 ± 1.90	107.90 ± 5.40
NGC 0821	495.40 ± 5.93	586.10 ± 7.02	474.40 ± 8.30	185.90 ± 9.30	103.10 ± 5.16	48.73 ± 2.44	36.72 ± 1.84
NGC 0855	84.75 ± 2.03	99.07 ± 3.10	80.06 ± 3.32	35.93 ± 1.80	22.11 ± 1.11	24.68 ± 1.23	50.18 ± 2.51
NGC 1016	250.10 ± 3.46	305.90 ± 4.79	254.60 ± 5.63	136.00 ± 6.80	81.35 ± 4.07	37.16 ± 1.86	26.40 ± 1.32
NGC 1023	2248.00 ± 35.19	2681.00 ± 44.45	2193.00 ± 42.41	993.70 ± 49.68	574.00 ± 28.70	833.50 ± 41.67	309.30 ± 15.46
NGC 1199	238.40 ± 1.32	302.50 ± 1.95	259.30 ± 2.15	...	98.60 ± 4.93	...	42.37 ± 2.12
NGC 1266	106.40 ± 2.74	118.00 ± 4.24	110.80 ± 4.80	52.06 ± 2.60	34.88 ± 1.74	43.01 ± 2.15	108.30 ± 5.42
NGC 1316	4334.00 ± 67.87	4729.00 ± 78.40	3994.00 ± 69.89	2003.00 ± 100.20	987.20 ± 49.36	502.80 ± 25.14	509.50 ± 25.48
NGC 1374	394.60 ± 4.00	476.80 ± 6.15	372.70 ± 7.21	185.10 ± 9.25	102.90 ± 5.15	59.88 ± 2.99	43.12 ± 2.16
NGC 1377	93.01 ± 2.31	110.20 ± 3.15	89.00 ± 3.77	53.95 ± 2.70	77.34 ± 3.87	333.00 ± 16.65	434.90 ± 21.74
NGC 1386	421.60 ± 3.50	497.00 ± 4.58	407.20 ± 5.25	224.00 ± 11.20	176.90 ± 8.84	258.00 ± 12.90	436.80 ± 21.84
NGC 1395	1207.00 ± 22.24	1441.00 ± 29.21	1198.00 ± 30.91	...	...	...	...
NGC 1399	2150.00 ± 37.63	2512.00 ± 48.58	2060.00 ± 51.22	...	...	...	...
NGC 1404	1284.00 ± 20.10	1546.00 ± 25.63	1283.00 ± 24.81	617.90 ± 30.89	347.00 ± 17.35	232.40 ± 11.62	165.50 ± 8.27
NGC 1407	1442.00 ± 25.23	1686.00 ± 31.05	1430.00 ± 32.93	...	...	...	...
NGC 1426	244.20 ± 2.70	291.80 ± 3.49	233.20 ± 4.51	143.80 ± 7.19	83.11 ± 4.16	44.77 ± 2.24	31.57 ± 1.58
NGC 1427	402.30 ± 4.45	494.20 ± 6.83	380.70 ± 7.71	207.80 ± 10.39	117.90 ± 5.89	74.31 ± 3.71	46.90 ± 2.35
NGC 1439	275.80 ± 4.06	316.20 ± 5.53	255.70 ± 6.83	150.90 ± 7.55	85.24 ± 4.26	55.25 ± 2.76	33.09 ± 1.66
NGC 1510	50.27 ± 1.76	90.52 ± 2.50	49.41 ± 2.91	15.39 ± 0.77	9.72 ± 0.49	11.73 ± 0.59	22.49 ± 1.12
NGC 1522	15.66 ± 1.13	24.27 ± 1.68	19.22 ± 1.70	9.72 ± 0.49	6.46 ± 0.32	6.56 ± 0.33	14.22 ± 0.71

Table 2
(Continued)

Name	J (mJy)	H (mJy)	Ks (mJy)	$i3.6$ (mJy)	$i4.5$ (mJy)	$i5.8$ (mJy)	$i8.0$ (mJy)
NGC 1533	626.50 ± 7.50	757.80 ± 10.47	611.20 ± 11.82	2303.00 ± 115.10	...	108.50 ± 5.43	...
NGC 1543	767.90 ± 14.15	898.50 ± 19.04	719.40 ± 18.56	462.80 ± 23.14	273.00 ± 13.65	152.70 ± 7.63	167.00 ± 8.35
NGC 1553	2200.00 ± 32.43	2654.00 ± 41.56	2108.00 ± 34.94	...	...	...	...
NGC 1700	404.50 ± 3.73	492.00 ± 4.98	399.00 ± 6.62	203.20 ± 10.16	120.30 ± 6.01	107.70 ± 5.38	43.94 ± 2.20
NGC 2110	325.20 ± 3.59	430.50 ± 5.55	379.00 ± 6.63	...	...	...	...
NGC 2300	597.70 ± 10.46	718.40 ± 14.56	610.60 ± 12.37	...	...	...	...
NGC 2325	500.90 ± 6.92	593.10 ± 9.29	478.40 ± 11.90	...	...	...	...
NGC 2434	462.70 ± 6.39	583.40 ± 10.21	480.60 ± 10.62	...	...	...	...
NGC 2685	328.80 ± 6.06	389.40 ± 8.61	312.30 ± 7.48	151.30 ± 7.56	87.96 ± 4.40	65.24 ± 3.26	202.60 ± 10.13
NGC 2768	1102.00 ± 23.34	1359.00 ± 33.79	1090.00 ± 31.12	547.60 ± 27.38	255.30 ± 12.76	260.50 ± 13.03	156.40 ± 7.82
NGC 2778	113.60 ± 1.88	136.80 ± 2.52	107.30 ± 2.87	52.43 ± 2.62	30.44 ± 1.52	17.63 ± 0.88	12.31 ± 0.62
NGC 2787	848.20 ± 5.47	1039.00 ± 8.62	853.10 ± 8.64	377.20 ± 18.86	249.90 ± 12.49	157.10 ± 7.86	128.20 ± 6.41
NGC 2832	222.30 ± 2.87	267.10 ± 4.43	227.50 ± 4.82	87.94 ± 4.40	79.43 ± 3.97	26.07 ± 1.30	17.51 ± 0.88
NGC 2970	28.74 ± 0.74	34.35 ± 1.17	26.27 ± 1.09	17.51 ± 0.88	7.00 ± 0.35	6.28 ± 0.31	3.46 ± 0.17
NGC 2974	2073.00 ± 3.82	1902.00 ± 7.01	2159.00 ± 9.94	463.20 ± 23.16	308.20 ± 15.41	177.70 ± 8.88	170.60 ± 8.53
NGC 2986	632.30 ± 12.81	764.10 ± 15.48	603.40 ± 17.23	...	...	...	...
NGC 3011	29.06 ± 0.48	30.79 ± 0.77	23.41 ± 0.71	13.06 ± 0.65	8.23 ± 0.41	10.12 ± 0.51	17.81 ± 0.89
NGC 3032	105.70 ± 1.56	121.80 ± 1.79	94.84 ± 2.10	55.78 ± 2.79	34.74 ± 1.74	53.10 ± 2.65	145.10 ± 7.26
NGC 3073	31.31 ± 1.33	41.68 ± 2.23	32.70 ± 2.32	21.15 ± 1.06	8.60 ± 0.43	8.57 ± 0.43	18.12 ± 0.91
NGC 3115	3157.00 ± 46.53	3767.00 ± 55.51	3041.00 ± 47.61	1281.00 ± 64.06	699.60 ± 34.98	624.70 ± 31.24	368.20 ± 18.41
NGC 3125	46.61 ± 1.25	48.93 ± 1.85	42.36 ± 2.11	29.44 ± 1.47	20.64 ± 1.03	43.13 ± 2.16	109.30 ± 5.46
NGC 3156	114.00 ± 2.21	125.00 ± 3.22	104.00 ± 3.54	52.17 ± 2.61	28.70 ± 1.44	22.92 ± 1.15	24.31 ± 1.22
NGC 3226	283.00 ± 6.00	294.80 ± 8.42	256.00 ± 8.72	197.10 ± 9.85	79.79 ± 3.99	47.72 ± 2.39	48.88 ± 2.44
NGC 3265	46.27 ± 0.90	56.38 ± 1.14	45.77 ± 1.22	26.39 ± 1.32	17.39 ± 0.87	41.98 ± 2.10	228.00 ± 11.40
NGC 3377	796.00 ± 13.93	937.40 ± 19.00	724.10 ± 19.34	310.00 ± 15.50	192.10 ± 9.60	138.20 ± 6.91	65.45 ± 3.27
NGC 3379	2227.00 ± 32.82	2679.00 ± 41.95	2129.00 ± 35.30	829.10 ± 41.46	452.90 ± 22.64	354.00 ± 17.70	164.60 ± 8.23
NGC 3384	1406.00 ± 20.73	1672.00 ± 26.17	1368.00 ± 23.95	571.50 ± 28.57	354.00 ± 17.70	310.30 ± 15.51	178.10 ± 8.91
NGC 3412	634.00 ± 3.50	755.70 ± 4.87	586.40 ± 5.94	262.70 ± 13.13	161.40 ± 8.07	87.75 ± 4.39	56.48 ± 2.82
NGC 3489	807.10 ± 3.72	1005.00 ± 5.56	773.00 ± 6.41	343.00 ± 17.15	205.40 ± 10.27	166.10 ± 8.31	157.00 ± 7.85
NGC 3516	252.90 ± 4.66	282.10 ± 6.50	270.00 ± 6.71	164.20 ± 8.21	134.70 ± 6.73	176.20 ± 8.81	265.90 ± 13.30
NGC 3522	54.52 ± 0.90	63.15 ± 1.57	48.55 ± 1.48	27.80 ± 1.39	15.74 ± 0.79	7.25 ± 0.36	6.62 ± 0.33
NGC 3557	893.10 ± 8.23	1057.00 ± 12.65	901.50 ± 14.12	449.40 ± 22.47	271.10 ± 13.55	215.20 ± 10.76	132.40 ± 6.62
NGC 3585	1482.00 ± 23.21	1772.00 ± 29.37	1429.00 ± 27.64	655.60 ± 32.78	380.00 ± 19.00	352.80 ± 17.64	193.20 ± 9.66
NGC 3593	711.40 ± 13.11	936.60 ± 19.84	740.30 ± 19.09	390.00 ± 19.50	245.30 ± 12.26	582.90 ± 29.14	1504.00 ± 75.22
NGC 3607	1125.00 ± 18.66	1298.00 ± 25.10	1093.00 ± 23.15	517.10 ± 25.86	253.10 ± 12.66	203.90 ± 10.20	176.00 ± 8.80
NGC 3608	431.00 ± 3.57	471.10 ± 5.64	396.10 ± 5.47	217.60 ± 10.88	114.90 ± 5.75	77.33 ± 3.87	33.05 ± 1.65
NGC 3610	479.60 ± 3.53	570.60 ± 6.31	471.00 ± 5.21	243.80 ± 12.19	141.30 ± 7.06	116.70 ± 5.83	68.58 ± 3.43
NGC 3640	691.40 ± 8.28	805.30 ± 10.38	674.50 ± 14.29	374.20 ± 18.71	197.20 ± 9.86	111.00 ± 5.55	59.68 ± 2.98
NGC 3706	476.10 ± 4.82	563.30 ± 7.26	473.60 ± 8.29	256.20 ± 12.81	153.30 ± 7.66	108.80 ± 5.44	59.47 ± 2.97
NGC 3773	41.05 ± 1.29	37.67 ± 1.84	36.12 ± 2.10	20.08 ± 1.00	10.95 ± 0.55	22.14 ± 1.11	53.18 ± 2.66
NGC 3870	36.35 ± 0.77	40.77 ± 1.43	32.22 ± 1.25	22.75 ± 1.14	13.43 ± 0.67	27.71 ± 1.39	64.72 ± 3.24
NGC 3923	1766.00 ± 34.15	2095.00 ± 42.45	1723.00 ± 47.60	688.90 ± 34.44	366.40 ± 18.32	298.80 ± 14.94	133.50 ± 6.68
NGC 3941	832.80 ± 4.60	1002.00 ± 7.38	812.40 ± 7.48	379.40 ± 18.97	223.70 ± 11.18	173.40 ± 8.67	113.50 ± 5.67
NGC 3945	644.00 ± 11.27	951.40 ± 18.40	669.60 ± 15.42	333.30 ± 16.67	186.80 ± 9.34	193.30 ± 9.66	156.00 ± 7.80
NGC 3962	615.60 ± 5.67	737.80 ± 7.47	588.00 ± 10.29	361.20 ± 18.06	213.10 ± 10.65	...	...
NGC 4026	644.00 ± 10.08	809.70 ± 13.42	634.70 ± 11.11	291.20 ± 14.56	179.70 ± 8.99	167.70 ± 8.38	97.69 ± 4.88
NGC 4073	270.70 ± 4.74	346.40 ± 6.06	275.80 ± 7.62	157.00 ± 7.85	94.03 ± 4.70	51.91 ± 2.60	33.71 ± 1.69
NGC 4117	69.91 ± 1.22	77.54 ± 2.00	65.67 ± 1.88	34.05 ± 1.70	21.11 ± 1.06	16.56 ± 0.83	24.53 ± 1.23
NGC 4125	1277.00 ± 21.17	1523.00 ± 26.66	1242.00 ± 26.32	655.50 ± 32.78	356.40 ± 17.82	273.60 ± 13.68	163.80 ± 8.19
NGC 4138	368.90 ± 2.72	453.70 ± 5.01	359.20 ± 4.63	188.20 ± 9.41	118.60 ± 5.93	138.30 ± 6.92	247.30 ± 12.36
NGC 4150	176.10 ± 1.78	210.80 ± 2.91	174.20 ± 2.73	102.00 ± 5.10	66.14 ± 3.31	61.96 ± 3.10	78.07 ± 3.90
NGC 4168	295.20 ± 3.26	352.50 ± 5.52	289.30 ± 5.60	164.20 ± 8.21	75.26 ± 3.76	37.01 ± 1.85	22.25 ± 1.11
NGC 4203	776.50 ± 6.44	932.30 ± 9.45	747.80 ± 9.64	350.00 ± 17.50	214.90 ± 10.75	105.00 ± 5.25	130.50 ± 6.52
NGC 4251	557.90 ± 3.60	667.90 ± 4.92	556.40 ± 5.64	270.00 ± 13.50	159.00 ± 7.95	121.00 ± 6.05	72.91 ± 3.65
NGC 4261	859.20 ± 15.04	1046.00 ± 20.23	853.10 ± 22.00	417.10 ± 20.86	242.40 ± 12.12	142.10 ± 7.11	72.67 ± 3.63
NGC 4267	530.80 ± 6.36	627.40 ± 9.25	500.50 ± 10.60	240.00 ± 12.00	131.60 ± 6.58	77.13 ± 3.86	45.32 ± 2.27
NGC 4278	957.00 ± 6.17	1142.00 ± 9.46	917.50 ± 9.29	428.20 ± 21.41	248.70 ± 12.44	169.20 ± 8.46	125.50 ± 6.28
NGC 4291	294.10 ± 2.98	366.10 ± 3.71	294.70 ± 4.07	124.80 ± 6.24	82.33 ± 4.12	62.51 ± 3.12	32.50 ± 1.62
NGC 4308	42.47 ± 0.86	46.72 ± 1.51	38.71 ± 1.35	20.06 ± 1.00	9.97 ± 0.50	7.27 ± 0.36	4.65 ± 0.23
NGC 4344	47.09 ± 0.61	56.75 ± 0.99	44.24 ± 0.98	39.98 ± 6.12	23.19 ± 4.86	...	...
NGC 4350	512.10 ± 2.83	661.20 ± 4.26	513.10 ± 3.78	246.10 ± 12.30	145.30 ± 7.26	111.20 ± 5.56	85.08 ± 4.25
NGC 4352	91.73 ± 2.11	100.50 ± 2.78	77.59 ± 3.22	...	22.23 ± 1.11	...	5.54 ± 0.28
NGC 4365	1578.00 ± 29.07	1895.00 ± 38.39	1514.00 ± 40.45	647.70 ± 32.38	400.70 ± 20.04	303.40 ± 15.17	205.10 ± 10.26
NGC 4371	594.50 ± 7.12	694.30 ± 10.23	561.00 ± 11.89	300.40 ± 15.02	171.40 ± 8.57	104.90 ± 5.25	39.23 ± 1.96

Table 2
(Continued)

Name	J (mJy)	H (mJy)	Ks (mJy)	$i3.6$ (mJy)	$i4.5$ (mJy)	$i5.8$ (mJy)	$i8.0$ (mJy)
NGC 4374	2319.00 ± 38.45	2729.00 ± 55.29	2225.00 ± 47.14	886.80 ± 44.34	490.00 ± 24.50	291.80 ± 14.59	124.50 ± 6.22
NGC 4377	210.50 ± 1.94	251.20 ± 3.24	201.60 ± 2.97	...	...	...	...
NGC 4379	226.00 ± 2.50	275.10 ± 4.05	213.90 ± 3.55	...	...	...	...
NGC 4382	2462.00 ± 38.55	2862.00 ± 52.73	2389.00 ± 46.21	944.50 ± 47.22	567.50 ± 28.37	422.70 ± 21.14	268.00 ± 13.40
NGC 4386	272.00 ± 3.01	346.10 ± 4.14	274.30 ± 4.29	88.34 ± 4.42	77.56 ± 3.88	60.85 ± 3.04	41.43 ± 2.07
NGC 4406	2583.00 ± 49.96	3110.00 ± 74.48	2483.00 ± 64.04	1426.00 ± 71.30	887.90 ± 44.39	234.70 ± 11.74	166.40 ± 8.32
NGC 4417	393.50 ± 6.52	452.00 ± 5.83	369.00 ± 9.52	...	...	...	...
NGC 4421	214.20 ± 2.76	254.90 ± 4.23	207.90 ± 4.02	117.50 ± 5.88	65.13 ± 3.26	39.09 ± 1.96	31.05 ± 1.55
NGC 4434	153.20 ± 2.40	176.70 ± 3.09	141.80 ± 3.79	...	...	...	...
NGC 4435	702.30 ± 8.41	1445.00 ± 13.31	826.80 ± 12.18	285.00 ± 14.25	156.00 ± 7.80	136.90 ± 6.84	129.80 ± 6.49
NGC 4442	849.00 ± 14.86	1059.00 ± 19.50	829.10 ± 18.33	402.60 ± 20.13	231.50 ± 11.58	151.00 ± 7.55	92.51 ± 4.63
NGC 4458	134.40 ± 1.73	157.00 ± 2.75	128.90 ± 2.61	67.89 ± 3.40	37.78 ± 1.89	25.80 ± 1.29	14.54 ± 0.73
NGC 4459	940.40 ± 6.93	1155.00 ± 10.64	944.90 ± 9.57	504.10 ± 25.20	255.00 ± 12.75	168.90 ± 8.45	176.20 ± 8.81
NGC 4460	168.60 ± 3.11	202.60 ± 4.11	163.60 ± 4.97	90.83 ± 4.54	55.99 ± 2.80	82.04 ± 4.10	147.50 ± 7.38
NGC 4464	108.60 ± 1.60	125.90 ± 2.44	101.00 ± 2.60	...	29.20 ± 1.46	...	10.43 ± 0.52
NGC 4472	4564.00 ± 67.26	5315.00 ± 78.33	4303.00 ± 67.38	2662.00 ± 133.10	1048.00 ± 52.42	682.80 ± 34.14	368.00 ± 18.40
NGC 4473	997.50 ± 16.54	1162.00 ± 22.47	940.60 ± 19.93	415.60 ± 20.78	238.20 ± 11.91	160.20 ± 8.01	90.57 ± 4.53
NGC 4474	233.80 ± 3.02	273.40 ± 4.03	227.10 ± 3.14	...	...	...	...
NGC 4476	115.80 ± 1.60	136.50 ± 2.14	112.30 ± 2.07	...	...	...	...
NGC 4477	799.70 ± 7.37	963.70 ± 10.65	785.90 ± 9.41	411.60 ± 20.58	223.10 ± 11.15	135.80 ± 6.79	93.48 ± 4.67
NGC 4478	327.90 ± 2.42	397.30 ± 4.03	312.00 ± 3.74	154.50 ± 7.72	92.11 ± 4.61	76.11 ± 3.81	43.34 ± 2.17
NGC 4479	91.31 ± 1.60	103.40 ± 2.76	84.53 ± 2.34	...	24.21 ± 1.21	...	9.58 ± 0.48
NGC 4482	52.06 ± 1.73	51.14 ± 2.64	40.12 ± 3.00	...	13.99 ± 0.70	...	3.50 ± 0.17
NGC 4483	148.40 ± 2.60	167.20 ± 3.54	132.20 ± 3.90	...	...	...	...
NGC 4486	3368.00 ± 52.73	3926.00 ± 65.09	3246.00 ± 56.81	1772.00 ± 88.62	1153.00 ± 57.67	670.20 ± 33.51	358.30 ± 17.91
NGC 4489	131.50 ± 2.30	153.60 ± 3.68	123.10 ± 3.17	...	...	...	...
NGC 4494	1131.00 ± 19.79	1330.00 ± 28.18	1089.00 ± 24.07	482.20 ± 24.11	273.40 ± 13.67	162.60 ± 8.13	134.90 ± 6.74
NGC 4515	86.48 ± 1.03	99.80 ± 1.75	76.03 ± 1.61	...	20.97 ± 1.05	...	6.04 ± 0.30
NGC 4526	1711.00 ± 26.80	2204.00 ± 36.54	1766.00 ± 32.53	991.90 ± 49.60	526.30 ± 26.31	410.80 ± 20.54	445.90 ± 22.30
NGC 4528	184.00 ± 2.20	233.50 ± 3.23	177.40 ± 3.60	...	...	...	...
NGC 4552	1470.00 ± 24.37	1762.00 ± 35.70	1396.00 ± 30.87	781.10 ± 39.05	445.90 ± 22.30	303.40 ± 15.17	139.30 ± 6.97
NGC 4564	464.40 ± 5.56	613.70 ± 7.91	458.60 ± 8.87	204.80 ± 10.24	113.50 ± 5.67	75.54 ± 3.78	49.52 ± 2.48
NGC 4570	592.80 ± 4.37	713.70 ± 5.92	574.60 ± 6.88	265.10 ± 13.25	157.80 ± 7.89	117.90 ± 5.89	74.85 ± 3.74
NGC 4578	299.90 ± 5.52	373.90 ± 7.92	298.30 ± 9.07	140.30 ± 7.01	80.34 ± 4.02	51.84 ± 2.59	33.82 ± 1.69
NGC 4589	541.20 ± 9.47	683.50 ± 13.22	540.70 ± 11.46	264.00 ± 13.20	162.10 ± 8.10	136.00 ± 6.80	69.53 ± 3.48
NGC 4612	280.10 ± 3.87	313.30 ± 4.91	257.90 ± 6.18	99.16 ± 4.96	75.72 ± 3.79	43.60 ± 2.18	25.16 ± 1.26
NGC 4621	1431.00 ± 25.05	1725.00 ± 31.77	1373.00 ± 32.89	571.50 ± 28.58	340.70 ± 17.04	207.80 ± 10.39	124.20 ± 6.21
NGC 4623	123.70 ± 2.39	147.80 ± 2.99	112.10 ± 3.82	...	...	...	...
NGC 4636	1956.00 ± 41.43	2430.00 ± 60.43	1851.00 ± 59.68	628.60 ± 31.43	358.10 ± 17.90	182.50 ± 9.13	107.70 ± 5.39
NGC 4638	367.20 ± 3.72	435.30 ± 4.81	356.90 ± 6.25	185.80 ± 9.29	102.40 ± 5.12	71.44 ± 3.57	42.07 ± 2.10
NGC 4649	3523.00 ± 55.16	4203.00 ± 65.81	3472.00 ± 67.16	1381.00 ± 69.07	784.10 ± 39.21	495.70 ± 24.79	334.60 ± 16.73
NGC 4660	373.70 ± 2.75	446.20 ± 3.70	357.90 ± 5.60	169.80 ± 8.49	102.60 ± 5.13	70.84 ± 3.54	45.78 ± 2.29
NGC 4694	184.40 ± 3.06	214.20 ± 3.75	179.60 ± 4.80	165.40 ± 8.27	63.50 ± 3.17	62.34 ± 3.12	370.20 ± 18.51
NGC 4696	944.80 ± 15.66	1179.00 ± 19.55	953.70 ± 21.08	503.10 ± 25.16	270.50 ± 13.53	206.80 ± 10.34	100.70 ± 5.03
NGC 4697	2094.00 ± 36.64	2432.00 ± 44.80	1947.00 ± 48.43	784.20 ± 39.21	563.30 ± 28.17	378.70 ± 18.93	196.50 ± 9.83
NGC 4709	404.50 ± 4.84	501.60 ± 6.01	427.90 ± 8.67	269.30 ± 13.46	162.30 ± 8.11	128.30 ± 6.42	40.79 ± 2.04
NGC 4754	778.60 ± 15.06	925.40 ± 18.75	742.30 ± 20.51	334.80 ± 16.74	205.70 ± 10.28	119.90 ± 6.00	60.32 ± 3.02
NGC 4762	863.20 ± 16.70	1093.00 ± 21.15	825.30 ± 22.05	378.60 ± 18.93	215.20 ± 10.76	160.10 ± 8.01	98.03 ± 4.90
NGC 4786	221.10 ± 3.05	273.90 ± 4.54	223.60 ± 5.56	129.60 ± 6.48	70.07 ± 3.50	52.68 ± 2.63	31.86 ± 1.59
NGC 4915	211.90 ± 2.34	259.90 ± 3.11	212.10 ± 4.49	101.70 ± 5.09	60.41 ± 3.02	43.24 ± 2.16	23.55 ± 1.18
NGC 4936	552.20 ± 6.10	677.90 ± 8.12	554.40 ± 10.21	373.70 ± 18.68	233.30 ± 11.66	182.40 ± 9.12	131.40 ± 6.57
NGC 5018	558.90 ± 5.15	643.80 ± 7.71	552.80 ± 7.13	297.60 ± 14.88	171.90 ± 8.60	134.50 ± 6.72	113.60 ± 5.68
NGC 5044	560.90 ± 5.17	673.50 ± 6.82	565.20 ± 10.41	321.60 ± 16.08	173.60 ± 8.68	111.90 ± 5.60	54.09 ± 2.71
NGC 5061	866.40 ± 6.38	1032.00 ± 11.40	832.90 ± 10.74	425.00 ± 21.25	267.40 ± 13.37	231.00 ± 11.55	126.40 ± 6.32
NGC 5077	344.30 ± 3.49	422.60 ± 4.67	354.60 ± 6.21	183.50 ± 9.18	87.64 ± 4.38	54.09 ± 2.71	38.48 ± 1.92
NGC 5173	72.66 ± 1.27	83.24 ± 1.53	65.73 ± 1.76	36.92 ± 1.85	20.85 ± 1.04	21.87 ± 1.09	35.85 ± 1.79
NGC 5273	259.70 ± 3.11	308.10 ± 4.54	234.50 ± 5.18	116.20 ± 5.81	66.79 ± 3.34	44.42 ± 2.22	38.80 ± 1.94
NGC 5322	997.50 ± 18.38	1204.00 ± 26.62	938.00 ± 23.33	423.70 ± 21.19	235.70 ± 11.79	168.50 ± 8.43	97.71 ± 4.88
NGC 5338	53.32 ± 2.46	61.99 ± 3.31	48.42 ± 4.29	26.86 ± 1.34	15.43 ± 0.77	15.90 ± 0.80	28.05 ± 1.40
NGC 5353	642.90 ± 4.14	857.30 ± 5.53	611.20 ± 6.75	310.40 ± 15.52	157.80 ± 7.89	109.20 ± 5.46	67.78 ± 3.39
NGC 5419	667.00 ± 13.52	778.30 ± 19.36	674.50 ± 19.88	339.00 ± 16.95	177.00 ± 8.85	94.80 ± 4.74	62.49 ± 3.12
NGC 5481	124.90 ± 2.30	152.30 ± 2.95	121.10 ± 3.68	60.97 ± 3.05	37.36 ± 1.87	19.34 ± 0.97	9.64 ± 0.48
NGC 5557	401.50 ± 3.33	487.00 ± 4.49	402.00 ± 5.92	227.90 ± 11.40	118.20 ± 5.91	77.85 ± 3.89	44.61 ± 2.23
NGC 5576	523.00 ± 5.78	686.00 ± 6.95	507.40 ± 9.81	276.70 ± 13.84	157.10 ± 7.85	101.40 ± 5.07	54.56 ± 2.73
NGC 5596	48.23 ± 0.84	58.02 ± 1.18	47.23 ± 1.61	23.83 ± 1.19	13.95 ± 0.70	10.65 ± 0.53	13.85 ± 0.69

Table 2
(Continued)

Name	J (mJy)	H (mJy)	Ks (mJy)	$i3.6$ (mJy)	$i4.5$ (mJy)	$i5.8$ (mJy)	$i8.0$ (mJy)
NGC 5813	755.30 ± 13.91	937.40 ± 16.41	743.00 ± 21.22	315.00 ± 15.75	177.40 ± 8.87	96.53 ± 4.83	45.91 ± 2.29
NGC 5831	297.90 ± 3.57	355.70 ± 4.26	289.30 ± 6.93	158.90 ± 7.95	90.15 ± 4.51	47.58 ± 2.38	30.63 ± 1.53
NGC 5845	153.10 ± 1.27	189.60 ± 1.40	155.40 ± 2.58	74.82 ± 3.74	38.64 ± 1.93	26.44 ± 1.32	19.11 ± 0.96
NGC 5846	1147.00 ± 19.02	1406.00 ± 23.31	1139.00 ± 27.28	522.70 ± 26.13	299.00 ± 14.95	161.70 ± 8.09	77.68 ± 3.88
NGC 5866	1207.00 ± 17.79	1482.00 ± 23.20	1222.00 ± 20.26	667.20 ± 33.36	364.20 ± 18.21	360.90 ± 18.05	342.70 ± 17.13
NGC 5982	381.70 ± 3.87	477.20 ± 6.15	376.50 ± 5.90	200.50 ± 10.03	124.80 ± 6.24	68.59 ± 3.43	42.75 ± 2.14
NGC 6482	299.30 ± 2.76	379.80 ± 4.20	307.20 ± 3.68	...	...	...	...
NGC 6684	983.80 ± 12.69	1476.00 ± 20.39	1039.00 ± 19.14	440.50 ± 22.02	251.00 ± 12.55	160.90 ± 8.04	108.30 ± 5.42
NGC 6703	352.30 ± 3.25	418.00 ± 5.00	344.00 ± 5.39	227.00 ± 11.35	121.00 ± 6.05	64.26 ± 3.21	32.73 ± 1.64
NGC 6776	168.30 ± 2.17	184.10 ± 3.22	165.70 ± 3.51	113.90 ± 5.70	66.85 ± 3.34	40.20 ± 2.01	30.83 ± 1.54
NGC 6849	124.90 ± 2.30	151.10 ± 3.34	117.80 ± 3.47	68.62 ± 3.43	35.78 ± 1.79	23.17 ± 1.16	16.48 ± 0.82
NGC 7077	19.54 ± 1.04	19.82 ± 1.68	19.29 ± 1.78	10.37 ± 0.52	6.55 ± 0.33	7.41 ± 0.37	13.91 ± 0.70
NGC 7176	424.70 ± 5.09	515.20 ± 7.59	428.30 ± 8.29	210.10 ± 10.51	...	129.70 ± 6.48	...
NGC 7360	38.03 ± 0.95	48.21 ± 1.64	38.74 ± 1.53	19.82 ± 0.99	11.90 ± 0.59	8.07 ± 0.40	15.33 ± 0.77
NGC 7457	372.30 ± 4.46	431.70 ± 6.36	362.60 ± 8.02	183.50 ± 9.18	101.30 ± 5.06	71.68 ± 3.58	50.35 ± 2.52
NGC 7619	415.10 ± 4.97	479.40 ± 7.07	419.70 ± 7.35	166.90 ± 8.34	117.30 ± 5.87	60.52 ± 3.03	37.35 ± 1.87
NGC 7626	413.20 ± 5.71	519.00 ± 8.13	420.10 ± 8.51	167.20 ± 8.36	123.10 ± 6.16	85.07 ± 4.25	35.64 ± 1.78
NGC 7785	269.20 ± 3.72	328.70 ± 4.84	285.60 ± 5.26	133.80 ± 6.69	77.04 ± 3.85	57.52 ± 2.88	39.77 ± 1.99
UGC01503	41.32 ± 0.88	47.72 ± 1.27	40.68 ± 1.31	...	...	...	...
UGC06570	35.10 ± 0.84	41.64 ± 1.19	35.04 ± 1.36	19.81 ± 0.99	13.16 ± 0.66	25.16 ± 1.26	81.27 ± 4.06
UGC06637	16.21 ± 0.46	18.91 ± 0.80	13.92 ± 0.76	7.64 ± 0.38	4.71 ± 0.24	8.30 ± 0.41	15.92 ± 0.80
UGC06655	12.83 ± 0.40	14.23 ± 0.79	10.30 ± 0.65	6.66 ± 0.33	4.32 ± 0.22	7.50 ± 0.37	14.48 ± 0.72
UGC06805	17.94 ± 0.55	19.23 ± 1.04	17.74 ± 0.90	9.33 ± 0.47	5.89 ± 0.29	13.31 ± 0.67	31.83 ± 1.59
UGC07436	22.85 ± 1.16	26.62 ± 1.99	19.89 ± 1.91	...	...	...	...
UGC07580	13.90 ± 1.29	18.89 ± 1.85	16.63 ± 2.20	...	...	...	...
UGC07854	10.29 ± 0.63	12.99 ± 0.84	8.20 ± 1.08	...	...	...	...
UGC08876	53.67 ± 0.84	65.88 ± 1.21	52.70 ± 1.70	...	...	...	...

the NED. The aperture size is inspected by eye to check for multiple sources or complex morphology. We obtained data for 75 galaxies and detected at the 5σ confidence level 31 sources at 250 μm, 31 at 350 μm, and 25 at 500 μm.

3. SED FITTING

To fit the SED of our galaxies, we use CIGALEMC[13] (Serra et al. 2011) which is a modified version of the Code Investigating GALaxy Emission (CIGALE; Noll et al. 2009; Giovannoli et al. 2011). CIGALEMC uses a Markov Chain Monte Carlo sampling of the CIGALE parameters which allows us to increase the size of the parameter space covered and a more efficient sampling of it. CIGALEMC uses the Maraston (2005) stellar population model and we use the Salpeter initial mass function (IMF) (Salpeter 1955). The Salpeter IMF is in general a better match for massive, ETGs as has been previously found (Grillo et al. 2009; Auger et al. 2010; Treu et al. 2010; Spiniello et al. 2011) using stellar dynamics and gravitational lensing. The Maraston (2005) stellar population model includes a realistic treatment of the thermally pulsating asymptotic giant branch (TP-AGB). The TP-AGB phase modeling is important to derive an accurate stellar mass (Maraston et al. 2006; Ilbert et al. 2010). When fitting the data, we assume an exponentially decreasing SFR for both the old and new star populations following Giovannoli et al. (2011). The age of the old stellar population is fixed to 10 Gyr, and the e-folding time of the new population is fixed to 20 Gyr, which corresponds effectively to a constant bursting time (Giovannoli et al. 2011; Serra et al. 2011). We use the Calzetti et al. (1994) and Calzetti (1997) attenuation to describe the dust absorption of star light. We do not add any modification to the Calzetti curve, like a 2175 Å UV bump or a change of slope. The attenuation is modeled independently for the old and young star populations, the attenuation factor for the young population is $A_{\rm ySP}$ (V-band attenuation), and there is a reduction factor f_V for the old stellar population ($A_{\rm ySP} \times f_V$).

The IR emission from the dust is computed using the Dale & Helou (2002) model, which is composed of 64 templates parameterized by a slope α. This slope represents the power-law slope of the dust mass over the heating intensity. Dale & Helou (2002) followed Desert et al. (1990) approach by dividing their dust emission sources into large grains, small grains and polycyclic aromatic hydrocarbons (PAHs). They normalized these components using observations from *IRAS*, *Infrared Space Observatory*, and SCUBA. CIGALEMC also includes a model for the AGN emission, using the AGN templates from Siebenmorgen et al. (2004a, 2004b) and a parameter for its amplitude $f_{\rm AGN}$.

The eight free parameters of the fit, $\tau_{\rm old}$, $t_{\rm new}$, $f_{\rm ySP}$, $A_{\rm ySP}$, f_V, α, $f_{\rm AGN}$, $M_{\rm gal}$, are described in Table 5 along with their priors.

In the analysis of the SEDs, we use some derived parameters: SFR, age$_{D4000}$, $L_{\rm bol}$, $L_{\rm dust}$, M_*; these are computed either from the fitted parameters and/or from the fitted SED (Table 6). The SFR is computed from the contribution of the young and old star populations; however, the young star population gives, in general, the dominant contribution. Therefore, the SFR mostly depends on the fitted parameters $M_{\rm gal}$ the normalization, $f_{\rm ySP}$ the fraction of young stars, and $t_{\rm new}$ the age of the young star population. SFR increases with $M_{\rm gal}$ and $f_{\rm ySP}$, and it decreases slightly as young stellar populations age, i.e., as $t_{\rm new}$ gets larger. Apart from its $M_{\rm gal}$ dependency, the SFR is

[13] http://cigale.oamp.fr/

Table 3
Fluxes (24–160 μm *Spitzer* MIPS, 12–100 μm *IRAS*) Used in This Study; Data Were Collected According to Section 2

Name	$24_{\mu m}$ (mJy)	$70_{\mu m}$ (mJy)	$160_{\mu m}$ (mJy)	$I12_{\mu m}$ (mJy)	$I25_{\mu m}$ (mJy)	$I60_{\mu m}$ (mJy)	$I100_{\mu m}$ (mJy)	Hα (erg s^{-1} cm^{-2})
Eso103-35	1693.0 ± 81.0	1774.0 ± 112.0	...	360 ± 73	40 ± 59	410 ± 321	15170 ± 3886	...
Eso428-14	1448.0 ± 80.0	4714.0 ± 389.0	...	20 ± 37	340 ± 70	430 ± 80	70 ± 348	...
Eso462-15	6.1 ± 0.7	0.0 ± 19.4	0.0 ± 26.8	810 ± 21871	...	1790 ± 1432	4960 ± 774	...
Eso483-13	29.8 ± 3.8	417.0 ± 23.0	579.0 ± 69.0	40 ± 41	...	150 ± 57	1310 ± 228	...
IC0798	0.6 ± 0.2	...	...	20 ± 34	120 ± 68	160 ± 43	470 ± 191	16.05 ± 3.72
IC1144	1.4 ± 0.3	...	...	...	120 ± 35	160 ± 103	...	...
IC1459	60.9 ± 4.3	542.0 ± 32.0	627.0 ± 72.0	...	...	...	...	...
IC1639	3.7 ± 0.4	...	...	20 ± 35	160 ± 50	280 ± 44	1210 ± 158	49.57 ± 10.38
IC3032	0.0 ± 0.1	...	...	100 ± 60	...	10 ± 78	270 ± 222	−1.91 ± 1.38
IC3101	0.0 ± 0.1	...	...	...	670 ± 70	270 ± 57	700 ± 180	3.56 ± 1.38
IC3328	0.5 ± 0.1	...	...	...	...	...	...	7.42 ± 6.02
IC3370	32.8 ± 3.4	680.0 ± 51.0	958.0 ± 128.0	30 ± 346	30 ± 143	0 ± 67	...	...
IC3381	0.5 ± 0.1	...	...	30 ± 33	50 ± 42	20 ± 49	...	5.25 ± 2.42
IC3383	0.0 ± 0.1	...	...	30 ± 27	...	...	...	−0.97 ± 1.93
IC3461	0.0 ± 0.1	...	...	240 ± 27	250 ± 32	480 ± 43	1260 ± 131	−3.22 ± 3.38
IC3468	0.2 ± 0.1	...	...	280 ± 28	1100 ± 47	4680 ± 41	3250 ± 121	9.64 ± 2.68
IC3470	0.0 ± 0.1	...	...	190 ± 135	100 ± 76	40 ± 62	1020 ± 330	17.69 ± 3.10
IC3487	0.0 ± 0.1	...	...	130 ± 27	360 ± 44	1520 ± 44	1950 ± 196	19.60 ± 5.23
IC3501	0.2 ± 0.1	...	...	20 ± 39	130 ± 40	...	...	10.73 ± 2.85
IC3586	0.0 ± 1.0	...	...	240 ± 41	290 ± 31	...	190 ± 224	−0.53 ± 1.73
IC3602	0.7 ± 0.1	...	...	10 ± 26	...	100 ± 54	550 ± 166	...
IC3633	0.0 ± 0.1	...	...	240 ± 27	1100 ± 40	14360 ± 48	16890 ± 180	3.82 ± 2.25
IC3652	0.2 ± 0.1	...	...	550 ± 29	430 ± 28	3620 ± 373	8340 ± 1389	14.50 ± 7.53
IC3653	0.8 ± 0.1	...	...	80 ± 23	...	70 ± 32	260 ± 92	34.98 ± 5.64
IC3735	0.0 ± 0.1	...	...	560 ± 27	1980 ± 37	7650 ± 30	6020 ± 117	...
IC3773	0.3 ± 0.1	...	...	550 ± 19	1500 ± 20	6120 ± 33	9070 ± 92	−3.72 ± 3.19
IC3779	0.0 ± 0.1	...	...	220 ± 23	60 ± 26	110 ± 31	290 ± 92	4.93 ± 1.70
IC4296	21.4 ± 8.0	118.0 ± 12.0	71.0 ± 12.0	250 ± 26	180 ± 26	70 ± 36	150 ± 80	...
IC4329	7.2 ± 1.5	0.0 ± 18.5	0.0 ± 25.8	100 ± 31	80 ± 22	70 ± 38	30 ± 111	...
IC5063	2170.0 ± 78.0	4425.0 ± 321.0	...	170 ± 22	110 ± 39	...	...	...
NGC 0221	175.0 ± 16.0	25.0 ± 18.0	...	...	...	...	150 ± 102	...
NGC 0315	94.0 ± 6.0	331.0 ± 17.0	536.0 ± 48.0	50 ± 20	30 ± 20	...	520 ± 108	...
NGC 0404	135.0 ± 8.0	2919.0 ± 202.0	3499.0 ± 366.0	60 ± 21	80 ± 21	...	...	...
NGC 0410	6.1 ± 0.8	0.0 ± 24.0	0.0 ± 45.0	130 ± 24	150 ± 25	1160 ± 39	1560 ± 118	...
NGC 0474	5.1 ± 2.2	38.2 ± 7.5	107.0 ± 22.0	0 ± 20	120 ± 21	1010 ± 35	1310 ± 87	...
NGC 0507	...	0.0 ± 18.8	0.0 ± 22.1	90 ± 26	10 ± 19	320 ± 34	1440 ± 95	...
NGC 0516	1.2 ± 0.3	...	...	120 ± 16	110 ± 16	120 ± 26	900 ± 104	...
NGC 0526	307.0 ± 28.0	294.0 ± 41.0	...	260 ± 18	220 ± 16	580 ± 28	650 ± 90	...
NGC 0533	7.2 ± 3.1	24.8 ± 4.9	28.7 ± 5.6	0 ± 27	110 ± 33	...	960 ± 231	...
NGC 0584	48.5 ± 7.6	52.3 ± 6.9	0.0 ± 18.9	240 ± 34	680 ± 43	3580 ± 247	760 ± 1414	...
NGC 0596	16.2 ± 4.6	22.5 ± 5.1	18.4 ± 7.3	0 ± 23	...	170 ± 48	1240 ± 285	...
NGC 0636	10.5 ± 3.6	0.0 ± 17.2	0.0 ± 26.9	210 ± 35	130 ± 27	150 ± 54	1910 ± 335	...
NGC 0720	26.1 ± 5.1	19.2 ± 4.9	0.0 ± 23.1	20 ± 15	10 ± 16	...	250 ± 172	...
NGC 0777	8.2 ± 2.7	6.3 ± 2.8	0.0 ± 18.4	120 ± 24	20 ± 31	350 ± 47	1530 ± 229	...
NGC 0807	59.9 ± 3.2	198.0 ± 9.0	2233.0 ± 235.0	140 ± 20	50 ± 24	340 ± 43	1190 ± 158	...
NGC 0814	697.0 ± 42.0	3007.0 ± 265.0	1952.0 ± 182.0	150 ± 28	30 ± 39	40 ± 41	260 ± 122	...
NGC 0821	15.4 ± 4.8	0.0 ± 16.3	0.0 ± 27.3	110 ± 48	40 ± 33	570 ± 54	1490 ± 572	...
NGC 0855	87.8 ± 8.5	1700.0 ± 136.0	2486.0 ± 246.0	260 ± 27	...	400 ± 43	1300 ± 150	...
NGC 1016	5.1 ± 2.9	0.0 ± 15.4	0.0 ± 28.5	120 ± 30	...	20 ± 48	10 ± 156	...
NGC 1023	60.1 ± 5.6	0.0 ± 29.6	0.0 ± 34.8	390 ± 29	...	480 ± 39	1860 ± 184	...
NGC 1199	10.5 ± 1.2	88.0 ± 13.0	...	...	100 ± 27	...	290 ± 234	...
NGC 1266	872.0 ± 32.0	12690.0 ± 535.0	10300.0 ± 843.0	...	40 ± 40	320 ± 35	200 ± 118	...
NGC 1316	430.0 ± 21.0	5440.0 ± 312.0	12610.0 ± 886.0	210 ± 26	160 ± 43	1960 ± 51	3690 ± 116	...
NGC 1374	9.2 ± 1.4	0.0 ± 18.5	0.0 ± 28.0	...	...	230 ± 46	500 ± 240	...
NGC 1377	1835.0 ± 84.0	6350.0 ± 371.0	3380.0 ± 248.0	600 ± 35	80 ± 42	90 ± 51	710 ± 242	...
NGC 1386	1211.0 ± 66.0	6900.0 ± 412.0	...	360 ± 34	830 ± 43	5610 ± 89	7120 ± 680	...
NGC 1395	46.4 ± 6.5	135.0 ± 11.0	213.0 ± 14.0	...	100 ± 57	230 ± 44	610 ± 97	...
NGC 1399	61.9 ± 7.3	16.4 ± 7.6	26.5 ± 8.6	830 ± 30	1540 ± 54	7640 ± 43	15070 ± 116	...
NGC 1404	56.6 ± 6.3	32.6 ± 6.3	0.0 ± 32.2	60 ± 30	480 ± 45	2530 ± 44	3180 ± 105	...
NGC 1407	43.4 ± 6.4	0.0 ± 21.1	0.0 ± 38.9	180 ± 41	40 ± 58	70 ± 59	870 ± 129	...
NGC 1426	8.3 ± 2.1	0.0 ± 14.4	0.0 ± 21.4	60 ± 51	...	...	...	...
NGC 1427	9.5 ± 1.4	27.3 ± 1.1	0.0 ± 13.3	160 ± 32	110 ± 118	90 ± 49	190 ± 153	...
NGC 1439	8.2 ± 0.8	72.0 ± 6.2	37.5 ± 8.0	...	...	...	...	...
NGC 1510	126.0 ± 13.0	862.0 ± 35.0	1237.0 ± 103.0	...	...	...	...	...
NGC 1522	88.0 ± 4.0	924.0 ± 63.0	749.0 ± 66.0	340 ± 25	910 ± 22	2080 ± 50	2920 ± 293	...

Table 3
(Continued)

Name	$24_{\mu m}$ (mJy)	$70_{\mu m}$ (mJy)	$160_{\mu m}$ (mJy)	$I12_{\mu m}$ (mJy)	$I25_{\mu m}$ (mJy)	$I60_{\mu m}$ (mJy)	$I100_{\mu m}$ (mJy)	Hα (erg s^{-1} cm^{-2})
NGC 1533	15.8 ± 2.3	374.0 ± 18.0	...	...	...	...	...	...
NGC 1543	18.2 ± 2.9	...	...	80 ± 28	...	...	...	...
NGC 1553	86.7 ± 8.9	527.0 ± 24.0	322.0 ± 21.0	200 ± 32	250 ± 36	110 ± 48	...	...
NGC 1700	19.0 ± 4.9	30.4 ± 5.3	44.1 ± 7.2	1690 ± 68	2150 ± 62	20550 ± 59	35050 ± 142	...
NGC 2110	641.0 ± 32.0	4966.0 ± 422.0	...	...	...	...	...	...
NGC 2300	13.3 ± 2.1	...	...	...	...	...	...	...
NGC 2325	27.5 ± 4.4	38.3 ± 6.8	23.9 ± 6.4	50 ± 45	40 ± 26	...	210 ± 103	...
NGC 2434	11.3 ± 0.4	47.3 ± 6.9	0.0 ± 16.8	220 ± 65	260 ± 72	...	...	...
NGC 2685	...	...	...	140 ± 32	...	...	...	...
NGC 2768	47.5 ± 5.2	728.0 ± 26.0	414.0 ± 29.0	150 ± 35	210 ± 49	1680 ± 44	2790 ± 150	...
NGC 2778	4.1 ± 1.3	0.0 ± 18.4	0.0 ± 28.2	70 ± 24	120 ± 28	1180 ± 33	2240 ± 135	...
NGC 2787	36.0 ± 5.0	1017.0 ± 46.0	705.0 ± 48.0	190 ± 36	40 ± 42	...	250 ± 356	...
NGC 2832	3.5 ± 0.5	0.0 ± 21.0	0.0 ± 38.0	...	...	...	...	...
NGC 2970	1.3 ± 0.2	...	...	80 ± 22	10 ± 20	350 ± 47	1550 ± 320	106.07 ± 5.51
NGC 2974	63.7 ± 4.4	716.0 ± 48.0	2076.0 ± 154.0	60 ± 35	0 ± 74	100 ± 55	1000 ± 224	...
NGC 2986	13.9 ± 3.8	0.0 ± 9.8	0.0 ± 18.5	130 ± 19	200 ± 30	...	...	...
NGC 3011	19.2 ± 3.2	...	...	50 ± 45	140 ± 75	240 ± 49	350 ± 174	1567.43 ± 21.48
NGC 3032	151.0 ± 8.0	2772.0 ± 184.0	3044.0 ± 273.0	...	...	...	...	...
NGC 3073	9.4 ± 1.5	218.0 ± 8.0	515.0 ± 42.0	180 ± 31	160 ± 25	610 ± 47	570 ± 229	645.78 ± 9.30
NGC 3115	97.0 ± 4.0	52.0 ± 4.0	0.0 ± 45.0	...	...	...	...	...
NGC 3125	636.0 ± 32.0	4714.0 ± 273.0	4337.0 ± 327.0	70 ± 20	140 ± 31	1350 ± 97	2300 ± 277	...
NGC 3156	16.7 ± 4.2	254.0 ± 18.0	203.0 ± 21.0	80 ± 40	50 ± 50	110 ± 68	810 ± 295	545.61 ± 14.83
NGC 3226	26.9 ± 3.2	327.0 ± 14.0	...	230 ± 77	150 ± 42	600 ± 49	1870 ± 140	...
NGC 3265	292.0 ± 17.0	2719.0 ± 144.0	2692.0 ± 159.0	...	240 ± 55	140 ± 57	540 ± 220	12125.80 ± 101.61
NGC 3377	17.6 ± 5.4	84.6 ± 5.7	77.7 ± 9.2	100 ± 58	240 ± 60	220 ± 44	450 ± 210	...
NGC 3379	66.8 ± 8.8	63.5 ± 8.0	65.2 ± 8.2	30 ± 27	20 ± 54	310 ± 66	920 ± 324	...
NGC 3384	61.3 ± 7.8	44.6 ± 17.2	...	230 ± 39	90 ± 35	730 ± 51	1760 ± 148	...
NGC 3412	14.9 ± 1.9	0.0 ± 18.0	0.0 ± 24.0	50 ± 19	130 ± 19	...	200 ± 119	...
NGC 3489	91.6 ± 6.7	1756.0 ± 78.0	2814.0 ± 128.0	20 ± 28	60 ± 44	...	...	...
NGC 3516	712.0 ± 32.0	...	...	170 ± 46	200 ± 38	480 ± 44	2050 ± 113	...
NGC 3522	1.7 ± 0.3	...	...	0 ± 43	120 ± 40	410 ± 52	1030 ± 142	446.04 ± 19.25
NGC 3557	30.6 ± 4.5	276.0 ± 19.0	271.0 ± 28.0	40 ± 36	80 ± 55	...	...	...
NGC 3585	37.2 ± 3.8	80.2 ± 5.2	38.2 ± 8.2	240 ± 31	30 ± 78	...	...	...
NGC 3593	1497.0 ± 110.0	19400.0 ± 88.0	...	150 ± 38	40 ± 60	140 ± 49	1480 ± 169	...
NGC 3607	84.9 ± 6.7	1761.0 ± 98.0	2215.0 ± 186.0	330 ± 41	...	670 ± 62	870 ± 241	...
NGC 3608	18.7 ± 4.2	69.5 ± 8.2	103.0 ± 21.0	130 ± 31	70 ± 58	490 ± 58	2070 ± 239	...
NGC 3610	18.4 ± 4.5	21.1 ± 7.3	36.5 ± 16.5	...	40 ± 43	...	...	...
NGC 3640	19.6 ± 1.6	0.0 ± 18.3	0.0 ± 26.8	160 ± 29	670 ± 51	...	...	...
NGC 3706	16.5 ± 4.4	0.0 ± 18.6	0.0 ± 22.3	150 ± 19	130 ± 23	80 ± 33	760 ± 158	...
NGC 3773	139.0 ± 9.0	1591.0 ± 183.0	2379.0 ± 232.0	60 ± 86	...	...	...	...
NGC 3870	92.1 ± 5.1	...	...	50 ± 39	...	300 ± 51	760 ± 163	9116.76 ± 74.08
NGC 3923	43.7 ± 6.7	23.8 ± 5.4	48.4 ± 7.8	...	...	30 ± 50	70 ± 122	...
NGC 3941	23.3 ± 3.1	...	...	...	...	...	140 ± 152	...
NGC 3945	39.9 ± 4.1	284.0 ± 19.0	2836.0 ± 216.0	90 ± 37	100 ± 59	2410 ± 70	9520 ± 189	...
NGC 3962	21.8 ± 5.6	392.0 ± 18.0	544.0 ± 24.0	0 ± 39	...	...	...	...
NGC 4026	23.7 ± 3.0	141.0 ± 13.0	106.0 ± 23.0	110 ± 28	...	...	...	...
NGC 4073	5.3 ± 3.0	0.0 ± 17.7	0.0 ± 22.6	880 ± 36	290 ± 68	2260 ± 71	5010 ± 307	51.83 ± 34.01
NGC 4117	31.4 ± 3.4	...	...	20 ± 58	...	3600 ± 66	6210 ± 462	2442.03 ± 27.28
NGC 4125	74.7 ± 6.9	1105.0 ± 98.0	1735.0 ± 187.0	40 ± 36	...	...	...	...
NGC 4138	167.0 ± 16.0	2505.0 ± 162.0	6144.0 ± 642.0	390 ± 31	680 ± 66	...	...	...
NGC 4150	69.3 ± 8.0	1522.0 ± 121.0	1720.0 ± 168.0	270 ± 44	340 ± 57	90 ± 83	240 ± 222	...
NGC 4168	5.2 ± 1.3	0.0 ± 15.0	0.0 ± 26.0	...	100 ± 56	30 ± 45	580 ± 216	273.94 ± 22.91
NGC 4203	43.3 ± 3.5	933.0 ± 111.0	2701.0 ± 259.0	280 ± 54	200 ± 50	720 ± 52	1290 ± 148	...
NGC 4251	17.3 ± 2.4	...	...	130 ± 35	60 ± 57	420 ± 63	260 ± 141	...
NGC 4261	51.5 ± 3.2	127.0 ± 11.0	375.0 ± 18.0	20 ± 45	430 ± 67	...	...	...
NGC 4267	11.7 ± 0.3	0.0 ± 16.9	0.0 ± 20.9	...	230 ± 69	...	...	...
NGC 4278	44.7 ± 12.7	829.0 ± 68.0	1491.0 ± 128.0	80 ± 29	...	...	80 ± 297	...
NGC 4291	...	0.0 ± 18.0	...	30 ± 29	...	...	...	...
NGC 4308	1.5 ± 0.3	...	...	440 ± 34	200 ± 61	510 ± 42	0 ± 198	51.31 ± 6.62
NGC 4344	40.2 ± 4.5	779.0 ± 62.0	1986.0 ± 226.0	...	...	...	...	31.41 ± 2.78
NGC 4350	29.8 ± 3.3	474.0 ± 32.0	1168.0 ± 112.0	130 ± 32	280 ± 41	310 ± 43	340 ± 145	...
NGC 4352	1.7 ± 0.3	...	...	260 ± 33	...	140 ± 47	610 ± 150	58.63 ± 7.16
NGC 4365	22.2 ± 4.7	67.0 ± 8.0	58.2 ± 7.3	550 ± 449	500 ± 203	6460 ± 72	15390 ± 167	...
NGC 4371	13.6 ± 0.7	24.5 ± 2.7	14.1 ± 7.0	230 ± 29	...	210 ± 58	1150 ± 317	...
NGC 4374	66.6 ± 8.6	617.0 ± 41.0	535.0 ± 61.0	200 ± 36	130 ± 55	300 ± 54	870 ± 306	...

Table 3
(Continued)

Name	$24_{\mu m}$ (mJy)	$70_{\mu m}$ (mJy)	$160_{\mu m}$ (mJy)	$I12_{\mu m}$ (mJy)	$I25_{\mu m}$ (mJy)	$I60_{\mu m}$ (mJy)	$I100_{\mu m}$ (mJy)	Hα (erg s^{-1} cm^{-2})
NGC 4377	3.2 ± 0.3	...	...	20 ± 34	10 ± 51	...	420 ± 265	...
NGC 4379	4.3 ± 0.3	...	...	40 ± 32	10 ± 54	...	...	...
NGC 4382	52.4 ± 6.7	23.6 ± 6.5	24.7 ± 9.0	10 ± 44	0 ± 47	...	500 ± 141	...
NGC 4386	...	178.0 ± 14.0	...	0 ± 22	50 ± 28	120 ± 47	...	...
NGC 4406	27.5 ± 3.2	64.0 ± 8.0	90.0 ± 12.0	...	100 ± 56	20 ± 51	...	...
NGC 4417	8.8 ± 1.2	...	...	170 ± 32	380 ± 55	340 ± 50	1510 ± 203	...
NGC 4421	3.3 ± 0.4	0.0 ± 25.0	0.0 ± 30.0	120 ± 41	...	270 ± 44	30 ± 102	100.24 ± 11.42
NGC 4434	4.8 ± 0.9	...	...	30 ± 39	260 ± 61	330 ± 52	270 ± 161	...
NGC 4435	111.0 ± 10.2	2210.0 ± 186.0	3022.0 ± 327.0	130 ± 34	...	...	...	...
NGC 4442	20.2 ± 2.2	...	...	640 ± 28	1030 ± 63	3520 ± 59	10580 ± 218	...
NGC 4458	3.3 ± 1.1	0.0 ± 18.5	0.0 ± 23.8	200 ± 43	...	90 ± 159	340 ± 505	...
NGC 4459	107.0 ± 8.0	2400.0 ± 175.0	3461.0 ± 431.0	80 ± 33	210 ± 54	1250 ± 111	1130 ± 696	...
NGC 4460	274.0 ± 31.0	4413.0 ± 389.0	4488.0 ± 461.0	150 ± 31	50 ± 31	190 ± 43	1120 ± 265	...
NGC 4464	2.0 ± 0.3	...	...	230 ± 36	540 ± 54	620 ± 55	640 ± 264	...
NGC 4472	74.7 ± 8.6	61.1 ± 7.6	66.4 ± 7.8	70 ± 29	...	80 ± 80	2580 ± 703	...
NGC 4473	26.3 ± 6.7	0.0 ± 18.0	0.0 ± 25.5	...	40 ± 49	...	...	...
NGC 4474	5.4 ± 0.8	...	...	340 ± 40	...	100 ± 58	670 ± 311	...
NGC 4476	35.7 ± 4.1	528.0 ± 89.0	1323.0 ± 135.0	140 ± 31	220 ± 50	390 ± 163	410 ± 595	289.65 ± 11.54
NGC 4477	39.0 ± 0.8	507.0 ± 12.0	514.0 ± 29.0	150 ± 32	...	...	...	...
NGC 4478	12.6 ± 3.9	0.0 ± 17.9	0.0 ± 23.7	200 ± 29	...	400 ± 182	1410 ± 779	...
NGC 4479	1.2 ± 0.3	...	...	110 ± 35	...	1150 ± 62	2730 ± 224	31.18 ± 4.45
NGC 4482	0.3 ± 0.2	...	...	90 ± 43	480 ± 84	...	...	14.60 ± 2.93
NGC 4483	3.0 ± 0.3	...	...	140 ± 30	100 ± 58	50 ± 51	400 ± 171	86.30 ± 14.41
NGC 4486	154.0 ± 9.0	483.0 ± 44.0	896.0 ± 91.0	210 ± 46	30 ± 85	560 ± 64	4670 ± 174	...
NGC 4489	3.2 ± 0.3	...	...	60 ± 33	...	190 ± 66	...	90.15 ± 11.65
NGC 4494	34.5 ± 4.5	316.0 ± 12.5	235.0 ± 19.6	140 ± 28	310 ± 44	880 ± 40	950 ± 168	...
NGC 4515	1.9 ± 0.2	...	...	110 ± 22	180 ± 22	450 ± 30	640 ± 66	118.99 ± 10.28
NGC 4526	267.0 ± 12.0	8134.0 ± 632.0	13710.0 ± 1267.0	140 ± 39	430 ± 61	360 ± 50	810 ± 179	...
NGC 4528	4.4 ± 0.7	...	...	220 ± 34	370 ± 33	530 ± 61	2480 ± 142	...
NGC 4552	58.5 ± 7.8	96.3 ± 10.2	188.0 ± 16.0	220 ± 28	...	60 ± 56	260 ± 226	...
NGC 4564	23.9 ± 3.7	...	...	80 ± 21	120 ± 19	450 ± 42	1180 ± 221	...
NGC 4570	18.7 ± 6.0	0.0 ± 23.3	0.0 ± 29.6	70 ± 60	...	...	430 ± 119	...
NGC 4578	5.2 ± 0.9	0.0 ± 19.0	0.0 ± 26.0	40 ± 44	90 ± 48	50 ± 100	1160 ± 513	...
NGC 4589	15.3 ± 4.5	275.0 ± 16.0	396.0 ± 21.0	100 ± 27	170 ± 29	90 ± 43	440 ± 143	...
NGC 4612	6.0 ± 0.8	...	...	230 ± 32	50 ± 44	270 ± 39	630 ± 112	...
NGC 4621	34.9 ± 6.3	33.7 ± 5.7	47.4 ± 6.6	50 ± 30	20 ± 43	190 ± 43	880 ± 163	...
NGC 4623	1.8 ± 0.2	...	...	10 ± 28	...	20 ± 50	...	...
NGC 4636	31.8 ± 5.6	197.0 ± 12.0	185.0 ± 24.0	160 ± 25	100 ± 38	30 ± 40	...	...
NGC 4638	12.7 ± 0.1	4.3 ± 1.1	0.8 ± 1.3	340 ± 19	340 ± 15	5700 ± 28	16170 ± 73	...
NGC 4649	108.0 ± 10.0	48.6 ± 6.8	0.0 ± 30.4	80 ± 20	10 ± 19	100 ± 37	...	...
NGC 4660	15.5 ± 4.3	38.3 ± 6.2	59.1 ± 8.2	30 ± 20	...	620 ± 63	2940 ± 323	...
NGC 4694	110.0 ± 9.0	1545.0 ± 112.0	3278.0 ± 334.0	60 ± 26	...	0 ± 45	340 ± 293	...
NGC 4696	23.4 ± 4.7	133.0 ± 13.0	295.0 ± 21.0	30 ± 27	20 ± 30	130 ± 136	2280 ± 936	...
NGC 4697	44.7 ± 6.7	618.0 ± 55.0	830.0 ± 68.0	...	...	310 ± 74	...	...
NGC 4709	8.2 ± 0.2	0.0 ± 15.5	0.0 ± 27.0	70 ± 36	40 ± 48	10 ± 55	600 ± 231	...
NGC 4754	17.1 ± 2.9	0.0 ± 12.2	0.0 ± 22.2	160 ± 38	100 ± 50	450 ± 52	660 ± 180	...
NGC 4762	39.1 ± 6.5	12.1 ± 2.6	0.0 ± 24.2	280 ± 46	390 ± 72	3350 ± 708	11680 ± 2656	...
NGC 4786	25.3 ± 1.2	303.0 ± 26.0	161.0 ± 19.0	740 ± 72	340 ± 80	...	...	...
NGC 4915	11.7 ± 5.5	30.6 ± 4.8	59.7 ± 8.9	40 ± 31	280 ± 36	10 ± 56	760 ± 405	...
NGC 4936	21.7 ± 0.9	465.0 ± 45.0	894.0 ± 76.0	10 ± 45	340 ± 133	150 ± 89	...	...
NGC 5018	61.7 ± 9.1	1174.0 ± 134.0	1855.0 ± 241.0	...	...	...	...	...
NGC 5044	23.5 ± 5.3	241.0 ± 23.0	266.0 ± 28.0	120 ± 42	...	140 ± 50	690 ± 239	...
NGC 5061	32.8 ± 0.5	18.2 ± 5.2	0.0 ± 23.5	20 ± 35	250 ± 109	...	...	...
NGC 5077	33.2 ± 5.7	133.0 ± 11.0	155.0 ± 18.0	70 ± 20	...	10 ± 33	460 ± 156	...
NGC 5173	21.1 ± 1.5	...	...	160 ± 26	120 ± 38	360 ± 49	490 ± 220	1572.38 ± 29.91
NGC 5273	83.1 ± 4.5	657.0 ± 44.0	836.0 ± 79.0	40 ± 29	30 ± 59	110 ± 72	900 ± 430	4263.61 ± 44.94
NGC 5322	42.2 ± 6.4	477.0 ± 23.0	687.0 ± 77.0	...	330 ± 49	...	220 ± 243	...
NGC 5338	35.2 ± 5.0	...	...	...	190 ± 48	110 ± 48	210 ± 144	2388.48 ± 25.11
NGC 5353	24.7 ± 3.3	492.0 ± 38.0	490.0 ± 52.0	...	...	20 ± 47	400 ± 129	...
NGC 5419	12.9 ± 0.1	0.0 ± 18.3	0.0 ± 21.7	220 ± 32	...	740 ± 47	3460 ± 217	...
NGC 5481	1.8 ± 0.3	10.2 ± 3.4	0.0 ± 22.0	530 ± 49	430 ± 60	160 ± 55	210 ± 192	...
NGC 5557	13.4 ± 5.0	26.4 ± 7.5	0.0 ± 46.0	40 ± 31	...	...	...	...
NGC 5576	16.5 ± 4.2	0.0 ± 12.7	0.0 ± 19.8	...	40 ± 54	...	440 ± 313	...
NGC 5596	6.5 ± 0.5	...	...	90 ± 34	400 ± 64	40 ± 61	700 ± 235	321.03 ± 15.84
NGC 5813	15.3 ± 4.9	61.3 ± 7.6	38.3 ± 5.9	...	140 ± 62	...	810 ± 378	...

Table 3
(Continued)

Name	$24_{\mu m}$ (mJy)	$70_{\mu m}$ (mJy)	$160_{\mu m}$ (mJy)	$I12_{\mu m}$ (mJy)	$I25_{\mu m}$ (mJy)	$I60_{\mu m}$ (mJy)	$I100_{\mu m}$ (mJy)	Hα (erg s^{-1} cm^{-2})
NGC 5831	14.8 ± 4.6	0.0 ± 18.8	0.0 ± 24.6	40 ± 36	860 ± 93	...	...	209.85 ± 73.30
NGC 5845	7.8 ± 3.2	108.0 ± 12.0	169.0 ± 23.0	110 ± 49	350 ± 55	...	...	...
NGC 5846	39.3 ± 6.2	107.0 ± 10.0	129.0 ± 12.0	10 ± 36	200 ± 74	170 ± 55	230 ± 264	298.25 ± 12.67
NGC 5866	194.0 ± 7.1	8753.0 ± 605.0	17540.0 ± 1297.0	...	160 ± 49	210 ± 39	230 ± 179	...
NGC 5982	13.8 ± 5.1	39.0 ± 7.2	65.8 ± 11.7	210 ± 43	...	...	430 ± 142	...
NGC 6482	9.5 ± 0.8	33.6 ± 12.1	0.0 ± 45.2	80 ± 33	220 ± 72	220 ± 47	770 ± 192	...
NGC 6684	17.7 ± 2.0	...	...	...	...	...	0 ± 170	...
NGC 6703	20.3 ± 4.5	43.5 ± 6.4	21.7 ± 5.1	20 ± 30	...	0 ± 54	170 ± 209	...
NGC 6776	16.4 ± 1.3	126.0 ± 12.0	58.1 ± 19.3	...	0 ± 59	200 ± 57	470 ± 286	...
NGC 6849	3.3 ± 0.1	0.0 ± 12.6	0.0 ± 19.8	10 ± 37	260 ± 56	...	50 ± 157	...
NGC 7077	28.7 ± 3.1	411.0 ± 37.0	452.0 ± 42.0	90 ± 44	60 ± 60	...	640 ± 263	...
NGC 7176	2.6 ± 0.4	...	...	210 ± 29	380 ± 46	120 ± 93	...	...
NGC 7360	9.6 ± 0.6	...	...	1230 ± 26	4110 ± 35	5740 ± 146	1870 ± 561	...
NGC 7457	8.4 ± 2.5	0.0 ± 25.9	0.0 ± 33.5	660 ± 29	2460 ± 32	2730 ± 44	1480 ± 187	...
NGC 7619	10.2 ± 4.7	0.0 ± 13.7	0.0 ± 23.5	410 ± 28	1870 ± 27	4790 ± 74	3980 ± 601	...
NGC 7626	12.4 ± 3.6	18.0 ± 0.3	0.0 ± 25.3	110 ± 25	...	150 ± 48	...	...
NGC 7785	8.2 ± 0.7	18.0 ± 0.9	0.0 ± 19.0	20 ± 24	70 ± 25	610 ± 40	1410 ± 131	...
UGC01503	39.6 ± 1.8	362.0 ± 66.0	1384.0 ± 139.0	110 ± 32	100 ± 33	690 ± 43	1620 ± 140	...
UGC06570	266.0 ± 33.0	...	...	140 ± 54	640 ± 84	1960 ± 131	2510 ± 210	8164.21 ± 64.04
UGC06637	18.0 ± 2.3	...	...	...	...	...	...	497.72 ± 7.42
UGC06655	18.4 ± 6.0	...	...	40 ± 32	450 ± 54	1650 ± 56	1540 ± 188	4977.99 ± 41.40
UGC06805	42.0 ± 3.6	...	...	40 ± 22	10 ± 36	350 ± 32	690 ± 119	7902.42 ± 63.48
UGC07436	0.0 ± 1.0	...	...	...	...	...	340 ± 141	5.34 ± 1.72
UGC07580	0.0 ± 0.1	...	...	70 ± 40	370 ± 67	10 ± 53	100 ± 152	1.49 ± 6.74
UGC07854	0.0 ± 0.1	...	...	...	...	60 ± 52	...	2.90 ± 1.59
UGC08876	1.5 ± 0.3	...	...	10 ± 30	...	...		274.75 ± 85.49

constrained by the UV, optical, and NIR part of the spectrum via the stellar population synthesis of Maraston (2005). The age$_{D4000}$ is calculated on the unreddened, fitted SED by taking the ratio of the average flux per frequency unit of the wavelength ranges 4000–4100 Å (red continuum) and 3850–3950 Å (blue continuum) and matching this ratio to the age calculated on Maraston models (Maraston 2005). $L_{\rm dust}$ is composed of an AGN contribution fitted with a Siebenmorgen et al. (2004a, 2004b) and a dust component, the dust component part of $L_{\rm dust}$ is constrained by the fitted absorption in UV and optical and the FIR emission consistently. M_* is calculated by integrating over the evolution track of the Maraston (2005) model, and depends primarily on the UV, optical, and NIR part of the spectrum, except for the overall normalization defined by $M_{\rm gal}$. $L_{\rm bol}$ is the total luminosity, and it is computed by integrating the fitted spectrum and therefore depends on the full SED.

Figure 1 shows the SED fit of one elliptical galaxy NGC 4660 and one lenticular galaxy NGC 5273. The red diamonds represent our data points, the black solid line represents the model spectrum, the blue dashed line represents the unabsorbed stellar spectrum, and the orange dot–dashed line represents the dust emission. Modeled spectra are in pretty good agreement with measurements from 1539 Å *GALEX* to 500 μm *Herschel*-SPIRE. Dust absorption and emission are significantly larger in the lenticular galaxy NGC 5273.

Typical constraints provided by CIGALEMC are depicted in Figure 2 (NGC 4660; corresponding SED is at the top of Figure 1). Diagonal elements of this figure show the marginalized (integrated over all the other parameters) probability distribution function (PDF) of each parameter. The off-diagonal elements show the two-dimensional marginalized PDF for pairs of parameters and allow us to quantify the level of degeneracy between pairs of parameters. Parameters age$_{D4000}$, $L_{\rm bol}$, M_*, SFR, and $L_{\rm dust}$ are constrained respectively at the 11%, 14%, 16%, 53%, and 87% level (median of the relative 68% confidence interval). Among these parameters, the correlation is fairly small except for the pair ($L_{\rm bol}$, M_*) because they depend both mostly on the normalization parameter $M_{\rm gal}$.

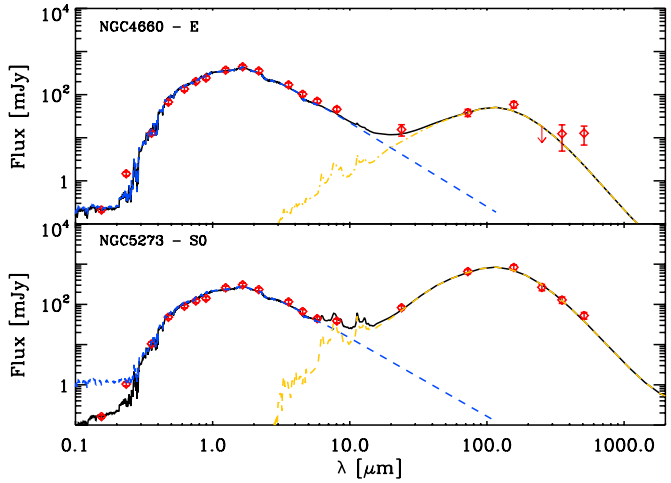

Figure 1. Example of an SED fit performed with CIGALEMC. For each galaxy, the data are two *GALEX*, five SDSS, three 2MASS, four IRAC, three MIPS, and three SPIRE bands. The top panel shows the fit (black solid line) of NGC 4660 (Elliptical galaxy) data (red diamond) with its unabsorbed stellar component (blue dashed line), and the dust emission model (orange dot–dashed line). The bottom panel shows the fit (black solid line) of NGC 5273 (lenticular galaxy) data (red diamond) with its unabsorbed stellar component (blue dashed line).
(A color version of this figure is available in the online journal.)

Out of a sample of 221 galaxies (116 E and 105 S0), our model converges to a solution for 193 galaxies. The reduced χ^2 of the fit is between 0.2 and 42, the overall reduced

Table 4
Herschel SPIRE Fluxes Used in This Work

Name	$250_{\mu m}$ (mJy)	$350_{\mu m}$ (mJy)	$500_{\mu m}$ (mJy)
IC3032	0.0 ± 3.2	0.0 ± 2.9	0.0 ± 2.1
IC3101	0.0 ± 3.4	0.0 ± 2.8	0.0 ± 2.1
IC3328	0.0 ± 3.8	0.0 ± 3.6	0.6 ± 2.6
IC3381	1.1 ± 5.4	0.6 ± 4.8	4.0 ± 3.9
IC3501	0.0 ± 3.7	0.0 ± 3.3	0.0 ± 2.6
IC5063	1723.8 ± 258.7	848.1 ± 134.0	279.4 ± 53.1
NGC 0584	0.8 ± 13.9	6.2 ± 13.4	2.7 ± 9.7
NGC 0855	788.2 ± 118.3	351.6 ± 53.0	139.9 ± 36.7
NGC 1266	3610.5 ± 541.6	1479.6 ± 225.4	415.4 ± 70.3
NGC 1316	3895.5 ± 584.4	1650.4 ± 249.6	502.9 ± 79.5
NGC 1377	945.5 ± 141.9	361.7 ± 54.6	131.4 ± 35.1
NGC 1386	3414.1 ± 512.2	1509.8 ± 229.9	460.8 ± 76.8
NGC 1399	1.5 ± 35.3	17.1 ± 31.6	26.0 ± 4.8
NGC 1404	0.7 ± 13.4	0.0 ± 12.5	0.0 ± 9.3
NGC 3226	381.8 ± 57.5	159.0 ± 24.5	65.1 ± 10.7
NGC 3265	926.6 ± 139.1	399.8 ± 60.2	137.6 ± 21.2
NGC 3608	0.6 ± 10.3	6.2 ± 9.4	6.6 ± 7.8
NGC 3640	0.7 ± 14.8	7.2 ± 14.4	6.1 ± 12.0
NGC 3773	669.0 ± 100.5	286.1 ± 43.3	82.0 ± 13.0
NGC 3941	14.0 ± 16.5	15.6 ± 13.2	5.8 ± 11.0
NGC 3945	1974.2 ± 296.5	899.8 ± 137.8	290.8 ± 48.7
NGC 4125	680.2 ± 102.4	374.8 ± 57.1	185.8 ± 38.5
NGC 4138	3140.3 ± 471.1	1395.4 ± 213.2	463.3 ± 69.5
NGC 4168	0.7 ± 9.3	4.6 ± 7.9	0.0 ± 5.5
NGC 4203	1152.9 ± 173.2	526.1 ± 83.8	191.1 ± 30.4
NGC 4251	0.1 ± 9.1	3.0 ± 8.6	3.2 ± 6.3
NGC 4261	237.4 ± 35.9	309.0 ± 56.9	216.7 ± 33.0
NGC 4267	20.6 ± 3.7	16.6 ± 13.0	7.4 ± 8.8
NGC 4350	246.3 ± 37.0	64.6 ± 10.1	22.2 ± 4.0
NGC 4352	0.5 ± 5.0	11.5 ± 4.9	9.2 ± 3.6
NGC 4365	1.2 ± 23.2	13.5 ± 22.3	15.4 ± 15.3
NGC 4371	0.7 ± 16.2	2.1 ± 13.3	0.0 ± 9.1
NGC 4374	239.3 ± 36.1	146.1 ± 22.4	119.5 ± 18.4
NGC 4377	275.0 ± 41.4	66.3 ± 10.4	28.9 ± 5.0
NGC 4379	0.1 ± 12.4	3.9 ± 11.1	0.0 ± 7.7
NGC 4406	1.0 ± 27.0	6.5 ± 27.0	7.6 ± 20.5
NGC 4417	1.3 ± 9.9	10.2 ± 8.8	7.5 ± 7.0
NGC 4434	0.0 ± 6.4	0.0 ± 5.6	0.0 ± 4.1
NGC 4435	1621.1 ± 243.2	656.5 ± 98.7	186.8 ± 28.4
NGC 4442	0.0 ± 11.1	0.0 ± 11.3	0.0 ± 8.3
NGC 4458	0.0 ± 6.6	0.5 ± 5.8	1.1 ± 4.4
NGC 4459	1451.5 ± 217.8	507.2 ± 76.2	154.3 ± 23.4
NGC 4464	0.7 ± 4.5	2.9 ± 4.0	8.1 ± 3.3
NGC 4472	12.9 ± 44.7	13.4 ± 41.5	11.8 ± 31.6
NGC 4473	0.2 ± 16.2	2.5 ± 13.3	0.0 ± 9.6
NGC 4474	0.1 ± 8.3	0.2 ± 7.1	5.6 ± 4.8
NGC 4476	701.8 ± 105.4	270.4 ± 40.8	83.8 ± 13.1
NGC 4477	414.8 ± 62.4	154.9 ± 23.8	42.2 ± 7.9
NGC 4478	36.6 ± 5.9	29.5 ± 5.2	26.2 ± 4.7
NGC 4479	0.0 ± 6.2	3.4 ± 5.5	3.9 ± 4.6
NGC 4482	0.0 ± 4.3	0.0 ± 4.4	0.8 ± 3.6
NGC 4483	0.0 ± 5.8	0.7 ± 5.1	0.7 ± 3.9
NGC 4486	706.0 ± 106.0	1065.6 ± 163.1	1280.9 ± 194.0
NGC 4494	74.2 ± 11.3	37.4 ± 6.3	13.3 ± 10.8
NGC 4526	7884.3 ± 1183.4	3157.6 ± 475.0	994.8 ± 151.1
NGC 4528	1.4 ± 7.9	8.6 ± 5.7	0.0 ± 5.3
NGC 4552	2.2 ± 27.0	21.4 ± 4.0	18.4 ± 16.9
NGC 4564	0.3 ± 10.5	0.0 ± 9.3	0.0 ± 6.5
NGC 4570	0.1 ± 7.4	0.4 ± 6.6	0.0 ± 4.8
NGC 4578	0.0 ± 10.7	7.4 ± 9.7	5.9 ± 7.3
NGC 4612	0.8 ± 6.8	7.1 ± 6.5	12.4 ± 4.5
NGC 4621	0.5 ± 17.4	0.0 ± 17.8	0.0 ± 15.0
NGC 4636	87.5 ± 13.4	33.3 ± 5.7	11.2 ± 15.8
NGC 4638	0.0 ± 6.4	0.0 ± 6.5	0.0 ± 4.1
NGC 4649	0.1 ± 31.0	0.0 ± 28.5	0.0 ± 19.5
NGC 4660	4.7 ± 7.1	12.4 ± 7.4	12.7 ± 5.8
NGC 4696	112.8 ± 17.1	41.6 ± 6.7	25.2 ± 4.5
NGC 4697	220.1 ± 33.1	65.6 ± 10.2	19.4 ± 17.8
NGC 4754	0.0 ± 14.2	0.6 ± 13.3	0.0 ± 8.6
NGC 4762	1.2 ± 13.8	2.0 ± 14.8	3.0 ± 10.9
NGC 5273	266.2 ± 40.0	129.1 ± 19.7	52.8 ± 8.5
NGC 5576	0.9 ± 9.7	8.4 ± 9.2	1.5 ± 7.2
NGC 5866	7434.1 ± 1115.2	2983.6 ± 449.0	976.0 ± 149.3
UGC07436	0.0 ± 4.5	3.8 ± 3.9	0.0 ± 3.0
UGC07580	18.9 ± 4.4	5.5 ± 3.1	3.9 ± 2.5

Table 5
Parameters Fitted by CIGALEMC to the Galaxy SEDs, with Priors Chosen

Parameters	Priors	Description
τ_{old}	$0 < \tau_{old} < 10$ Gyr	Old star population e-folding time
t_{new}	$0 < t_{new} < 5$ Gyr	Age of the new stellar population
f_{ySP}	$0 < f_{ySP} < 1$	Fraction of young stars
A_{ySP}	$0 < A_{ySP} < 5$ mag	Dust extinction for young stars
f_V	$0 < f_V < 1$	Factor for dust extinction of old stars
α	$0.06 < \alpha < 4$	Slope of the dust mass over heating
f_{AGN}	$0 < f_{AGN} < 1$	AGN fraction of the dust luminosity
M_{gal}	$6 < M_{gal} < 13$	Logarithm of the galaxy mass

χ^2 is well fitted by a Gaussian distribution centered on 2.5 with a standard deviation of 4.5. We decide to reduce the sample by removing 38 poorly fitted galaxies (reduced $\chi^2 > 10$). Finally, in order to include only strongly constrained galaxies, we select the sub-sample where the galaxy mass is constrained by better than a factor 10 at 68% confidence level; this removes 12 additional galaxies. We check that this last cut does not bias the selection by selecting only massive galaxies. Our reduced sample is composed of 75 elliptical galaxies (type < -3) and 68 lenticular galaxies (type > -3), with a respective average reduced χ^2 of 4.7 ± 2.6 and 3.9 ± 2.4. On average, lenticular galaxies are a better fit to our model.

To check our CIGALEMC estimate of SFR in our galaxy sample, we use the SFR estimate at 24 μm of Calzetti et al. (2007):

$$\mathrm{SFR}(M_\odot\ \mathrm{yr}^{-1}) = 1.27 \times 10^{-38}\ [L_{24\,\mu m}(\mathrm{erg\ s}^{-1})]^{0.8850}. \quad (1)$$

We find a good agreement with the 143 galaxies for which we obtain a SFR as indicated by Figure 3 (left).

Given that CIGALEMC SFR is constrained by the UV/optical/NIR part of the SED, the agreement with the 24 μm estimate gives us good confidence in CIGALEMC SFR estimates. Using DR9 SDSS spectrometric measurements of Hα obtained for 50 of our galaxies, we use Calzetti et al. (2007) relation between the Hα flux and SFR to compare with the CIGALEMC SFR estimate:

$$\mathrm{SFR}(M_\odot\ \mathrm{yr}^{-1}) = 5.3 \times 10^{-42} L(\mathrm{H}\alpha)(\mathrm{erg\ s}^{-1}). \quad (2)$$

Using Hα to estimate the SFR, we see a large difference with our estimate (blue dashed line on the right Figure 3 compared to the data points), the Hα SFR estimate is about a factor 10 time smaller than our SED SFR estimate. Calzetti et al. (2007) proposed to add a correction with the 24 μm luminosity (5.3×10^{-42} 0.031 $L_{24\,\mu m}$) but this correction is larger than

Table 6
Parameters Fitted by CIGALEMC Using *GALEX*, SDSS, 2MASS, IRAC, and MIPS Data When Available

Name	Log(f_{ysp})	Log(M_{gal}) ($M_\odot$)	Log($M_\star$) ($M_\odot$)	Log(SFR) ($M_\odot$ yr^{-1})	t_{D4000} (Gyr)	Log(L_{bol}) ($L_\odot$)	Log(L_d) ($L_\odot$)
Eso462-15	-3.25 ± 0.83	11.65 ± 0.89	11.51 ± 0.89	-1.01 ± 0.28	9.27 ± 2.53	11.09 ± 0.61	8.66 ± 0.40
Eso483-13	-1.23 ± 0.57	9.10 ± 0.18	8.97 ± 0.18	-1.22 ± 0.09	0.59 ± 0.20	9.00 ± 0.07	8.04 ± 0.15
IC0798	-4.53 ± 0.93	9.63 ± 0.06	9.49 ± 0.06	-3.19 ± 0.64	9.09 ± 0.94	9.02 ± 0.06	6.41 ± 0.55
IC1144	-0.46 ± 0.45	7.77 ± 0.96	7.64 ± 0.96	-1.94 ± 0.94	0.37 ± 0.38	8.35 ± 0.84	8.24 ± 0.88
IC1459	-2.52 ± 1.05	11.04 ± 1.05	10.90 ± 1.04	-0.92 ± 0.22	7.39 ± 3.60	10.61 ± 0.66	8.87 ± 0.15
IC1639	-3.01 ± 0.42	11.09 ± 0.06	10.94 ± 0.06	-1.32 ± 0.23	8.91 ± 0.91	10.47 ± 0.05	8.53 ± 0.38
IC3328	-0.65 ± 0.55	6.44 ± 0.33	6.31 ± 0.33	-3.55 ± 0.40	0.53 ± 0.65	6.62 ± 0.29	6.48 ± 0.33
IC3370	-1.16 ± 0.72	11.40 ± 0.20	11.27 ± 0.19	1.04 ± 0.44	1.16 ± 1.52	11.32 ± 0.16	9.32 ± 0.20
IC3381	-3.63 ± 0.46	9.14 ± 0.06	8.99 ± 0.06	-3.91 ± 0.34	9.99 ± 0.44	8.51 ± 0.06	5.48 ± 0.54
IC3383	-3.23 ± 0.55	9.61 ± 0.07	9.46 ± 0.07	-3.03 ± 0.42	9.35 ± 0.85	8.98 ± 0.07	6.19 ± 0.56
IC3461	-2.77 ± 0.45	9.13 ± 0.06	8.99 ± 0.06	-2.98 ± 0.19	7.81 ± 1.07	8.53 ± 0.06	5.66 ± 0.57
IC3468	-2.36 ± 0.53	9.73 ± 0.07	9.59 ± 0.07	-1.89 ± 0.23	5.31 ± 1.28	9.17 ± 0.06	5.63 ± 0.59
IC3470	-3.02 ± 0.42	9.83 ± 0.06	9.68 ± 0.06	-2.57 ± 0.18	8.89 ± 0.79	9.21 ± 0.05	5.81 ± 0.57
IC3487	-3.34 ± 0.92	8.86 ± 0.88	8.71 ± 0.87	-3.97 ± 0.41	9.23 ± 2.93	8.28 ± 0.69	5.92 ± 0.46
IC3501	-3.90 ± 1.75	8.95 ± 1.24	8.81 ± 1.23	-3.56 ± 0.39	8.16 ± 3.67	8.48 ± 0.92	6.03 ± 0.68
IC3586	-2.92 ± 0.60	9.53 ± 0.07	9.38 ± 0.07	-2.82 ± 0.47	8.46 ± 1.64	8.92 ± 0.06	7.25 ± 0.53
IC3602	-3.21 ± 0.52	9.15 ± 0.06	9.00 ± 0.06	-3.47 ± 0.39	9.36 ± 0.89	8.53 ± 0.06	6.59 ± 0.43
IC3633	-3.27 ± 0.49	9.36 ± 0.07	9.22 ± 0.07	-3.28 ± 0.34	9.41 ± 0.77	8.74 ± 0.07	6.39 ± 0.55
IC3652	-3.52 ± 0.46	9.09 ± 0.06	8.94 ± 0.06	-3.83 ± 0.30	9.90 ± 0.48	8.46 ± 0.06	5.11 ± 0.60
IC3653	-3.50 ± 0.43	9.15 ± 0.06	9.01 ± 0.06	-3.76 ± 0.22	9.93 ± 0.45	8.52 ± 0.05	5.55 ± 0.54
IC3773	-3.25 ± 0.42	9.64 ± 0.06	9.50 ± 0.06	-3.03 ± 0.24	9.59 ± 0.56	9.02 ± 0.06	5.56 ± 0.58
IC3779	-3.52 ± 0.44	9.06 ± 0.07	8.92 ± 0.07	-3.87 ± 0.28	9.90 ± 0.45	8.43 ± 0.06	5.84 ± 0.58
IC4296	-3.27 ± 0.38	11.87 ± 0.07	11.72 ± 0.07	-0.80 ± 0.16	9.63 ± 0.48	11.25 ± 0.07	8.85 ± 0.29
IC4329	-3.28 ± 0.37	11.93 ± 0.06	11.79 ± 0.06	-0.76 ± 0.14	9.71 ± 0.44	11.31 ± 0.06	8.14 ± 0.50
IC5063	-1.41 ± 0.52	11.28 ± 0.18	11.14 ± 0.18	0.51 ± 0.23	1.65 ± 1.18	11.05 ± 0.06	10.80 ± 0.09
NGC 0315	-2.87 ± 0.42	11.84 ± 0.07	11.69 ± 0.07	-0.47 ± 0.26	8.65 ± 1.06	11.22 ± 0.06	9.79 ± 0.14
NGC 0404	-3.90 ± 1.08	9.77 ± 0.08	9.63 ± 0.08	-2.52 ± 0.27	8.03 ± 0.99	9.18 ± 0.07	7.69 ± 0.22
NGC 0410	-3.22 ± 0.39	11.84 ± 0.06	11.69 ± 0.06	-0.80 ± 0.18	9.61 ± 0.50	11.21 ± 0.05	8.40 ± 0.48
NGC 0474	-3.35 ± 0.40	11.09 ± 0.06	10.94 ± 0.06	-1.68 ± 0.23	9.76 ± 0.49	10.46 ± 0.06	8.06 ± 0.37
NGC 0507	-3.10 ± 0.38	11.75 ± 0.06	11.61 ± 0.06	-0.77 ± 0.18	9.43 ± 0.60	11.13 ± 0.06	8.90 ± 0.52
NGC 0516	-0.54 ± 0.51	6.93 ± 0.65	6.80 ± 0.64	-2.90 ± 0.62	0.46 ± 0.63	7.34 ± 0.53	7.21 ± 0.56
NGC 0533	-3.10 ± 0.41	11.80 ± 0.07	11.65 ± 0.07	-0.70 ± 0.18	9.27 ± 0.66	11.17 ± 0.06	8.63 ± 0.36
NGC 0584	-4.45 ± 0.79	11.23 ± 0.06	11.08 ± 0.06	-1.97 ± 0.41	9.90 ± 0.46	10.60 ± 0.06	7.84 ± 0.39
NGC 0596	-4.41 ± 0.81	11.05 ± 0.06	10.90 ± 0.06	-2.11 ± 0.42	9.85 ± 0.48	10.42 ± 0.05	7.50 ± 0.44
NGC 0636	-3.53 ± 0.46	11.00 ± 0.06	10.85 ± 0.06	-1.94 ± 0.28	9.93 ± 0.46	10.36 ± 0.05	7.76 ± 0.45
NGC 0777	-2.98 ± 0.37	11.74 ± 0.06	11.59 ± 0.06	-0.68 ± 0.17	9.14 ± 0.72	11.11 ± 0.06	8.28 ± 0.45
NGC 0807	-2.08 ± 0.48	11.09 ± 0.14	10.95 ± 0.14	-0.32 ± 0.20	4.33 ± 1.28	10.57 ± 0.10	9.72 ± 0.17
NGC 0814	-0.38 ± 0.36	9.32 ± 0.20	9.19 ± 0.19	-0.38 ± 0.17	0.34 ± 0.10	9.70 ± 0.10	9.54 ± 0.14
NGC 0855	-1.58 ± 0.50	9.32 ± 0.12	9.18 ± 0.12	-1.42 ± 0.13	1.42 ± 0.76	9.00 ± 0.06	8.26 ± 0.17
NGC 1016	-3.40 ± 0.47	11.95 ± 0.06	11.80 ± 0.06	-0.90 ± 0.35	9.86 ± 0.52	11.32 ± 0.05	8.82 ± 0.46
NGC 1023	-4.38 ± 0.79	11.26 ± 0.06	11.12 ± 0.06	-1.83 ± 0.24	9.84 ± 0.45	10.64 ± 0.05	7.20 ± 0.48
NGC 1199	-3.23 ± 0.43	11.23 ± 0.06	11.08 ± 0.06	-1.42 ± 0.23	9.59 ± 0.60	10.60 ± 0.06	8.42 ± 0.39
NGC 1266	-1.02 ± 0.54	10.52 ± 0.22	10.38 ± 0.21	0.12 ± 0.23	0.82 ± 0.82	10.38 ± 0.08	10.21 ± 0.12
NGC 1316	-2.90 ± 0.46	12.06 ± 0.08	11.91 ± 0.08	-0.28 ± 0.29	8.66 ± 1.13	11.44 ± 0.08	9.92 ± 0.17
NGC 1374	-3.30 ± 0.39	10.85 ± 0.06	10.70 ± 0.06	-1.86 ± 0.14	9.71 ± 0.44	10.22 ± 0.06	7.14 ± 0.48
NGC 1377	-0.50 ± 0.43	9.99 ± 0.21	9.87 ± 0.20	0.15 ± 0.16	0.39 ± 0.18	10.33 ± 0.08	10.14 ± 0.09
NGC 1386	-1.74 ± 0.48	10.48 ± 0.11	10.33 ± 0.11	-0.66 ± 0.25	3.03 ± 1.41	10.03 ± 0.06	9.59 ± 0.10
NGC 1404	-3.28 ± 0.37	11.75 ± 0.06	11.60 ± 0.06	-0.95 ± 0.14	9.71 ± 0.45	11.12 ± 0.06	8.02 ± 0.38
NGC 1426	-3.47 ± 0.40	10.78 ± 0.06	10.64 ± 0.06	-2.08 ± 0.15	9.88 ± 0.43	10.15 ± 0.06	7.30 ± 0.46
NGC 1427	-3.20 ± 0.37	10.94 ± 0.06	10.79 ± 0.06	-1.67 ± 0.14	9.57 ± 0.50	10.32 ± 0.06	7.42 ± 0.24
NGC 1439	-2.51 ± 1.30	10.01 ± 1.44	9.86 ± 1.43	-1.92 ± 0.24	7.08 ± 4.39	9.66 ± 0.97	7.69 ± 0.24
NGC 1510	-0.50 ± 0.37	9.13 ± 0.18	9.00 ± 0.18	-0.78 ± 0.09	0.39 ± 0.06	9.30 ± 0.07	8.51 ± 0.14
NGC 1522	-0.34 ± 0.32	8.64 ± 0.20	8.52 ± 0.20	-1.04 ± 0.11	0.33 ± 0.07	9.00 ± 0.07	8.31 ± 0.16
NGC 1543	-3.66 ± 0.40	11.11 ± 0.06	10.97 ± 0.06	-1.98 ± 0.21	10.11 ± 0.41	10.48 ± 0.06	7.63 ± 0.55
NGC 1700	-2.66 ± 0.62	11.66 ± 0.08	11.51 ± 0.08	-0.41 ± 0.51	7.33 ± 2.05	11.06 ± 0.06	8.55 ± 0.33
NGC 2685	-1.29 ± 0.68	10.23 ± 0.14	10.09 ± 0.13	-0.36 ± 0.41	1.51 ± 1.37	10.01 ± 0.16	9.57 ± 0.42
NGC 2768	-3.08 ± 0.41	11.03 ± 0.07	10.89 ± 0.07	-1.48 ± 0.24	9.35 ± 0.73	10.41 ± 0.06	8.52 ± 0.20
NGC 2778	-3.35 ± 0.46	10.69 ± 0.06	10.54 ± 0.06	-2.10 ± 0.34	9.77 ± 0.56	10.06 ± 0.05	7.63 ± 0.46
NGC 2787	-3.37 ± 0.44	10.66 ± 0.07	10.52 ± 0.07	-2.15 ± 0.28	9.81 ± 0.49	10.03 ± 0.07	7.98 ± 0.19
NGC 2832	-3.10 ± 0.89	11.53 ± 0.90	11.39 ± 0.89	-1.07 ± 0.32	9.06 ± 2.69	10.98 ± 0.62	8.69 ± 0.51
NGC 2970	-2.84 ± 0.42	9.92 ± 0.06	9.77 ± 0.06	-2.29 ± 0.19	8.25 ± 1.00	9.31 ± 0.05	6.93 ± 0.47
NGC 2974	-3.21 ± 0.43	11.69 ± 0.07	11.55 ± 0.07	-0.98 ± 0.27	9.57 ± 0.61	11.07 ± 0.07	9.21 ± 0.17
NGC 3011	-1.58 ± 0.53	9.65 ± 0.12	9.50 ± 0.12	-1.02 ± 0.12	1.16 ± 0.65	9.35 ± 0.05	8.49 ± 0.24
NGC 3032	-1.44 ± 0.51	10.19 ± 0.13	10.05 ± 0.13	-0.43 ± 0.13	1.06 ± 0.65	9.92 ± 0.06	9.43 ± 0.12
NGC 3073	-1.88 ± 0.46	9.61 ± 0.10	9.47 ± 0.10	-1.52 ± 0.14	3.05 ± 0.87	9.14 ± 0.06	8.19 ± 0.17

Table 6
(Continued)

Name	Log(f_{ysp})	Log(M_{gal}) ($M_\odot$)	Log($M_\star$) ($M_\odot$)	Log(SFR) ($M_\odot$ yr^{-1})	t_{D4000} (Gyr)	Log(L_{bol}) ($L_\odot$)	Log(L_d) ($L_\odot$)
NGC 3115	-3.44 ± 0.35	11.19 ± 0.06	11.04 ± 0.06	-1.70 ± 0.15	9.94 ± 0.42	10.56 ± 0.06	7.25 ± 0.29
NGC 3125	-0.29 ± 0.26	9.10 ± 0.20	8.98 ± 0.19	-0.33 ± 0.13	0.25 ± 0.09	9.68 ± 0.08	9.32 ± 0.15
NGC 3156	-2.77 ± 0.45	10.31 ± 0.07	10.16 ± 0.07	-1.83 ± 0.22	7.91 ± 1.14	9.70 ± 0.06	8.16 ± 0.22
NGC 3226	-2.51 ± 0.61	10.49 ± 0.08	10.34 ± 0.08	-1.37 ± 0.48	6.43 ± 2.16	9.91 ± 0.05	8.41 ± 0.25
NGC 3265	-0.99 ± 0.55	9.67 ± 0.16	9.53 ± 0.15	-0.58 ± 0.14	0.56 ± 0.26	9.63 ± 0.07	9.35 ± 0.12
NGC 3377	-3.36 ± 0.39	10.45 ± 0.07	10.30 ± 0.07	-2.35 ± 0.21	9.86 ± 0.46	9.82 ± 0.06	7.26 ± 0.27
NGC 3379	-3.02 ± 0.38	10.86 ± 0.07	10.71 ± 0.07	-1.58 ± 0.18	9.20 ± 0.71	10.24 ± 0.07	7.64 ± 0.32
NGC 3384	-3.26 ± 0.40	10.56 ± 0.07	10.41 ± 0.07	-2.11 ± 0.19	9.65 ± 0.50	9.93 ± 0.06	7.54 ± 0.38
NGC 3412	-3.47 ± 0.40	10.62 ± 0.05	10.47 ± 0.05	-2.26 ± 0.19	9.90 ± 0.43	9.99 ± 0.05	6.95 ± 0.46
NGC 3489	-2.63 ± 0.46	10.43 ± 0.07	10.28 ± 0.07	-1.60 ± 0.26	7.46 ± 1.30	9.83 ± 0.06	8.54 ± 0.15
NGC 3516	-1.59 ± 0.50	11.18 ± 0.12	11.04 ± 0.12	0.32 ± 0.18	1.90 ± 1.00	10.83 ± 0.06	10.35 ± 0.13
NGC 3522	-3.25 ± 0.46	9.94 ± 0.06	9.79 ± 0.06	-2.63 ± 0.21	9.34 ± 0.64	9.32 ± 0.06	6.78 ± 0.51
NGC 3557	-0.40 ± 0.39	8.51 ± 0.53	8.39 ± 0.52	-1.14 ± 0.36	0.34 ± 0.32	9.04 ± 0.28	8.95 ± 0.28
NGC 3585	-0.57 ± 0.61	8.19 ± 0.72	8.07 ± 0.71	-1.60 ± 0.41	0.53 ± 1.06	8.60 ± 0.39	8.09 ± 0.20
NGC 3593	-1.25 ± 0.53	10.28 ± 0.14	10.14 ± 0.13	-0.32 ± 0.21	1.13 ± 0.87	10.02 ± 0.07	9.80 ± 0.10
NGC 3607	-2.94 ± 0.43	10.99 ± 0.06	10.85 ± 0.06	-1.38 ± 0.25	8.90 ± 0.93	10.37 ± 0.06	8.70 ± 0.23
NGC 3608	-3.24 ± 0.38	10.83 ± 0.07	10.68 ± 0.07	-1.82 ± 0.16	9.61 ± 0.49	10.20 ± 0.06	7.77 ± 0.28
NGC 3610	-3.29 ± 1.36	10.48 ± 1.41	10.34 ± 1.40	-1.92 ± 0.37	8.04 ± 3.47	10.05 ± 0.99	7.89 ± 0.41
NGC 3640	-3.64 ± 0.45	11.01 ± 0.06	10.86 ± 0.06	-2.02 ± 0.24	10.01 ± 0.44	10.38 ± 0.05	7.42 ± 0.43
NGC 3706	-1.23 ± 1.28	8.64 ± 1.87	8.51 ± 1.86	-1.91 ± 0.79	2.83 ± 4.06	8.90 ± 1.33	7.96 ± 0.64
NGC 3773	-0.41 ± 0.38	9.06 ± 0.17	8.94 ± 0.17	-0.73 ± 0.09	0.36 ± 0.07	9.34 ± 0.06	8.74 ± 0.15
NGC 3870	-0.44 ± 0.38	8.84 ± 0.17	8.72 ± 0.16	-0.99 ± 0.10	0.37 ± 0.06	9.08 ± 0.06	8.48 ± 0.18
NGC 3923	-3.37 ± 0.38	11.71 ± 0.07	11.56 ± 0.07	-1.07 ± 0.15	9.78 ± 0.45	11.08 ± 0.06	7.78 ± 0.35
NGC 3941	-0.48 ± 0.46	7.09 ± 0.64	6.96 ± 0.64	-2.68 ± 0.64	0.39 ± 0.36	7.60 ± 0.51	7.50 ± 0.55
NGC 3945	-2.97 ± 0.49	10.77 ± 0.07	10.62 ± 0.07	-1.64 ± 0.37	8.86 ± 1.15	10.15 ± 0.06	8.66 ± 0.21
NGC 3962	-3.26 ± 0.39	11.37 ± 0.07	11.23 ± 0.07	-1.32 ± 0.20	9.65 ± 0.50	10.75 ± 0.07	8.73 ± 0.13
NGC 4026	-3.19 ± 0.85	10.41 ± 0.87	10.26 ± 0.86	-2.30 ± 0.25	9.22 ± 2.61	9.86 ± 0.58	7.67 ± 0.29
NGC 4073	-2.91 ± 0.38	11.81 ± 0.07	11.66 ± 0.07	-0.54 ± 0.18	8.98 ± 0.80	11.19 ± 0.06	8.71 ± 0.46
NGC 4117	-2.30 ± 0.48	9.78 ± 0.07	9.63 ± 0.07	-1.89 ± 0.24	5.60 ± 1.36	9.21 ± 0.05	8.11 ± 0.26
NGC 4125	-3.11 ± 0.48	11.18 ± 0.07	11.04 ± 0.07	-1.38 ± 0.35	9.30 ± 0.87	10.56 ± 0.06	8.95 ± 0.21
NGC 4138	-1.95 ± 0.48	10.41 ± 0.09	10.26 ± 0.09	-0.82 ± 0.17	3.45 ± 1.01	9.92 ± 0.06	9.12 ± 0.15
NGC 4150	-3.96 ± 1.08	10.39 ± 0.06	10.25 ± 0.06	-2.17 ± 0.50	8.76 ± 1.18	9.79 ± 0.05	8.60 ± 0.25
NGC 4168	-3.27 ± 0.41	11.12 ± 0.06	10.97 ± 0.06	-1.54 ± 0.20	9.58 ± 0.54	10.49 ± 0.05	7.56 ± 0.50
NGC 4203	-2.59 ± 0.44	10.65 ± 0.07	10.51 ± 0.07	-1.33 ± 0.24	7.26 ± 1.32	10.05 ± 0.06	8.72 ± 0.24
NGC 4251	-3.49 ± 0.50	10.72 ± 0.06	10.57 ± 0.06	-2.19 ± 0.35	9.90 ± 0.53	10.09 ± 0.05	7.85 ± 0.47
NGC 4261	-3.03 ± 0.39	11.51 ± 0.06	11.37 ± 0.06	-0.93 ± 0.19	9.16 ± 0.71	10.89 ± 0.06	8.78 ± 0.17
NGC 4267	-3.44 ± 0.42	10.59 ± 0.06	10.45 ± 0.06	-2.27 ± 0.21	9.92 ± 0.44	9.96 ± 0.05	7.08 ± 0.42
NGC 4278	-2.81 ± 0.40	10.52 ± 0.07	10.38 ± 0.07	-1.71 ± 0.20	8.45 ± 0.99	9.91 ± 0.06	8.18 ± 0.26
NGC 4308	-3.28 ± 0.44	9.19 ± 0.06	9.04 ± 0.06	-3.48 ± 0.26	9.57 ± 0.56	8.56 ± 0.05	6.12 ± 0.49
NGC 4344	-1.69 ± 0.47	9.82 ± 0.10	9.68 ± 0.09	-1.17 ± 0.19	2.37 ± 1.04	9.39 ± 0.06	8.66 ± 0.24
NGC 4350	-3.00 ± 0.45	10.84 ± 0.07	10.69 ± 0.07	-1.60 ± 0.30	9.02 ± 0.98	10.22 ± 0.06	8.53 ± 0.26
NGC 4352	-3.50 ± 0.42	10.58 ± 0.06	10.43 ± 0.06	-2.33 ± 0.25	9.89 ± 0.45	9.95 ± 0.06	6.97 ± 0.52
NGC 4365	-3.08 ± 0.37	11.21 ± 0.07	11.07 ± 0.07	-1.30 ± 0.18	9.37 ± 0.63	10.59 ± 0.06	7.67 ± 0.32
NGC 4371	-3.36 ± 0.41	10.65 ± 0.06	10.51 ± 0.06	-2.13 ± 0.21	9.81 ± 0.46	10.02 ± 0.06	7.01 ± 0.34
NGC 4374	-3.14 ± 0.39	11.31 ± 0.08	11.16 ± 0.08	-1.24 ± 0.16	9.42 ± 0.54	10.68 ± 0.07	8.30 ± 0.24
NGC 4377	-3.47 ± 0.45	10.58 ± 0.06	10.43 ± 0.05	-2.30 ± 0.28	9.88 ± 0.47	9.95 ± 0.05	6.68 ± 0.55
NGC 4379	-3.34 ± 0.40	10.41 ± 0.06	10.27 ± 0.06	-2.34 ± 0.17	9.81 ± 0.44	9.78 ± 0.05	6.66 ± 0.52
NGC 4382	-1.48 ± 1.36	8.15 ± 1.81	8.02 ± 1.80	-2.61 ± 0.69	3.45 ± 4.17	8.27 ± 1.26	7.15 ± 0.41
NGC 4417	-3.31 ± 0.38	10.41 ± 0.06	10.26 ± 0.06	-2.31 ± 0.16	9.71 ± 0.46	9.78 ± 0.05	7.01 ± 0.51
NGC 4421	-3.71 ± 0.45	10.73 ± 0.06	10.58 ± 0.06	-2.37 ± 0.24	10.11 ± 0.43	10.09 ± 0.05	7.04 ± 0.53
NGC 4434	-3.28 ± 0.40	10.26 ± 0.06	10.11 ± 0.06	-2.44 ± 0.19	9.67 ± 0.51	9.63 ± 0.05	7.10 ± 0.51
NGC 4435	-2.99 ± 0.53	10.75 ± 0.06	10.61 ± 0.06	-1.71 ± 0.39	8.95 ± 1.12	10.13 ± 0.06	8.60 ± 0.24
NGC 4442	-3.26 ± 0.37	10.31 ± 0.06	10.16 ± 0.06	-2.40 ± 0.21	9.74 ± 0.48	9.68 ± 0.05	7.09 ± 0.49
NGC 4458	-3.49 ± 0.41	9.78 ± 0.05	9.63 ± 0.05	-3.14 ± 0.22	9.95 ± 0.43	9.15 ± 0.05	6.48 ± 0.48
NGC 4459	-2.89 ± 0.46	11.17 ± 0.07	11.03 ± 0.07	-1.15 ± 0.30	8.60 ± 1.15	10.56 ± 0.07	9.08 ± 0.18
NGC 4460	-1.51 ± 0.50	9.47 ± 0.12	9.32 ± 0.12	-1.25 ± 0.14	1.34 ± 0.75	9.15 ± 0.06	8.59 ± 0.13
NGC 4464	-3.28 ± 0.40	10.21 ± 0.06	10.07 ± 0.06	-2.46 ± 0.17	9.65 ± 0.48	9.59 ± 0.05	6.63 ± 0.53
NGC 4472	-2.82 ± 0.40	11.16 ± 0.08	11.02 ± 0.08	-1.07 ± 0.20	8.46 ± 1.01	10.55 ± 0.07	7.70 ± 0.32
NGC 4473	-3.24 ± 0.38	11.54 ± 0.06	11.40 ± 0.06	-1.13 ± 0.18	9.68 ± 0.49	10.92 ± 0.05	8.06 ± 0.47
NGC 4474	-3.55 ± 0.40	10.77 ± 0.06	10.62 ± 0.06	-2.18 ± 0.22	9.94 ± 0.44	10.14 ± 0.05	7.38 ± 0.53
NGC 4476	-2.38 ± 0.47	10.70 ± 0.07	10.56 ± 0.07	-1.11 ± 0.29	6.38 ± 1.53	10.12 ± 0.06	9.00 ± 0.24
NGC 4477	-3.20 ± 0.41	11.10 ± 0.06	10.95 ± 0.06	-1.53 ± 0.23	9.59 ± 0.55	10.47 ± 0.06	8.47 ± 0.18
NGC 4478	-3.11 ± 0.38	10.68 ± 0.06	10.53 ± 0.06	-1.85 ± 0.17	9.43 ± 0.62	10.06 ± 0.06	7.54 ± 0.44
NGC 4479	-3.18 ± 0.40	9.85 ± 0.06	9.70 ± 0.06	-2.73 ± 0.19	9.46 ± 0.58	9.22 ± 0.05	6.19 ± 0.56
NGC 4482	-3.27 ± 0.98	9.90 ± 1.03	9.76 ± 1.02	-2.79 ± 0.45	9.21 ± 2.80	9.34 ± 0.76	6.47 ± 0.55

Table 6
(Continued)

Name	Log(f_{ysp})	Log(M_{gal}) ($M_\odot$)	Log($M_\star$) ($M_\odot$)	Log(SFR) ($M_\odot$ yr^{-1})	t_{D4000} (Gyr)	Log(L_{bol}) ($L_\odot$)	Log(L_d) ($L_\odot$)
NGC 4483	-3.36 ± 0.38	10.03 ± 0.06	9.88 ± 0.06	-2.74 ± 0.15	9.78 ± 0.44	9.40 ± 0.05	6.43 ± 0.52
NGC 4486	-2.92 ± 0.37	11.81 ± 0.07	11.66 ± 0.07	-0.52 ± 0.13	8.84 ± 0.77	11.19 ± 0.06	8.72 ± 0.18
NGC 4489	-3.36 ± 0.37	10.08 ± 0.06	9.94 ± 0.06	-2.73 ± 0.17	9.87 ± 0.43	9.45 ± 0.05	6.62 ± 0.50
NGC 4494	-0.87 ± 0.60	10.99 ± 0.17	10.85 ± 0.16	0.87 ± 0.29	0.61 ± 0.69	11.02 ± 0.14	8.28 ± 0.16
NGC 4515	-3.24 ± 0.41	9.89 ± 0.06	9.75 ± 0.06	-2.74 ± 0.20	9.55 ± 0.53	9.27 ± 0.06	6.27 ± 0.52
NGC 4526	-2.43 ± 0.52	10.31 ± 0.08	10.17 ± 0.08	-1.56 ± 0.35	6.63 ± 1.77	9.72 ± 0.06	8.77 ± 0.17
NGC 4528	-2.98 ± 0.86	10.22 ± 0.84	10.08 ± 0.84	-2.22 ± 0.26	8.78 ± 2.68	9.68 ± 0.57	7.51 ± 0.46
NGC 4552	-4.25 ± 0.89	11.19 ± 0.06	11.04 ± 0.06	-1.39 ± 0.34	8.84 ± 0.75	10.59 ± 0.06	7.97 ± 0.24
NGC 4564	-3.11 ± 0.41	10.73 ± 0.06	10.58 ± 0.06	-1.80 ± 0.22	9.34 ± 0.71	10.10 ± 0.05	7.99 ± 0.44
NGC 4570	-3.31 ± 0.38	11.22 ± 0.06	11.08 ± 0.06	-1.53 ± 0.19	9.78 ± 0.46	10.59 ± 0.06	7.83 ± 0.47
NGC 4578	-0.52 ± 0.50	7.13 ± 0.61	7.00 ± 0.61	-2.64 ± 0.58	0.39 ± 0.37	7.62 ± 0.50	7.46 ± 0.56
NGC 4589	-1.74 ± 1.26	9.99 ± 1.33	9.86 ± 1.32	-1.21 ± 0.22	4.84 ± 4.47	9.82 ± 0.85	8.68 ± 0.15
NGC 4612	-3.50 ± 0.42	10.93 ± 0.06	10.79 ± 0.06	-2.01 ± 0.27	9.97 ± 0.45	10.30 ± 0.05	7.52 ± 0.51
NGC 4621	-4.24 ± 0.88	11.20 ± 0.06	11.06 ± 0.06	-1.71 ± 0.42	9.64 ± 0.58	10.58 ± 0.05	7.45 ± 0.36
NGC 4623	-3.40 ± 0.43	10.58 ± 0.06	10.43 ± 0.06	-2.22 ± 0.23	9.78 ± 0.47	9.95 ± 0.05	6.81 ± 0.55
NGC 4636	-3.06 ± 0.41	10.85 ± 0.07	10.70 ± 0.07	-1.62 ± 0.21	9.23 ± 0.70	10.23 ± 0.06	7.86 ± 0.25
NGC 4638	-1.78 ± 1.81	8.03 ± 1.89	7.90 ± 1.88	-2.80 ± 0.66	3.45 ± 4.29	8.21 ± 1.32	6.89 ± 0.41
NGC 4649	-3.12 ± 0.38	11.64 ± 0.06	11.49 ± 0.06	-0.89 ± 0.14	9.40 ± 0.57	11.02 ± 0.06	7.64 ± 0.38
NGC 4660	-3.26 ± 0.38	10.65 ± 0.06	10.50 ± 0.06	-2.05 ± 0.20	9.73 ± 0.48	10.02 ± 0.06	7.48 ± 0.32
NGC 4694	-1.85 ± 0.46	10.34 ± 0.09	10.19 ± 0.09	-0.86 ± 0.20	3.33 ± 1.11	9.85 ± 0.06	9.12 ± 0.16
NGC 4696	-0.50 ± 0.48	8.65 ± 0.57	8.53 ± 0.56	-1.05 ± 0.31	0.36 ± 0.29	9.09 ± 0.25	8.90 ± 0.21
NGC 4697	-1.05 ± 1.06	9.15 ± 1.08	9.02 ± 1.07	-1.14 ± 0.20	1.93 ± 3.02	9.28 ± 0.61	8.60 ± 0.18
NGC 4709	-0.46 ± 0.45	8.15 ± 0.79	8.03 ± 0.78	-1.57 ± 0.65	0.38 ± 0.39	8.76 ± 0.41	8.52 ± 0.28
NGC 4754	-3.44 ± 0.40	11.02 ± 0.06	10.87 ± 0.06	-1.85 ± 0.24	9.92 ± 0.46	10.39 ± 0.05	7.39 ± 0.46
NGC 4762	-3.55 ± 0.43	10.80 ± 0.06	10.65 ± 0.06	-2.20 ± 0.28	10.05 ± 0.44	10.16 ± 0.06	7.09 ± 0.43
NGC 4786	-3.06 ± 0.81	11.54 ± 0.69	11.40 ± 0.68	-0.97 ± 0.28	9.01 ± 2.37	10.98 ± 0.43	9.21 ± 0.20
NGC 4915	-1.42 ± 1.34	9.09 ± 1.66	8.95 ± 1.64	-1.72 ± 0.41	3.74 ± 4.57	9.27 ± 1.02	8.44 ± 0.36
NGC 4936	-0.96 ± 1.00	9.61 ± 1.14	9.48 ± 1.13	-0.67 ± 0.33	2.05 ± 3.40	9.75 ± 0.69	9.25 ± 0.25
NGC 5018	-2.98 ± 0.50	11.70 ± 0.07	11.56 ± 0.07	-0.75 ± 0.38	8.96 ± 1.08	11.08 ± 0.07	9.57 ± 0.21
NGC 5044	-3.08 ± 0.39	11.68 ± 0.07	11.53 ± 0.07	-0.79 ± 0.15	9.24 ± 0.63	11.06 ± 0.06	8.82 ± 0.23
NGC 5061	-1.45 ± 1.36	9.16 ± 1.82	9.02 ± 1.80	-1.67 ± 0.51	3.78 ± 4.76	9.35 ± 1.14	8.12 ± 0.41
NGC 5077	-0.98 ± 0.67	11.14 ± 0.18	11.01 ± 0.17	0.96 ± 0.33	0.74 ± 0.90	11.14 ± 0.15	8.80 ± 0.16
NGC 5173	-2.03 ± 0.48	10.59 ± 0.08	10.45 ± 0.08	-0.72 ± 0.17	3.86 ± 1.01	10.08 ± 0.05	8.93 ± 0.31
NGC 5273	-2.76 ± 0.46	10.43 ± 0.06	10.29 ± 0.06	-1.76 ± 0.30	8.07 ± 1.26	9.83 ± 0.06	8.51 ± 0.16
NGC 5322	-3.15 ± 0.43	11.29 ± 0.06	11.15 ± 0.06	-1.30 ± 0.26	9.51 ± 0.68	10.67 ± 0.06	8.82 ± 0.22
NGC 5338	-2.00 ± 0.48	9.53 ± 0.08	9.39 ± 0.08	-1.81 ± 0.22	3.98 ± 1.21	9.02 ± 0.06	8.11 ± 0.24
NGC 5353	-3.13 ± 0.43	11.39 ± 0.07	11.24 ± 0.07	-1.16 ± 0.26	9.38 ± 0.73	10.76 ± 0.06	8.83 ± 0.28
NGC 5419	-3.44 ± 0.38	12.06 ± 0.06	11.91 ± 0.06	-0.82 ± 0.21	9.94 ± 0.44	11.42 ± 0.06	8.06 ± 0.48
NGC 5481	-2.43 ± 0.65	10.64 ± 0.08	10.49 ± 0.08	-1.13 ± 0.52	5.95 ± 2.36	10.07 ± 0.05	7.11 ± 0.51
NGC 5557	-0.48 ± 0.47	7.53 ± 0.73	7.40 ± 0.73	-2.20 ± 0.68	0.38 ± 0.37	8.12 ± 0.66	7.97 ± 0.73
NGC 5576	-3.42 ± 0.41	10.98 ± 0.06	10.83 ± 0.06	-1.87 ± 0.20	9.92 ± 0.45	10.34 ± 0.06	7.55 ± 0.46
NGC 5596	-2.41 ± 0.44	10.68 ± 0.07	10.53 ± 0.07	-1.09 ± 0.17	6.14 ± 1.03	10.09 ± 0.05	8.50 ± 0.36
NGC 5813	-3.03 ± 0.38	11.17 ± 0.07	11.02 ± 0.07	-1.28 ± 0.20	9.21 ± 0.71	10.55 ± 0.06	8.06 ± 0.33
NGC 5831	-3.25 ± 0.40	10.77 ± 0.06	10.62 ± 0.06	-1.91 ± 0.21	9.69 ± 0.51	10.14 ± 0.06	7.80 ± 0.44
NGC 5845	-3.00 ± 0.42	10.41 ± 0.07	10.26 ± 0.07	-2.04 ± 0.26	9.11 ± 0.85	9.79 ± 0.06	8.03 ± 0.27
NGC 5846	-2.91 ± 0.39	11.26 ± 0.07	11.11 ± 0.07	-1.06 ± 0.18	8.77 ± 0.89	10.64 ± 0.06	8.30 ± 0.24
NGC 5866	-2.58 ± 0.51	10.68 ± 0.07	10.53 ± 0.07	-1.36 ± 0.38	7.41 ± 1.70	10.07 ± 0.06	8.96 ± 0.22
NGC 5982	-3.28 ± 0.45	11.50 ± 0.06	11.35 ± 0.06	-1.16 ± 0.21	9.58 ± 0.54	10.87 ± 0.06	8.41 ± 0.34
NGC 6703	-1.88 ± 1.81	8.88 ± 1.82	8.75 ± 1.81	-2.37 ± 0.48	4.43 ± 4.96	9.08 ± 1.13	8.28 ± 0.42
NGC 6776	-0.49 ± 0.48	8.76 ± 0.64	8.63 ± 0.63	-0.97 ± 0.42	0.38 ± 0.33	9.26 ± 0.29	9.08 ± 0.27
NGC 7077	-1.60 ± 1.62	7.47 ± 0.42	7.34 ± 0.41	-2.25 ± 0.46	0.46 ± 0.92	8.06 ± 0.16	7.98 ± 0.20
NGC 7360	-2.10 ± 0.47	10.88 ± 0.08	10.74 ± 0.08	-0.48 ± 0.16	4.08 ± 0.98	10.36 ± 0.05	9.11 ± 0.31
NGC 7457	-3.19 ± 1.04	9.92 ± 1.03	9.77 ± 1.03	-2.76 ± 0.45	8.93 ± 3.07	9.39 ± 0.73	7.25 ± 0.40
NGC 7619	-3.31 ± 0.40	11.68 ± 0.06	11.53 ± 0.06	-1.05 ± 0.19	9.76 ± 0.48	11.05 ± 0.05	8.36 ± 0.46
NGC 7626	-3.26 ± 0.40	11.61 ± 0.06	11.46 ± 0.06	-1.09 ± 0.20	9.73 ± 0.48	10.98 ± 0.06	8.26 ± 0.27
NGC 7785	-2.50 ± 0.63	11.55 ± 0.08	11.40 ± 0.08	-0.34 ± 0.51	6.54 ± 2.27	10.96 ± 0.05	8.25 ± 0.25
UGC01503	-1.36 ± 0.59	10.69 ± 0.19	10.55 ± 0.19	0.13 ± 0.24	1.20 ± 1.18	10.47 ± 0.06	9.92 ± 0.16
UGC06570	-1.18 ± 0.52	9.84 ± 0.13	9.70 ± 0.13	-0.68 ± 0.26	1.02 ± 0.84	9.65 ± 0.09	9.33 ± 0.19
UGC06637	-1.11 ± 0.58	9.45 ± 0.13	9.31 ± 0.13	-0.79 ± 0.10	0.53 ± 0.16	9.39 ± 0.05	8.66 ± 0.20
UGC06655	-0.72 ± 0.51	8.49 ± 0.15	8.35 ± 0.15	-1.55 ± 0.10	0.44 ± 0.08	8.58 ± 0.05	7.86 ± 0.20
UGC06805	-1.02 ± 0.55	9.09 ± 0.14	8.96 ± 0.14	-1.12 ± 0.12	0.53 ± 0.18	9.06 ± 0.06	8.62 ± 0.15
UGC07436	-3.13 ± 0.50	9.44 ± 0.06	9.30 ± 0.06	-3.07 ± 0.34	9.06 ± 1.03	8.82 ± 0.05	6.86 ± 0.53
UGC07580	-2.92 ± 0.42	8.82 ± 0.07	8.67 ± 0.07	-3.46 ± 0.14	8.58 ± 0.85	8.21 ± 0.06	5.17 ± 0.57
UGC08876	-3.28 ± 0.39	10.39 ± 0.06	10.24 ± 0.06	-2.32 ± 0.19	9.71 ± 0.49	9.76 ± 0.06	7.12 ± 0.52

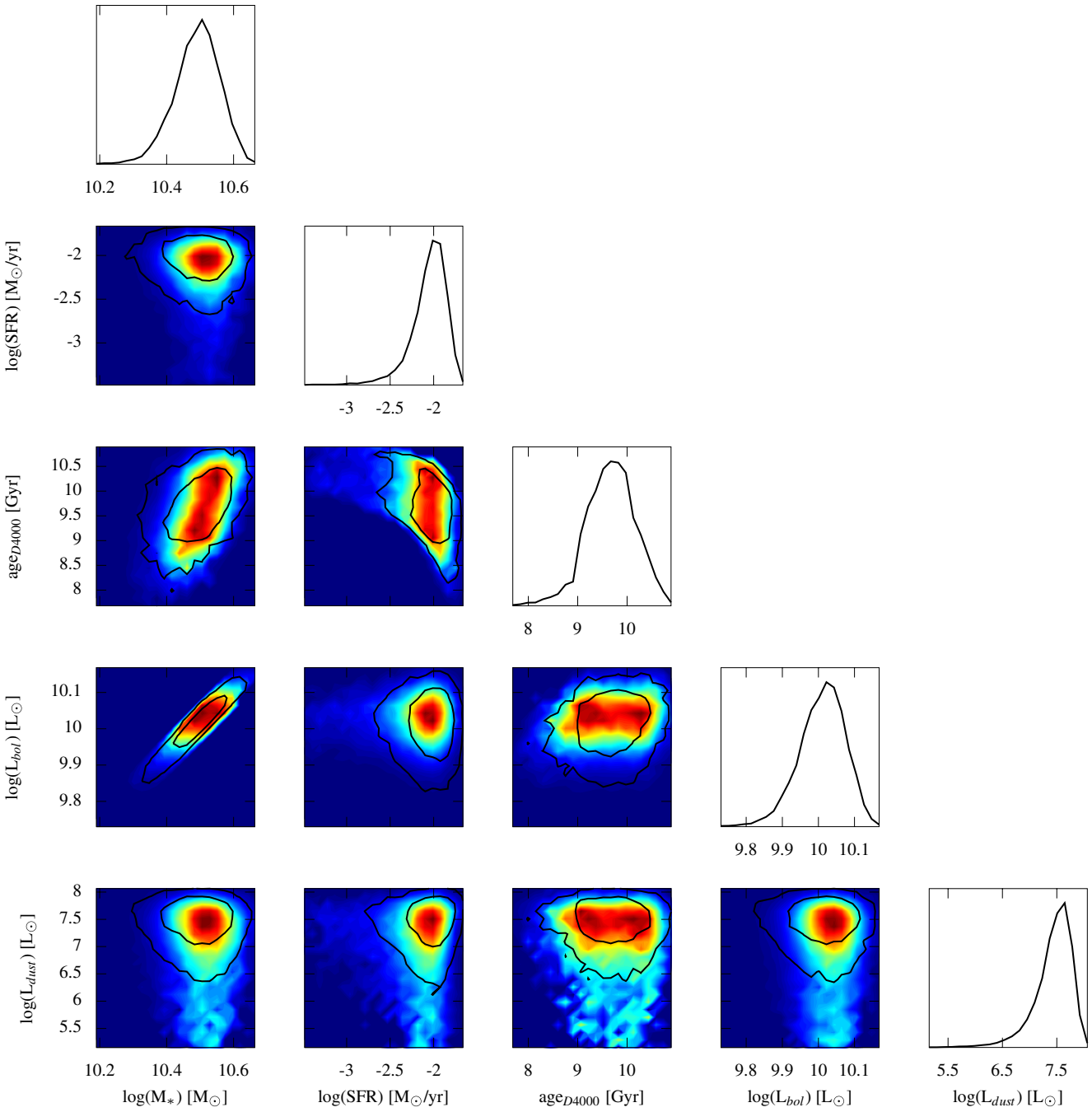

Figure 2. Constraints on some of the CIGALEMC parameters (M_*, SFR, age$_{D4000}$, $L_{\rm bol}$, $L_{\rm dust}$) for NGC 4660. The diagonal (solid black line) plots show the PDFs of each parameter, and the rainbow-color plots show the two-dimension PDFs of one parameter vs. another (solid black contours represent the 68% and 95% confidence intervals).

(A color version of this figure is available in the online journal.)

the Hα contribution in our sample. It is, in fact, about the same amplitude as the 24 μm SFR estimate itself (similar to the conclusions of Temi et al. 2009a on Hβ estimate), and would only reduce the Hα SFR estimate, whereas our plot indicates this estimate needs to be increased. The difference could be explained by the small aperture of SDSS spectroscopic data (around 3″) and the fact that the Calzetti et al. (2007) relation was estimated on a starburst whose star formation is dominated by the central bulge. Our sources might have a more extended star formation distribution, which is captured by our SED and 24 μm estimates, but underestimated by the SDSS spectroscopic data and the Calzetti et al. (2007) relation. If this difference of aperture was corrected for, the Hα SFR estimate might, on the contrary, overestimate the true SFR due to the gas photoionization by post-AGB stars (Yan & Blanton 2012; Sarzi et al. 2010), and an additional correction would be required. Indeed Yan & Blanton (2012) found a variation of the emission line ratio as a function of radius in ETGs that could potentially be explained by post-AGB stars (Binette et al. 1994) if they are more abundant or more closely distributed than expected, with respect to the gas. Previously, Sarzi et al. (2010) also concluded that post-AGB stars are their favorite candidate to power the

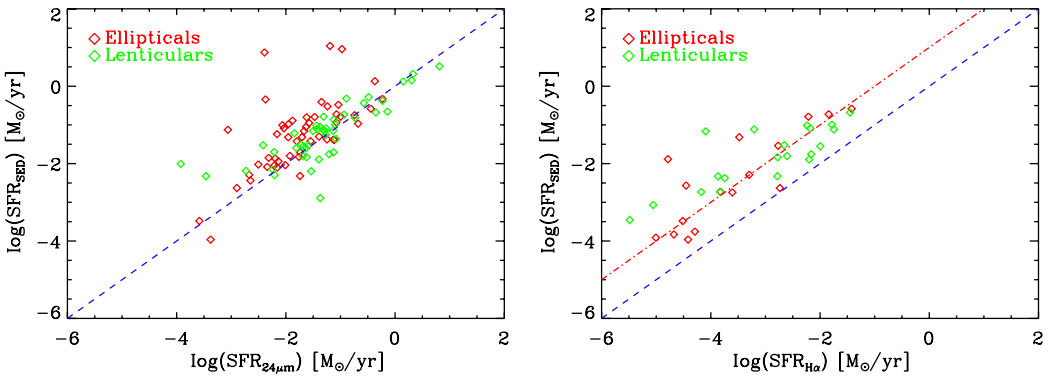

Figure 3. Left : CIGALEMC estimate of the SFR of our 143 galaxy sample vs. the 24 μm estimate as calibrated in Calzetti et al. (2007). Right: CIGALEMC estimate of SFR for a 50 galaxy subset compared to the SFR calculated from SDSS spectrometric measurements of the Hα flux and the Calzetti et al. (2007) relation. The blue dashed line indicates where the two estimates are equal and the red dot–dashed line indicates when the CIGALEMC estimate is ten times larger. Our SFR estimate is clearly correlated to the Hα luminosity, but the conversion coefficient in the Calzetti et al. (2007) would need to be multiplied by 10 for our sample.

(A color version of this figure is available in the online journal.)

ionized gas emission in ETGs based on the correlation of the Hβ line and the stellar surface brightness. Nevertheless, Hα luminosities correlate well with our SFR estimates and changing the relation to SFR ($M_\odot$ yr^{-1}) = 5.3 $\times$ $10^{-41} L$(Hα)(erg s^{-1}) leads to a good agreement with our sample (red dot–dashed line on the right of Figure 3). This implies that the star formation mechanism in the central part of our galaxies and in their outskirts is related and that the star formation is most likely distributed relatively homogeneously.

The distribution of the value of our parameters in our reduced sample of galaxies is shown on Figure 4. Ellipticals have more massive galaxies than lenticulars; about 40% of ellipticals are heavier than 10^{11} $M_\odot$, but only 12% of lenticulars are. The distribution of age$_{D4000}$ fitted on our galaxies is heavily clustered around 10 Gyr for both types; however, there are more young (age$_{D4000}$ < 8 Gyr) lenticulars (46% of S0) than ellipticals (23% of E). When normalizing the SFR and dust luminosity by the stellar mass of each galaxy, the lenticular galaxies are, on average, brighter and produce more stars. The proportion of E galaxies with a sSFR greater than $10^{-11.5}$ $M_\odot$ yr^{-1} $M_\odot^{-1}$ about 16%, and the proportion of E galaxies with a dust luminosity to stellar mass ratio greater than 10^{-2} is about 15%. For S0 galaxies, these proportions are, respectively, about 35% and 47%. These results are in agreement with previous studies using FIR photometric indicators (Temi et al. 2009a, 2009b), which showed that lenticulars are, on average, more star-forming and contain more dust. We also compared the sSFR with the slow/fast rotator classification of Emsellem et al. (2011), which classified galaxies with an angular momentum λ_R greater than $0.31\sqrt{\epsilon_e}$ as fast rotators. The number of galaxies, common to ATLAS^{3D} and our reduced sample of reasonably fitted galaxies (cf. previous χ^2 and galaxy mass constraints) is 46, with 11 slow rotators and 35 fast rotators. All the slow rotators except for one galaxy are ellipticals, and 24 fast rotators are lenticulars. Among the 46 galaxies, only three galaxies have a sSFR greater than $10^{-11.5}$ $M_\odot$ yr^{-1} $M_\odot^{-1}$. All of these galaxies are fast rotators (3/35), however the small size of this sample does not allow us to make a strong conclusion.

4. DUST MASS AND TEMPERATURE

To better understand the dust content of our sample, we decided to fit the FIR part of the spectrum with a variety of models parameterized by dust emissivity, temperature, and mass. Since CIGALEMC does not provide a direct estimate of the dust mass nor temperature, we apply two additional approaches to measure these quantities: (1) we run another SED modeling software MAGPHYS[14] (da Cunha et al. 2008), and (2) we fit some modified black-body spectra to the FIR portion of our data ($\lambda > 60\,\mu$m).

4.1. Full Spectrum Fit: MAGPHYS

Multi-wavelength Analysis of Galaxy Physical Properties (MAGPHYS) is a model able to simultaneously interpret the UV, optical, and IR emission from galaxies and determine the dust temperature. It separates contribution from dust in stellar birth clouds (BCs) and the ambient interstellar medium (ISM). The dust emission is decomposed in three components for the BCs. One models the PAHs and the NIR emission. The second corresponds to the hot MIR continuum emission, described as the sum of two graybodies with temperatures of 130 K and 250 K, respectively. The last component is dust grains in thermal equilibrium, with a temperature allowed to vary between 30 and 60 K. For the ambient ISM, to keep the number of free parameters manageable, the proportions of these three components are fixed and the temperature of the warm dust in the thermal equilibrium is fixed to 45 K. da Cunha et al. (2008) added a cold grain component in the ISM with a temperature that can vary from 15 to 25 K.

Whereas MAGPHYS fits a lot of parameters, our goal is to compute the cold dust temperature and mass of our sample, and we concentrate on these two parameters. All the galaxies in our sample are fitted using MAGPHYS, but several parameters are sometimes not well-constrained even if the reduced χ^2 of the fit seems acceptable. For instance, among the 221 sources without SPIRE data, 158 sources have good constraint on $M_{\rm dust}$, 132 on $L_{\rm dust}$, and only 36 (16% of the sample) on $T_C^{\rm ISM}$, hereafter $T_{\rm dust}$. Sources with SPIRE data available return similar results except for the temperature: among 75 sources in the initial SPIRE sample, 45 constrain the $M_{\rm dust}$ parameter, 30 constrain $L_{\rm dust}$, and 20 constrain $T_{\rm dust}$. FIR data are important to constrain $T_{\rm dust}$ accurately. 50% of the sources are constrained when the full FIR spectrum is available and less than 25% are constrained when SPIRE data are missing. This emphasizes the critical need of FIR data when determining the dust temperature using the MAGPHYS model.

[14] http://www.iap.fr/magphys/magphys/MAGPHYS.html

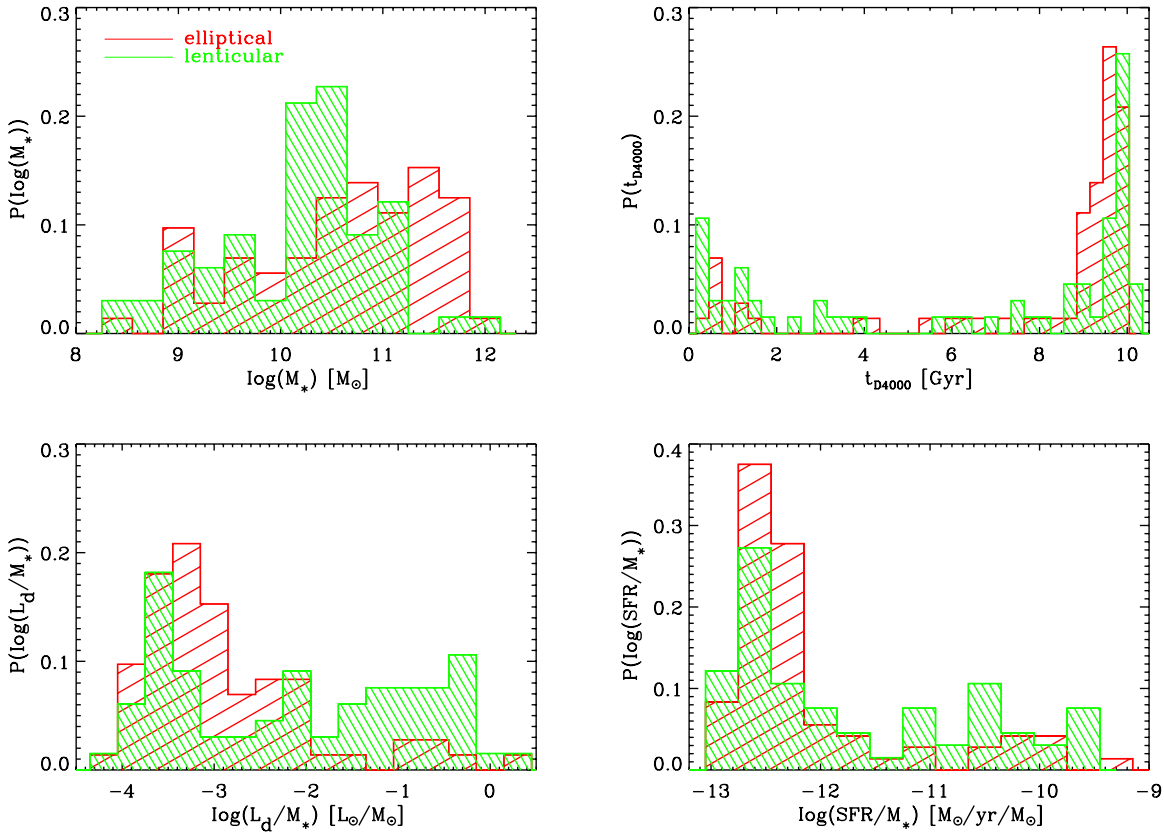

Figure 4. Distribution (renormalized to one) of the fitted parameters (from top to bottom and left to right: M_*, t_{D400}, L_d/M_*, SFR$/M_*$) for our galaxy sample. (A color version of this figure is available in the online journal.)

Among the galaxies constrained in temperature, we compare the value of $T_{\rm dust}$ obtained with MAGPHYS with and without SPIRE data. There is a huge discrepancy between these estimates and they do not correlate with each other. This result underlines the fact that values of $T_{\rm dust}$ will not be reliable without observations at FIR wavelengths. We estimate that in our sample, only the temperatures of the 20 sources with SPIRE data are accurate enough when using MAGPHYS. This encouraged us to explore other methods to determine the dust temperature of our sample, as detailed in the following sub-section.

4.2. Far-infrared Fit

Using only the FIR part of our data ($\lambda > 40\,\mu$m), contrarily to the MAGPHYS fitting method, we perform two types of fits on our sources.

1. A two-temperature fit with a standard emissivity β for big dust grains of 1.5 or 2.0 (Draine & Lee 1984; Agladze et al. 1996; Mennella et al. 1998; Reach et al. 1995; Boulanger et al. 1996; Dunne & Eales 2001), on *IRAS* 60, 100 μm, MIPS 70, 160 μm and 250, 350, 500 μm SPIRE data, the luminosity is then

$$L(\nu) \propto \alpha B\left(\nu, T_d^1\right)\nu^\beta + (1-\alpha)B\left(\nu, T_d^2\right)\nu^\beta, \qquad (3)$$

where $B(\nu,T)$ represents a blackbody spectrum of temperature T at frequency ν, α gives the luminosity ratio of the two dust species. T_d^1 is constrained between 10 and 45 K, and T_d^2 between 45 and 95 K.

2. A single-temperature fit with emissivity β, either 1.5 or 2.0, on *IRAS* 60, 100 μm, MIPS 70, 160 μm, and 250, 350, 500 μm SPIRE data. T_d is constrained between 10 and 95 K, and the luminosity is then expressed as

$$L(\nu) \propto B(\nu, T_d)\nu^\beta. \qquad (4)$$

We compute fluxes in each band by integrating over the various instrument filters f_i, which have been normalized so that $\int f_i(\nu)d\nu = 1$. We normalize fluxes with the total dust luminosity defined as $L_d = \int L(\nu)d\nu$. Fluxes in each band, F_i are then defined as

$$F_i = \frac{L_d}{4\pi D_l^2}\frac{\int L(\nu)f_i(\nu)d\nu}{\int L(\nu)d\nu}. \qquad (5)$$

To obtain the mass of the dust, we assume that dust grains are in thermal equilibrium and use the Hildebrand (1983) formula, which gives a relation between the dust temperature (T_d), the dust luminosity (L_d), and its mass (M_d):

$$L_d(\lambda) = 4\pi M_d \kappa(\lambda)B(\lambda, Td). \qquad (6)$$

We use the same hypothesis as Dunne et al. (2000) and take κ at 850 μm, $\kappa(850\,\mu$m), to be equal to 0.077 kg^{-1} m^{-2} (based on the calculations of Draine & Lee 1984; Hughes et al. 1993). We assume the emissivity to follow the relation $\kappa(\lambda) = \kappa(850\ \mu\text{m})(\lambda/850\ \mu\text{m})^{-\beta}$, the dust mass can then be expressed as

$$M_d = L_d \Big/ \int 4\pi\kappa(\lambda)B(\lambda, T)d\lambda. \qquad (7)$$

The results of the fit can be found in Figures 5 and 6 and Tables 7 and 8. When fitting with a two-temperature model, our

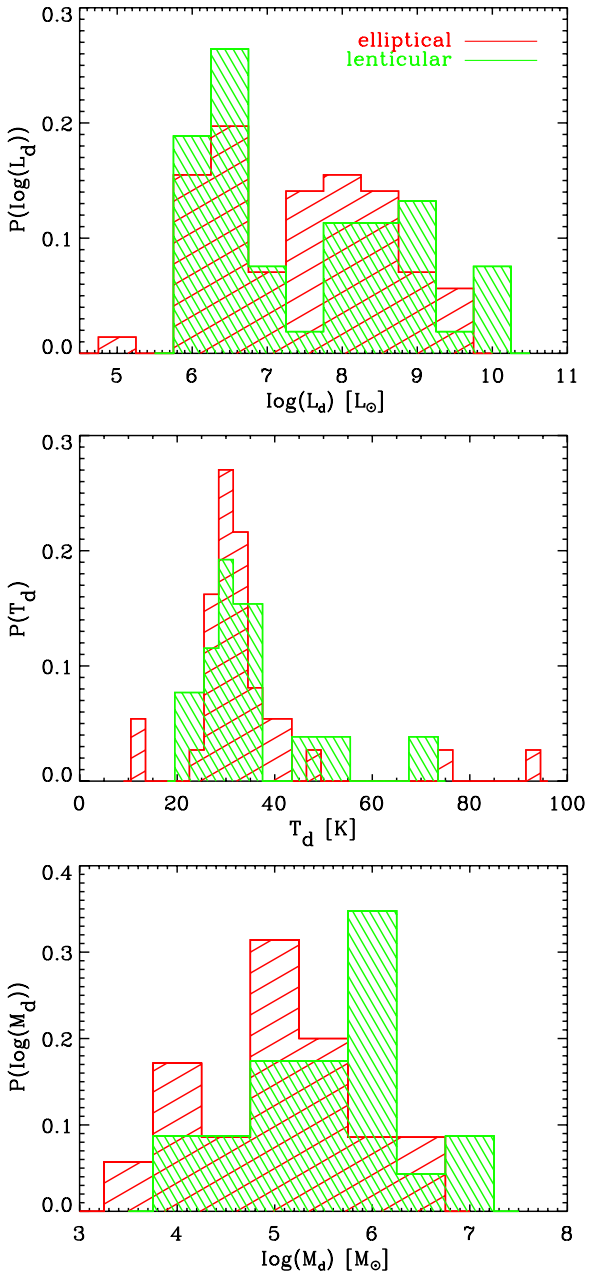

Figure 5. Distribution of the dust luminosity (top), temperature (middle), and mass (bottom), obtained by fitting our one temperature model with $\beta = 1.5$ to our data. The elliptical and lenticular galaxy histograms are, respectively, in red and green lines, and they both are normalized to one. A few more lenticulars than ellipticals reach a dust mass of 10^6 $M_\odot$.

(A color version of this figure is available in the online journal.)

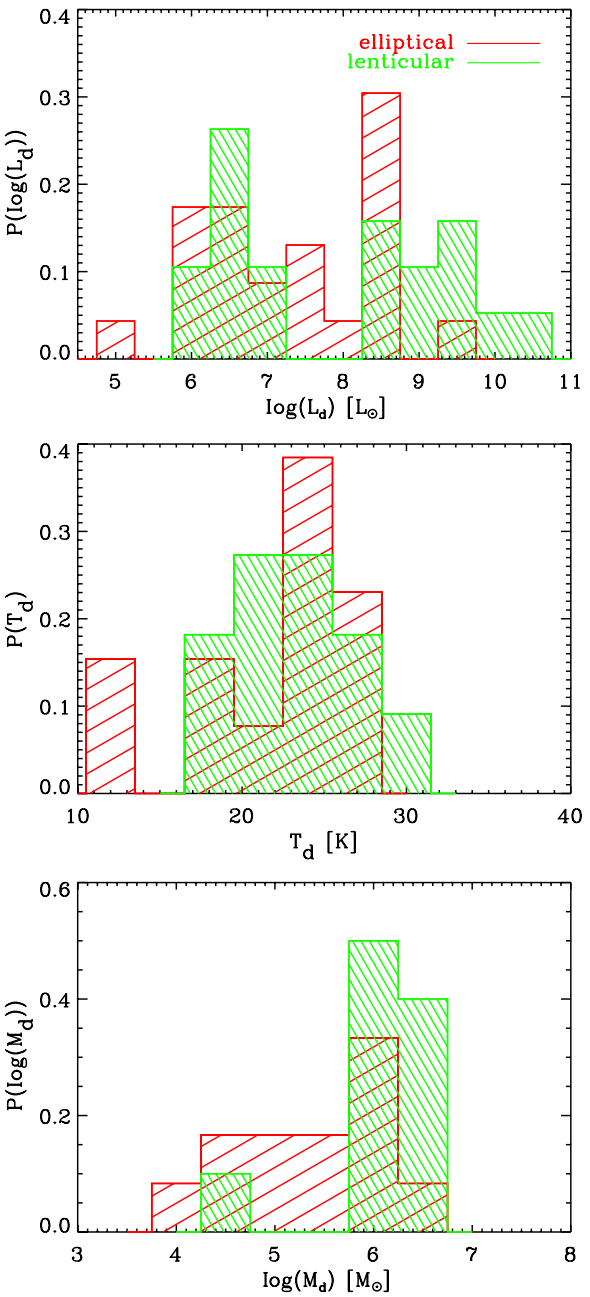

Figure 6. Distribution of the dust luminosity (top), cold temperature (center), and mass (bottom), obtained by fitting our two-temperature model with $\beta = 2.0$ to our data. The elliptical and lenticular galaxy histograms are, respectively, in red and green lines, and they both are normalized to one. Lenticulars appear slightly dustier and more luminous.

(A color version of this figure is available in the online journal.)

algorithm manages to converge on 42 galaxies (23 E and 19 S0), and when using the single-temperature model we constrain 124 galaxies (71 E and 53 S0) with a reduced χ^2 of 10 or better. The average reduced χ^2 of our two temperature fit is 3.4, the reduced χ^2 for our single-temperature fit is 3.3. Introducing a more complex model does not improve our fit on average, although our frequency coverage is limited in the FIR. Some of our galaxies are known to have a strong synchrotron emission (NGC 4267 and NGC 4486 for instance) as indicated in di Serego Alighieri et al. (2013), they only represent a small fraction of the sample and most of them have a very large reduced χ^2 and are therefore not included in the following analysis.

The fit is slightly better, on average, for a 2.0 emissivity than 1.5 in the two-temperature, but it is the opposite for the single-temperature. Changing the emissivity in the two-temperature fit from 1.5 to 2, increases the luminosity by 20%, decreases the cold temperature by 10%, and increases the dust mass by a factor of three. In our single-temperature case, we compare the fit with an emissivity β of 1.5 and 2 and find that the temperature and mass change, respectively, by $\sim -10\%$, -40% when using 2 instead of 1.5, but the luminosity is barely changed. In the following, we will only discuss our fit with an emissivity 2.0 for the two-temperature model, and 1.5 for the single-temperature model.

Table 7
Parameters Fitted with Single-temperature Model and Emissivity $\beta = 1.5$ on FIR Data

Name	Log(L_d) ($L_\odot$)	T (K)	Log(M_d) ($M_\odot$)	χ^2/ndf
Eso103-35	10.57 ± 0.05	88.33 ± 4.40	4.90 ± 0.06	10.10
Eso428-14	9.76 ± 0.02	54.14 ± 3.61	5.22 ± 0.14	1.05
Eso483-13	8.12 ± 0.02	31.45 ± 1.40	4.87 ± 0.11	50.00
IC1459	8.75 ± 0.02	31.76 ± 1.31	5.47 ± 0.10	1.18
IC3032	6.23 ± 0.82	61.10 ± 21.56	2.71 ± 2.20	0.06
IC3101	6.30 ± 0.87	60.61 ± 21.96	2.95 ± 2.27	0.05
IC3328	6.28 ± 0.79	61.56 ± 21.29	2.66 ± 2.40	3.12
IC3370	9.43 ± 0.02	30.07 ± 0.93	6.28 ± 0.08	67.35
IC3381	6.22 ± 0.77	61.96 ± 21.38	2.55 ± 2.38	0.94
IC3501	6.37 ± 0.91	60.58 ± 22.64	3.05 ± 2.15	0.05
IC4296	8.69 ± 0.05	39.12 ± 3.32	4.94 ± 0.16	2.39
IC4329	6.70 ± 1.00	55.18 ± 25.00	5.27 ± 4.60	0.80
IC5063	10.57 ± 0.07	70.45 ± 6.49	5.43 ± 0.15	22.78
NGC 0221	5.65 ± 0.46	12.20 ± 1.60	5.21 ± 0.77	16.03
NGC 0315	9.47 ± 0.02	28.57 ± 0.85	6.45 ± 0.08	5.92
NGC 0404	5.94 ± 0.02	30.63 ± 1.14	2.74 ± 0.09	0.31
NGC 0410	7.31 ± 1.19	56.10 ± 24.00	5.40 ± 5.19	19.31
NGC 0474	8.00 ± 0.07	25.28 ± 2.05	5.32 ± 0.21	7.27
NGC 0507	6.72 ± 1.04	54.32 ± 24.43	5.14 ± 3.97	1.19
NGC 0526	9.94 ± 0.11	21.62 ± 1.94	7.69 ± 0.33	11.36
NGC 0533	8.38 ± 0.07	31.84 ± 3.54	5.16 ± 0.22	0.63
NGC 0584	8.16 ± 0.20	76.06 ± 13.59	2.96 ± 0.51	5.32
NGC 0636	6.24 ± 0.76	55.95 ± 24.94	4.59 ± 4.78	1.26
NGC 0720	7.43 ± 0.31	63.23 ± 19.00	3.21 ± 1.57	9.92
NGC 0777	7.20 ± 0.86	55.01 ± 22.94	5.01 ± 4.98	5.18
NGC 0807	9.84 ± 0.04	18.17 ± 0.38	7.90 ± 0.09	47.69
NGC 0814	9.71 ± 0.01	55.91 ± 1.12	5.07 ± 0.04	27.90
NGC 0821	6.25 ± 0.74	53.97 ± 24.80	4.53 ± 4.50	4.93
NGC 0855	8.36 ± 0.01	34.96 ± 0.74	4.84 ± 0.06	8.41
NGC 1016	6.75 ± 1.03	53.93 ± 24.44	5.52 ± 8.51	1.81
NGC 1023	5.88 ± 0.54	55.71 ± 24.57	3.84 ± 3.17	0.52
NGC 1199	8.80 ± 0.41	31.89 ± 22.27	7.35 ± 0.76	2.65
NGC 1266	10.43 ± 0.00	42.42 ± 0.22	6.45 ± 0.01	24.33
NGC 1316	9.80 ± 0.02	28.75 ± 0.45	6.75 ± 0.04	5.98
NGC 1374	6.48 ± 0.76	57.36 ± 23.60	4.27 ± 4.49	5.59
NGC 1377	9.99 ± 0.00	51.26 ± 0.49	5.56 ± 0.02	8.40
NGC 1386	9.28 ± 0.00	38.04 ± 0.19	5.56 ± 0.01	10.54
NGC 1395	8.17 ± 0.02	28.48 ± 0.81	5.14 ± 0.06	0.85
NGC 1399	6.89 ± 0.11	12.66 ± 1.41	5.87 ± 0.19	2.78
NGC 1404	7.86 ± 0.24	66.18 ± 17.02	3.21 ± 0.78	0.18
NGC 1407	6.08 ± 0.66	52.92 ± 24.99	4.76 ± 3.75	7.10
NGC 1426	6.11 ± 0.66	54.77 ± 24.36	4.18 ± 3.66	1.21
NGC 1427	7.37 ± 0.18	55.84 ± 14.95	3.08 ± 0.58	11.60
NGC 1439	7.77 ± 0.05	41.42 ± 4.20	3.90 ± 0.18	3.95
NGC 1510	8.50 ± 0.05	49.25 ± 5.59	4.24 ± 0.24	84.27
NGC 1522	8.47 ± 0.01	40.53 ± 1.12	4.61 ± 0.06	17.03
NGC 1533	8.34 ± 0.05	20.46 ± 0.67	6.12 ± 0.13	24.34
NGC 1553	8.34 ± 0.02	42.28 ± 1.32	4.37 ± 0.06	14.66
NGC 2110	9.91 ± 0.04	47.10 ± 5.50	5.76 ± 0.26	6.42
NGC 2434	7.51 ± 0.19	52.98 ± 15.07	3.33 ± 0.52	5.73
NGC 2768	8.58 ± 0.01	37.40 ± 0.87	4.90 ± 0.05	10.80
NGC 2787	8.14 ± 0.02	35.67 ± 0.90	4.58 ± 0.06	1.76
NGC 2832	9.72 ± 0.14	87.51 ± 6.85	4.09 ± 0.13	63.60
NGC 2974	9.14 ± 0.02	25.00 ± 0.54	6.42 ± 0.06	4.65
NGC 2986	6.16 ± 0.70	54.06 ± 25.14	4.59 ± 3.98	5.56
NGC 3032	9.33 ± 0.01	34.04 ± 0.53	5.88 ± 0.04	2.77
NGC 3073	8.11 ± 0.02	25.65 ± 0.62	5.34 ± 0.07	3.47
NGC 3115	7.01 ± 0.18	55.33 ± 15.71	2.90 ± 0.96	4.21
NGC 3156	8.14 ± 0.03	35.20 ± 1.47	4.62 ± 0.09	5.56
NGC 3226	8.26 ± 0.02	26.19 ± 0.50	5.43 ± 0.06	0.17
NGC 3265	9.24 ± 0.01	38.76 ± 0.50	5.48 ± 0.03	12.43
NGC 3377	7.06 ± 0.03	33.27 ± 1.49	3.68 ± 0.10	17.23
NGC 3379	7.20 ± 0.04	32.07 ± 1.93	3.91 ± 0.13	2.42
NGC 3384	7.03 ± 0.42	57.97 ± 22.92	5.55 ± 6.88	1.88

Table 7
(Continued)

Name	Log(L_d) ($L_\odot$)	T (K)	Log(M_d) ($M_\odot$)	χ^2/ndf
NGC 3557	8.89 ± 0.03	31.84 ± 1.22	5.60 ± 0.09	12.57
NGC 3585	7.75 ± 0.08	46.54 ± 6.44	3.63 ± 0.23	1.70
NGC 3593	9.48 ± 0.00	36.61 ± 0.10	5.85 ± 0.01	9674.29
NGC 3608	7.53 ± 0.08	38.06 ± 7.02	3.93 ± 0.24	3.33
NGC 3610	7.30 ± 0.33	40.96 ± 19.20	4.39 ± 2.05	2.29
NGC 3640	6.10 ± 0.67	56.90 ± 24.45	3.68 ± 2.85	0.17
NGC 3773	8.84 ± 0.01	36.08 ± 0.55	5.24 ± 0.04	6.24
NGC 3923	7.45 ± 0.06	26.27 ± 2.18	4.66 ± 0.21	2.36
NGC 3941	6.79 ± 1.05	55.79 ± 24.01	3.77 ± 1.64	1.10
NGC 3945	8.69 ± 0.02	19.84 ± 0.25	6.53 ± 0.04	8.44
NGC 3962	8.65 ± 0.01	29.07 ± 0.53	5.57 ± 0.04	3.57
NGC 4125	8.83 ± 0.02	28.75 ± 0.63	5.78 ± 0.06	6.21
NGC 4138	8.93 ± 0.02	25.89 ± 0.45	6.13 ± 0.05	0.84
NGC 4150	7.44 ± 0.02	33.76 ± 1.15	4.02 ± 0.08	5.33
NGC 4168	6.29 ± 0.78	56.17 ± 24.16	3.78 ± 2.36	0.11
NGC 4203	8.71 ± 0.02	26.28 ± 0.48	5.88 ± 0.05	1.92
NGC 4251	6.39 ± 0.93	59.76 ± 23.06	3.25 ± 2.18	0.31
NGC 4261	8.52 ± 0.02	23.69 ± 0.55	5.94 ± 0.05	10.66
NGC 4267	6.44 ± 0.23	17.36 ± 5.00	4.94 ± 0.49	6.14
NGC 4278	8.18 ± 0.02	29.32 ± 0.79	5.08 ± 0.07	9.31
NGC 4291	6.38 ± 0.89	49.74 ± 26.08	6.50 ± 3.89	3.29
NGC 4344	8.72 ± 0.02	25.18 ± 0.62	5.99 ± 0.07	3.34
NGC 4350	8.36 ± 0.02	33.41 ± 0.74	4.95 ± 0.05	11.57
NGC 4352	6.80 ± 0.99	44.94 ± 27.44	4.91 ± 0.99	8.75
NGC 4365	7.49 ± 0.05	34.11 ± 2.04	4.05 ± 0.12	0.51
NGC 4371	7.07 ± 0.25	60.92 ± 19.77	2.71 ± 0.57	16.13
NGC 4374	8.37 ± 0.02	33.36 ± 0.87	4.96 ± 0.06	8.42
NGC 4377	8.65 ± 0.04	36.56 ± 1.03	5.02 ± 0.05	10.30
NGC 4379	6.46 ± 0.96	59.60 ± 23.13	3.29 ± 2.09	0.11
NGC 4382	6.58 ± 0.19	40.15 ± 15.01	3.30 ± 2.12	3.10
NGC 4386	8.76 ± 0.19	19.50 ± 2.22	6.84 ± 0.45	0.19
NGC 4406	5.02 ± 0.02	93.40 ± 1.34	−0.77 ± 0.03	9.77
NGC 4417	8.09 ± 0.14	69.58 ± 11.07	3.05 ± 0.26	5.52
NGC 4421	6.32 ± 0.76	55.95 ± 24.23	4.54 ± 3.78	0.29
NGC 4434	6.03 ± 0.66	57.94 ± 23.03	3.07 ± 2.20	0.85
NGC 4435	8.96 ± 0.01	30.62 ± 0.25	5.75 ± 0.02	100.32
NGC 4442	6.17 ± 0.76	62.86 ± 21.24	2.64 ± 2.88	0.06
NGC 4458	5.80 ± 0.53	61.33 ± 21.99	2.50 ± 2.94	0.05
NGC 4459	9.17 ± 0.01	33.56 ± 0.54	5.75 ± 0.04	8.84
NGC 4460	8.58 ± 0.01	35.68 ± 0.83	5.02 ± 0.06	3.67
NGC 4464	5.97 ± 0.63	51.16 ± 25.83	3.82 ± 1.44	3.09
NGC 4472	7.28 ± 0.04	31.78 ± 1.82	4.01 ± 0.12	0.16
NGC 4473	6.36 ± 0.82	56.01 ± 24.20	3.95 ± 2.47	0.45
NGC 4474	6.54 ± 0.92	58.30 ± 23.07	3.42 ± 2.21	2.79
NGC 4476	9.08 ± 0.02	29.59 ± 0.68	5.96 ± 0.05	7.72
NGC 4477	8.47 ± 0.01	31.53 ± 0.50	5.20 ± 0.04	5.88
NGC 4478	6.73 ± 0.07	11.61 ± 1.05	5.89 ± 0.15	2.35
NGC 4479	6.31 ± 0.87	60.85 ± 22.86	3.11 ± 2.32	0.93
NGC 4482	6.26 ± 0.83	58.44 ± 22.63	3.28 ± 2.54	0.35
NGC 4483	5.87 ± 0.59	58.19 ± 22.63	2.83 ± 2.34	0.71
NGC 4486	8.55 ± 0.02	27.98 ± 0.97	5.58 ± 0.09	24.88
NGC 4494	8.24 ± 0.02	36.63 ± 0.90	4.61 ± 0.05	1.20
NGC 4526	8.84 ± 0.00	31.24 ± 0.17	5.59 ± 0.01	6.30
NGC 4528	8.29 ± 0.24	72.81 ± 12.59	3.18 ± 0.33	4.35
NGC 4552	6.63 ± 0.03	29.78 ± 0.89	3.50 ± 0.06	8.41
NGC 4564	6.11 ± 0.70	57.59 ± 22.99	3.27 ± 2.31	1.67
NGC 4570	6.15 ± 0.73	58.18 ± 23.81	3.35 ± 2.27	0.37
NGC 4578	6.31 ± 0.78	53.98 ± 24.91	4.21 ± 2.28	2.86
NGC 4589	8.57 ± 0.02	28.90 ± 0.67	5.51 ± 0.05	3.11
NGC 4612	6.48 ± 0.81	48.96 ± 26.30	4.61 ± 1.26	2.79
NGC 4621	6.31 ± 0.05	30.94 ± 2.08	3.12 ± 0.14	18.48
NGC 4636	7.74 ± 0.02	33.12 ± 1.05	4.36 ± 0.07	3.17
NGC 4638	6.46 ± 0.30	66.50 ± 17.34	1.79 ± 1.26	3.99
NGC 4649	8.32 ± 0.03	94.04 ± 1.02	2.52 ± 0.03	1117.45
NGC 4660	7.18 ± 0.05	30.50 ± 1.88	4.01 ± 0.13	2.08

Table 7
(Continued)

Name	Log(L_d) ($L_\odot$)	T (K)	Log(M_d) ($M_\odot$)	χ^2/ndf
NGC 4694	8.93 ± 0.03	28.26 ± 1.07	5.93 ± 0.10	10.20
NGC 4696	8.69 ± 0.02	27.67 ± 0.60	5.73 ± 0.05	5.55
NGC 4697	8.53 ± 0.02	35.69 ± 0.88	4.97 ± 0.05	6.49
NGC 4709	6.68 ± 0.98	54.58 ± 24.57	5.22 ± 4.27	7.20
NGC 4754	6.00 ± 0.62	56.26 ± 24.22	3.52 ± 2.24	0.24
NGC 4762	6.73 ± 0.23	57.48 ± 18.47	2.77 ± 1.07	1.39
NGC 4786	9.31 ± 0.05	41.32 ± 2.73	5.41 ± 0.12	0.53
NGC 4915	8.04 ± 0.05	26.93 ± 1.66	5.18 ± 0.15	0.90
NGC 4936	9.26 ± 0.03	26.88 ± 0.94	6.38 ± 0.08	0.61
NGC 5018	9.63 ± 0.02	31.77 ± 1.02	6.35 ± 0.09	11.19
NGC 5044	8.76 ± 0.03	31.18 ± 1.40	5.53 ± 0.10	4.06
NGC 5061	7.56 ± 0.37	61.88 ± 20.01	3.54 ± 1.58	2.85
NGC 5077	8.60 ± 0.02	31.06 ± 1.14	5.37 ± 0.09	353.34
NGC 5273	8.49 ± 0.02	35.46 ± 0.88	4.94 ± 0.06	17.31
NGC 5322	8.70 ± 0.02	33.48 ± 1.57	5.30 ± 0.12	13.66
NGC 5353	9.02 ± 0.02	32.28 ± 0.97	5.69 ± 0.07	78.11
NGC 5419	6.72 ± 1.00	54.91 ± 24.39	4.96 ± 4.26	1.16
NGC 5557	7.94 ± 0.37	48.40 ± 19.54	4.70 ± 1.87	7.76
NGC 5576	6.09 ± 0.68	55.65 ± 24.40	3.66 ± 2.18	1.23
NGC 5813	7.93 ± 0.07	42.33 ± 4.29	4.01 ± 0.18	28.02
NGC 5831	7.23 ± 0.87	65.48 ± 21.68	3.78 ± 5.51	21.82
NGC 5845	7.88 ± 0.04	28.72 ± 1.67	4.86 ± 0.14	14.40
NGC 5846	8.00 ± 0.03	30.43 ± 1.22	4.83 ± 0.09	1.24
NGC 5866	9.20 ± 0.00	29.41 ± 0.07	6.09 ± 0.01	3.05
NGC 5982	8.11 ± 0.06	28.59 ± 2.39	5.12 ± 0.18	2.73
NGC 6482	8.99 ± 0.16	84.78 ± 9.05	3.48 ± 0.99	78.27
NGC 6703	7.94 ± 0.11	45.41 ± 7.75	3.91 ± 0.25	3.23
NGC 6776	9.48 ± 0.22	74.04 ± 15.54	4.45 ± 0.59	3.83
NGC 6849	6.67 ± 1.00	53.83 ± 25.04	5.33 ± 4.21	3.35
NGC 7077	8.28 ± 0.03	33.40 ± 1.33	4.88 ± 0.09	5.81
NGC 7457	6.01 ± 0.60	57.06 ± 24.20	4.05 ± 3.31	1.77
NGC 7619	6.58 ± 0.92	55.30 ± 24.95	5.07 ± 4.31	1.46
NGC 7785	8.09 ± 0.22	56.80 ± 18.52	3.92 ± 0.70	6.97
UGC01503	9.88 ± 0.02	28.32 ± 0.96	6.88 ± 0.09	41.94
UGC07436	5.93 ± 0.61	56.84 ± 23.00	2.97 ± 2.08	3.22
UGC07580	6.58 ± 0.42	31.53 ± 9.38	3.58 ± 0.52	0.41

The distributions in Figures 5 and 6 show that galaxies fitted by the two-temperature model have a lower temperature than the one fitted with the single-temperature model (22.4 K versus 32.3 K). This can be explained by the fact that our two-temperature model containing four free parameters requires five data points. This means that at least one data point from *Herschel*-SPIRE is required to fit the two-temperature model, whereas the one-temperature fit does not require *Herschel* data with only two free parameters. The two-temperature model is only possible on galaxies with colder dust. This result is in agreement with Skibba et al. (2011) where they find a higher dust to stellar flux ratio for *Herschel*-detected galaxies, because *Herschel* is tracing additional cold dust that was not detected with *Spitzer*. The 32.3 K average temperature derived on the single-temperature model is very close to average temperatures derived from other galaxy selections, such as the 35 K estimate from Elbaz et al. (2010), and the 28 K estimate from Amblard et al. (2010). Figures 5 and 6 also reveal that lenticular galaxies have slightly more dust than elliptical (more apparent in the two-temperature model), and slightly higher dust luminosity when their SED is modeled with two temperatures.

Figure 7 shows the evolution of the ratio of dust mass to stellar mass in a logarithmic scale versus the stellar mass in elliptical galaxies (in red) and in lenticular ones (in green) with

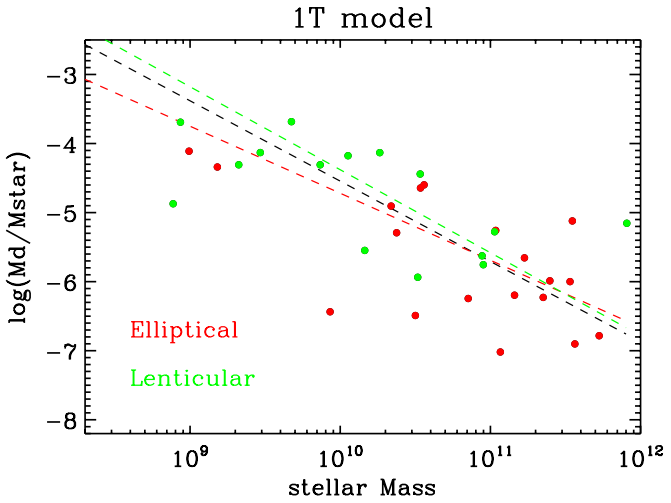

Figure 7. Ratio of dust mass to stellar mass in logarithmic scale vs. the stellar mass for Elliptical galaxies (in red) and for lenticular ones (in green) for sources with a secure fit (dust mass estimate with a relative error of 50% or less) with the 1T model. The dashed lines represent the best linear fit obtained for the whole sample (black), for elliptical galaxies (red) and for lenticular galaxies (green).
(A color version of this figure is available in the online journal.)

the single-temperature model, when selecting only sources with a secure dust mass (less than 50% relative error) and a good fit to the full SED and the FIR spectra (34 sources). We decide to present results only for the single-temperature model; we have similar results but with poorer statistics for the two-temperature model.

The dashed lines represent the best linear fit obtained with these 34 sources (black), with elliptical galaxies among this sample (red), and with lenticular galaxies (green). The general trend is that the ratio $M_{\rm dust}$ to $M_{\rm star}$ decreases with increasing stellar mass. This relation is statistically identical for both elliptical galaxies (red dashed line) and lenticular ones (green dashed line); the slopes being -1.16 ± 0.16, -0.97 ± 0.18, -1.20 ± 0.30 for the whole sample, the elliptical galaxies, and for the lenticular galaxies, respectively. The decreasing trend is in good agreement with other studies, and measurements from Smith et al. (2012) seem compatible with our fit although their stellar mass range is very small (10^{10}–10^{11} $M_\odot$). Agius et al. (2013) found a shallower slope of -0.55 with larger dust-to-stellar mass ratio ($10^{-2.5}$ to 10^{-4}), it uses a sample detected by the shallow H-ATLAS survey which could explain that it selects a higher dust-to-stellar mass ratio. (Rowlands et al. 2012) using data from H-ATLAS as well, found higher dust masses, around $7 < \log(M_d/M_\odot) < 9$ and higher dust-to-stellar mass ratios. Skibba et al. (2011) measured dust-to-stellar mass ratios in the same range as ours. Cortese et al. (2012) measured dust-to-stellar mass ratios on late-type galaxies ranging from 10^{-2} to 10^{-4} and on ETGs from $10^{-3.5}$ to 10^{-6}.

Figure 8 shows the evolution of the specific SFR (sSFR) as a function of the dust-to-stellar mass ratio for ellipticals (red triangles) and for lenticulars (green triangles) in a logarithmic scale. Figure 8 is similar in shape to the banana-shaped plots of Temi et al. (2009b) which show the relationship between $\log(L_{24}/L_K)$ and $\log(L_{\rm FIR}/L_K)$, and the information it contains is correlated with our plot. However, Figure 8 permits a better distinction of SFR and dust mass than the 24 μm and FIR (70 or 160 μm) luminosities could.

The sSFR is constant ($\log({\rm sSFR}) \sim -12.5\ M_\odot\ {\rm yr}^{-1}\ M_\odot^{-1}$) for a dust-to-star mass ratio less than 10^{-5}. This part of the diagram

Table 8
Parameters Fitted by a Two-temperature Model with an Emissivity $\beta = 2$ Using FIR Data

Name	Log(L_d) ($L_\odot$)	α	T_d^1 (K)	T_d^2 (K)	Log(M_d) ($M_\odot$)	χ^2/ndf
IC3328	6.45 ± 0.81	0.50 ± 0.29	27.48 ± 10.13	71.11 ± 14.39	4.75 ± 2.80	9.31
IC5063	10.63 ± 0.07	1.00 ± 0.00	16.53 ± 1.48	70.67 ± 5.36	8.63 ± 0.35	2.15
NGC 0584	8.34 ± 0.21	0.46 ± 0.27	26.86 ± 10.03	79.91 ± 11.67	6.11 ± 1.43	8.44
NGC 0855	8.36 ± 0.07	0.99 ± 0.01	22.61 ± 1.12	57.17 ± 7.27	5.48 ± 0.13	2.52
NGC 1266	10.56 ± 0.03	0.99 ± 0.00	27.60 ± 0.59	70.13 ± 3.06	7.15 ± 0.06	12.83
NGC 1316	9.61 ± 0.07	1.00 ± 0.00	24.11 ± 0.65	55.17 ± 8.73	6.56 ± 0.13	5.55
NGC 1377	10.17 ± 0.04	0.98 ± 0.00	29.83 ± 1.07	72.82 ± 4.15	6.55 ± 0.09	2.46
NGC 1386	9.34 ± 0.04	0.99 ± 0.00	24.18 ± 0.64	62.96 ± 4.13	6.27 ± 0.07	0.40
NGC 1399	7.40 ± 0.32	1.00 ± 0.00	11.52 ± 0.97	65.41 ± 14.85	6.43 ± 0.40	2.65
NGC 1404	8.02 ± 0.27	0.48 ± 0.28	27.25 ± 10.09	71.84 ± 14.05	5.79 ± 1.59	0.18
NGC 3265	9.31 ± 0.10	0.99 ± 0.01	24.43 ± 1.09	61.03 ± 10.47	6.21 ± 0.08	1.19
NGC 3640	6.23 ± 0.74	0.50 ± 0.29	27.54 ± 10.13	71.33 ± 14.29	4.53 ± 3.32	0.56
NGC 4125	8.66 ± 0.04	0.99 ± 0.00	20.34 ± 1.26	48.98 ± 3.51	6.07 ± 0.18	7.41
NGC 4138	8.75 ± 0.16	1.00 ± 0.00	21.62 ± 0.93	58.67 ± 12.09	6.04 ± 0.29	0.37
NGC 4168	6.44 ± 0.85	0.49 ± 0.29	27.45 ± 10.10	71.60 ± 14.50	4.87 ± 3.10	0.38
NGC 4203	8.55 ± 0.10	1.00 ± 0.00	21.62 ± 0.61	67.69 ± 13.69	5.79 ± 0.14	0.79
NGC 4267	7.23 ± 0.42	1.00 ± 0.00	16.95 ± 4.24	68.92 ± 14.54	5.76 ± 0.80	10.01
NGC 4350	8.26 ± 0.11	1.00 ± 0.01	27.34 ± 0.84	59.71 ± 13.42	4.90 ± 0.19	14.76
NGC 4365	7.48 ± 0.15	0.98 ± 0.02	27.10 ± 3.20	56.06 ± 10.45	4.34 ± 0.59	1.06
NGC 4371	7.18 ± 0.27	0.55 ± 0.30	28.46 ± 9.58	67.60 ± 14.46	4.88 ± 1.74	27.19
NGC 4374	8.46 ± 0.11	0.99 ± 0.00	18.13 ± 1.94	53.27 ± 7.67	6.21 ± 0.26	5.56
NGC 4377	8.54 ± 0.06	0.99 ± 0.01	30.36 ± 1.03	57.29 ± 12.21	4.89 ± 0.13	24.45
NGC 4406	5.04 ± 0.03	1.00 ± 0.00	19.48 ± 2.07	92.08 ± 2.34	2.65 ± 0.42	2.10
NGC 4417	8.02 ± 0.17	0.46 ± 0.28	28.22 ± 10.70	60.45 ± 12.15	5.77 ± 1.44	16.05
NGC 4434	6.14 ± 0.71	0.50 ± 0.29	27.60 ± 10.09	70.88 ± 14.32	4.34 ± 2.62	2.59
NGC 4435	8.71 ± 0.01	1.00 ± 0.00	26.93 ± 0.22	56.53 ± 11.44	5.36 ± 0.02	133.75
NGC 4458	5.92 ± 0.58	0.50 ± 0.29	27.34 ± 10.15	72.13 ± 14.35	4.05 ± 2.62	0.15
NGC 4459	9.24 ± 0.11	1.00 ± 0.00	25.87 ± 0.74	74.82 ± 13.39	6.01 ± 0.14	6.87
NGC 4464	6.14 ± 0.70	0.50 ± 0.29	27.37 ± 10.07	71.04 ± 14.27	4.36 ± 3.37	10.08
NGC 4472	7.33 ± 0.21	0.99 ± 0.01	24.58 ± 3.49	59.94 ± 12.69	4.63 ± 0.90	0.39
NGC 4473	6.54 ± 0.90	0.49 ± 0.29	27.19 ± 10.12	71.49 ± 14.29	5.01 ± 3.10	0.75
NGC 4474	6.71 ± 0.94	0.49 ± 0.29	27.50 ± 10.01	70.42 ± 14.41	5.08 ± 2.62	8.42
NGC 4476	9.29 ± 0.13	1.00 ± 0.00	22.02 ± 0.76	80.71 ± 10.37	6.49 ± 0.16	3.10
NGC 4477	8.52 ± 0.07	0.99 ± 0.00	19.35 ± 1.00	51.66 ± 4.36	6.06 ± 0.14	3.41
NGC 4478	6.77 ± 0.53	1.00 ± 0.00	11.03 ± 0.85	60.33 ± 12.82	6.05 ± 0.56	4.90
NGC 4483	6.04 ± 0.64	0.50 ± 0.29	27.39 ± 10.12	71.59 ± 14.46	4.20 ± 2.88	2.22
NGC 4486	8.58 ± 0.11	1.00 ± 0.00	12.67 ± 0.91	56.17 ± 7.32	7.24 ± 0.20	13.78
NGC 4494	8.36 ± 0.17	0.98 ± 0.02	26.75 ± 2.49	63.40 ± 14.30	5.14 ± 0.35	0.80
NGC 4528	8.30 ± 0.30	0.49 ± 0.28	27.69 ± 10.39	69.08 ± 13.78	6.07 ± 1.44	13.01
NGC 4552	6.59 ± 0.21	1.00 ± 0.00	24.83 ± 1.24	64.23 ± 13.99	3.57 ± 0.41	12.15
NGC 4564	6.17 ± 0.74	0.52 ± 0.29	27.26 ± 10.20	71.24 ± 14.27	4.48 ± 3.22	5.06
NGC 4570	6.26 ± 0.77	0.50 ± 0.29	27.42 ± 10.20	71.56 ± 14.37	4.63 ± 3.03	0.61
NGC 4578	6.43 ± 0.86	0.50 ± 0.28	27.35 ± 10.07	71.06 ± 14.27	4.90 ± 3.45	4.85
NGC 4612	6.65 ± 0.93	0.50 ± 0.29	27.55 ± 10.11	70.82 ± 14.22	5.12 ± 3.10	9.67
NGC 4621	6.52 ± 0.29	0.99 ± 0.01	23.42 ± 3.26	67.98 ± 14.92	3.91 ± 0.67	30.17
NGC 4638	6.57 ± 0.30	0.49 ± 0.28	27.46 ± 10.13	68.90 ± 14.26	4.37 ± 1.56	6.64
NGC 4649	8.53 ± 0.03	0.42 ± 0.28	21.70 ± 8.31	94.25 ± 0.75	6.48 ± 1.02	1847.70
NGC 4660	7.16 ± 0.19	0.99 ± 0.01	25.23 ± 2.49	58.57 ± 11.86	4.19 ± 0.71	3.66
NGC 4696	8.49 ± 0.10	1.00 ± 0.00	23.47 ± 0.92	56.97 ± 10.24	5.53 ± 0.21	7.97
NGC 4697	8.53 ± 0.11	0.99 ± 0.01	27.55 ± 1.47	59.99 ± 11.62	5.16 ± 0.22	7.28
NGC 4754	6.16 ± 0.70	0.50 ± 0.29	27.33 ± 10.04	71.97 ± 14.28	4.42 ± 3.33	0.41
NGC 4762	6.96 ± 0.29	0.50 ± 0.29	27.60 ± 10.10	71.37 ± 14.50	4.73 ± 1.63	2.25
NGC 5576	6.25 ± 0.75	0.50 ± 0.29	27.26 ± 10.18	71.28 ± 14.29	4.47 ± 2.57	2.08
NGC 5866	8.98 ± 0.01	1.00 ± 0.00	23.42 ± 0.50	49.03 ± 2.17	5.99 ± 0.06	0.91
UGC07580	6.98 ± 0.31	0.90 ± 0.17	27.61 ± 6.68	56.04 ± 11.51	4.31 ± 2.26	3.01

is mainly populated by elliptical galaxies (68% of sources). For a higher dust-to-star mass ratio ($\log(M_d/M_*) > -5$), which mainly contains S0 galaxies (72% of sources), the sSFR rises steeply with the dust-to-star mass ratio. A single outlier source, NGC 4494, lies at Log(sSFR) ~ -10 and $\log(M_d/M_*) \sim -6$. This elliptical galaxy has a high, sSFR but a surprisingly small dust-to-star mass ratio. NGC 4494 contains an AGN according to the Veron catalog Véron-Cetty & Véron (2010) and could have undergone a recent merger (O'Sullivan & Ponman 2004), which might be able to explain the low dust mass. However, we do not have *GALEX* or SDSS data for this galaxy, so the fit might have converged to an unphysical solution.

We compared our E/SO classification with the slow/fast rotator one from Emsellem et al. (2011) and obtained the same

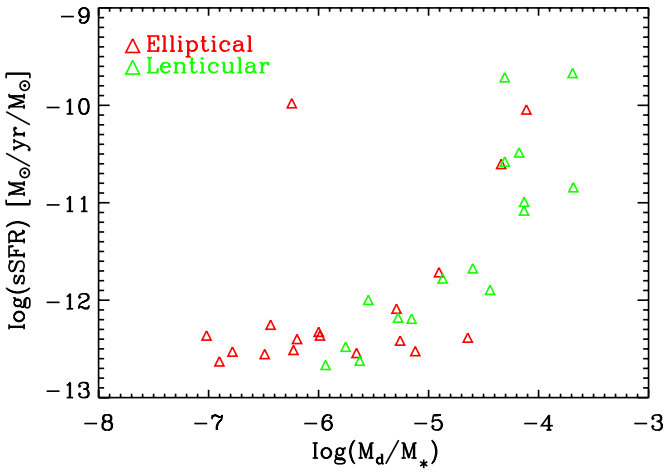

Figure 8. Specific star formation estimated with our CIGALEMC fit vs. the dust mass to stellar mass ratio, estimated with the one-temperature FIR model. We select data with a reduced χ^2 lower than 10, a dust mass error of less than 50%, and a dust luminosity logarithm error of less than 1 dex. Elliptical galaxies are indicated with red triangles, and lenticular galaxies with green triangles. The isolated triangle at Log(sSFR) ~ -10 and Log(M_d/M_*) ~ -6 represents NGC 4494.

(A color version of this figure is available in the online journal.)

sample of 46 galaxies of Section 3, that are in ATLAS^{3D} and are well fitted in our sample. Out of 35 fast rotators, 6 have a Log(M_d/M_*) greater than -5.5, but no slow rotator has such a high dust mass. This would indicate that fast rotators are the only ones with a large amount of dust, although the small size of this sample does not allow us to make a conclusion.

5. AGN ACTIVITY

AGN activity can influence the SFR of a galaxy. In order to better understand the variability in our sample of ETGs, we try to detect galaxies in our sample with a significant trace of AGN activity.

5.1. Spectroscopic Selection

To select AGN, we downloaded the DR9 SDSS spectroscopic line catalog[15] along with the spectroscopic information file and cross-identified it with our 221 galaxy sample. We identify 54 galaxies (27 S0 and 27 E, compared to the 147 galaxies for which we have photometric data), from which we selected the ones with at least four lines with a S/N of at least 3 out of the seven lines that we use to produce the Baldwin, Phillips, and Terlevich (BPT) diagrams (Baldwin et al. 1981), namely O III (5007 Å), N II(6584 Å), S II(6718 and 6731 Å), Hα (6563 Å), Hβ (4861 Å), O I (6300 Å). We obtain 21 galaxies (13 S0 and 8 E, ~40% of the sample) with enough optical lines detected, about the same rate as Rowlands et al. (2012) (45%) and twice the rate of Schawinski et al. (2007b) (~20%). Our 24 μm selection and the 250 μm selection of Rowlands et al. (2012) are more likely to select active ETGs than the optical selection of Schawinski et al. (2007b).

Using the three BTP diagrams of Figure 9, with SF, AGN, and LINER areas defined by Kewley et al. (2001, 2006), we identify five AGNs (5 S0), 11 SFGs (7 S0 and 5 E), and 4 (1 S0 and 3 E) undetermined galaxies (with some lines they are identified as AGN and some others as SF galaxy, SFG). We obtain a larger proportion (69%) of SFGs than the 57% of the 250 μm selected

[15] http://www.sdss3.org/dr9/spectro/spectro_access.php

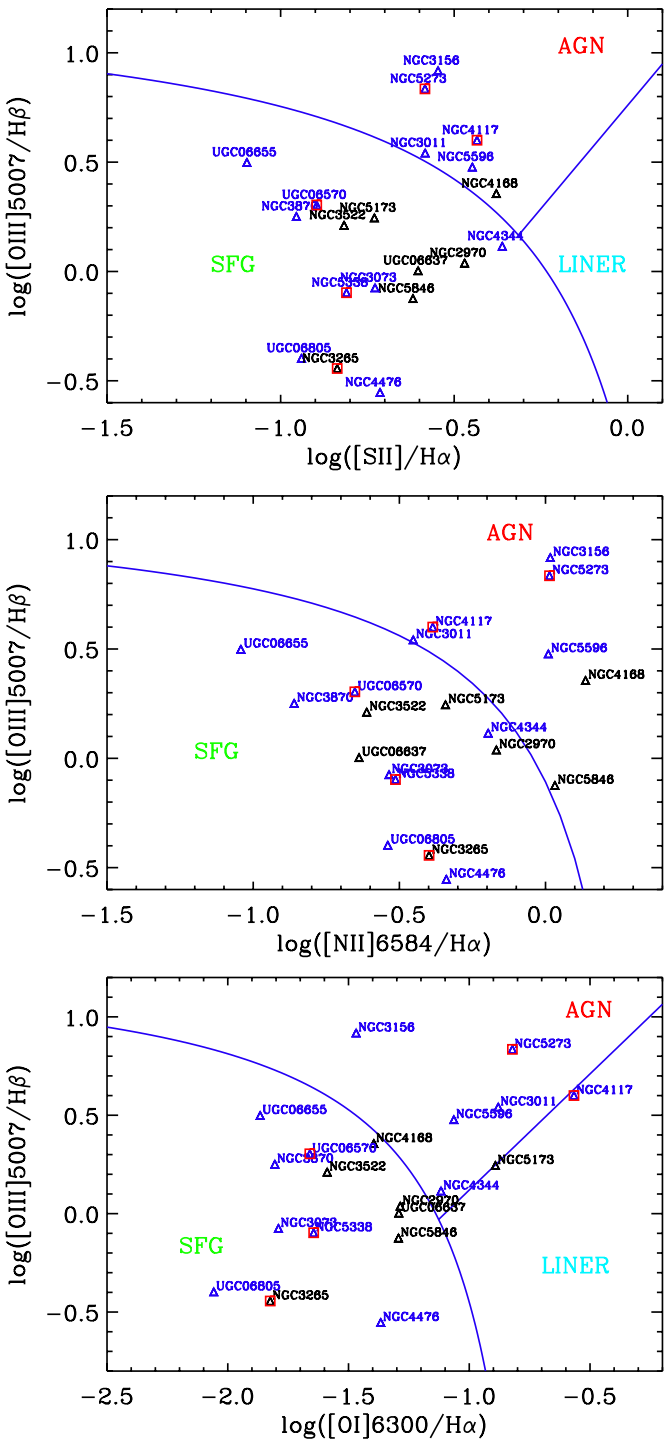

Figure 9. BPT diagrams of galaxies in our sample for which we have SDSS spectroscopic data, at least for emission lines detected. Lenticular galaxies are represented by blue triangles, and elliptical galaxies by black triangles. The blue solid line separates the star-forming galaxy (SFG) region from the AGN one. The red square indicates galaxies in which 24 μm morphology is point-like.

(A color version of this figure is available in the online journal.)

sample of Rowlands et al. (2012), although the difference is not statistically significant since both samples are quite small. Schawinski et al. (2007b), using a much larger sample of optically selected ETGs, found 61% of SFGs among sources with optical line detection. Starting with an equal number of E and S0 galaxies in the cross-sample with SDSS spectroscopic data, more S0 galaxies (65% of the detected galaxies) have

detected emission lines than E galaxies, and all AGN identified with the BPT diagrams are S0. Both Rowlands et al. (2012) and Schawinski et al. (2007b) did not separate their numbers between S0 and E morphology, but Schawinski et al. (2007b) found a time sequence for small to intermediate mass ETGs, going from a SF phase to an AGN phase to finish into a quiescent state. Our results would be consistent with such a picture if the S0 dominated the intermediate AGN phase. Overall, our S0 galaxies with SDSS spectroscopic are 52% quiescent, 19% AGN-dominated, and 26% SF-dominated, our E galaxies are 70% quiescent, 0% AGN-dominated, and 18% SF-dominated. Separating LINERs from other AGNs would not change our results, since our BPT diagrams do not seem to indicate any LINERs in our sample. Two galaxies are potentially borderline LINERs in one BPT diagram but are clearly not LINERs in another, and neither are classified as such in the NED and Hyperleda databases.

We mark, on our BPT diagrams, galaxies for which the 24 μm morphology is point-source like (red squares). Among galaxies identified with a 24 μm point-source morphology and for which we have SDSS spectroscopic data, all of them have detected lines. The 24 μm morphology seems to be a good indicator of galactic activity. They seem to split evenly between AGN emission (two) and SF emission (three), 24 μm morphology gives a ~50% accuracy in AGN detection in our sample.

5.2. NIR Selection

Another powerful way to select AGN is to use NIR selection. Indeed, the UV to MIR continuum for a galaxy is dominated by a black body emission that would dominate at 1.6 μm, while the UV to MIR continuum of an AGN is dominated by a power law. Different criteria have been proposed using IRAC–IRAC colors (e.g., Lacy et al. 2004; Stern et al. 2005) and more recently *WISE* colors (e.g., Stern et al. 2012). We apply these three criteria to our sample: nine sources are selected following Lacy et al. (2004), only one source (plus a boarder-line source) with Stern et al. (2005) criteria, and four sources following Stern et al. (2012) using *WISE* filters. Very few sources are selected by these criteria, and this might be explained by these criteria being designed in order to select highly obscured quasars, and our sample of ETGs is quite poor in dust.

Assef et al. (2013) underline the incompleteness and the unreliability of these criteria, stating a reliability of only 36% for the selection of Lacy et al. (2004) and a completeness of 79%, a 67% reliability/51% completeness for Stern et al. (2005), and a 45% reliability/70% completeness for Stern et al. (2012). This leads us to the conclusion that we should combine the three criteria to increase the reliability of the NIR selection in our sample. We finally have only two sources selected as AGN via the NIR-methods: NGC 1377 and IC5063. We do not have any SDSS spectra for these two sources so we cannot correlate this NIR classification with the BPT spectral classification. Both of these sources have a high $f_{\rm agn}$ fraction from the SED-fitting which could confirm their AGN activity. IC5063 is also detected in X-ray and has a luminosity $L_X > 10^{41}$ erg s^{-1}, pointing to some AGN activity. NGC 1377 is a power-law source, i.e., presenting Fl $_{\rm IRAC4}$ > Fl $_{\rm IRAC3}$ > Fl $_{\rm IRAC2}$ > Fl $_{\rm IRAC1}$, once again characterizing an AGN.

Figure 10 shows the distribution of our sample in the Lacy et al. (2004) diagram. Elliptical galaxies are represented with dots while lenticulars are represented with crosses. We add to this figure the information collected on the BPT diagrams with a color code. Black symbols represent galaxies for which we do not have emission lines or SDSS data, blue symbols represent AGN sources, pink ones represent the potential AGN, and green ones represent the SF sources. SF sources (green dots and crosses) are mainly distributed in the upper part of the diagram on the outside of the Lacy et al. (2004) box. Sources in this part of the color–color plot, with bluer $S_{5.8}/S_{3.6}$ colors and redder $S_{8.0}/S_{4.5}$ colors than the rest of the sample, are known (Lacy et al. 2004) to be low-redshift galaxies with their 6.2 and 7.7 μm PAH bands redshifted into the IRAC 8 μm filter. The presence of PAHs in these sources shows that they are forming stars and most likely present emission lines in their spectra. We also notice that AGNs from the BPT diagram (blue dots and crosses) are outside the NIR-selection, showing that these two methods select different types of AGN with different properties. The NIR-selection will select highly obscured quasars. Another trend noticeable on Figure 10 is the separation between ellipticals (dots), concentrated in the left-bottom part, and lenticulars (crosses). This shows that lenticular galaxies have more dust than ellipticals, which goes in the same direction that we have already noticed on Figures 5 and 6.

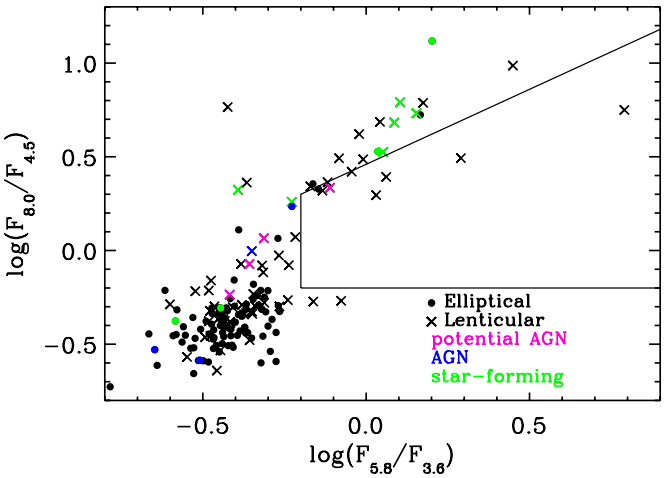

Figure 10. Distribution of the sources from our sample in the Lacy et al. (2004) diagram displaying $\log(S_{8.0}/S_{4.5})$ vs. $\log(S_{5.8}/S_{3.6})$. Ellipticals and lenticulars are represented by dots and crosses, respectively. We also show here the AGN activity vs. star-forming activity of our sample from our analysis of the BPT diagram: star forming (green), AGN (blue), and potential AGN (pink). The black quadrilateral shape corresponds to the Lacy et al. (2004) box where the highly obscured quasars lie.

(A color version of this figure is available in the online journal.)

Similar to the BPT diagram, the NIR-selected AGNs in our sample are mainly composed of S0 (~90%). Using these criteria, we find that 12.3% of S0 are AGN-dominated, while only 1.1% of elliptical galaxies are AGN-dominated. As we recalled previously, this estimator is not complete and it could also be biased for our selection, but it qualitatively matches the proportions we find with the BPT diagrams (19% for S0 and 0% for E).

As a comparison in Table 9, we indicate sources detected in X-ray with *Chandra* with a high X-ray luminosity, i.e., $L_X > 10^{41}$ erg s^{-1}, believed to be AGN sources as well. We also show if the SED-fit parameter $f_{\rm agn}$ indicates the presence of an AGN. $f_{\rm agn}$ is not strongly constrained by our SEDs, and we chose to report its value by indicating whether its lower 95% confidence level limit is greater than 10% at the 95% confidence level, i.e., the AGN luminosity in MIR contributes at least 10% of the total IR luminosity. Galaxies with lower AGN contribution in their SED are reported with an "inc." for inconclusive, since

Table 9
AGN Classification Using the Following Criteria: from the BPT Diagram, from the AGN Template in the SED Fit, from the NIR Color Criteria, from X-ray Luminosity

Name	Type	BPT	SED	NIR	X-ray
Eso103-35	S0	–	–	yes	–
Eso428-14	S0	–	–	no	yes
IC4296	E	–	inc.	no	yes
IC5063	S0	–	yes	yes	yes
NGC 0221	E	–	–	no	yes
NGC 0315	E	–	inc.	no	yes
NGC 0410	E	–	inc.	no	yes
NGC 0507	E	–	inc.	no	–
NGC 0533	E	–	inc.	–	–
NGC 0596	E	–	yes	no	–
NGC 0807	E	–	inc.	–	–
NGC 1016	E	–	inc.	no	–
NGC 1374	E	–	inc.	yes	–
NGC 1377	S0	–	yes	yes	–
NGC 1386	S0	–	inc.	yes	no
NGC 1407	S0	–	–	–	yes
NGC 1439	E	–	yes	no	–
NGC 1510	S0	–	inc.	yes	–
NGC 2832	E	–	inc.	no	yes
NGC 3011	S0	yes	inc.	yes	–
NGC 3156	S0	yes	inc.	–	no
NGC 3516	S0	–	inc.	yes	–
NGC 3593	S0	–	inc.	no	–
NGC 3610	E	–	yes	no	no
NGC 3706	E	–	yes	no	–
NGC 4117	S0	yes	inc.	no	no
NGC 4138	S0	–	inc.	yes	–
NGC 4168	E	yes	inc.	no	–
NGC 4261	E	–	inc.	no	yes
NGC 4344	S0	inc.	–	no	–
NGC 4382	S0	–	yes	no	no
NGC 4460	S0	–	inc.	yes	–
NGC 4638	S0	–	yes	no	no
NGC 4915	E	–	yes	no	no
NGC 5061	E	–	yes	no	–
NGC 5173	E	inc.	inc.	no	–
NGC 5273	S0	yes	inc.	no	yes
NGC 5419	E	–	inc.	no	yes
NGC 5596	S0	yes	inc.	no	–
NGC 5846	E	inc.	inc.	no	–
NGC 6703	S0	–	yes	no	–
NGC 7077	E	–	–	yes	–
NGC 7626	E	–	inc.	no	yes

Notes. A dash line indicates that we did not have data and "inc." indicates data were inconclusive.

we could not conclude for these galaxies how large the potential AGN contribution could be.

6. COLORS

Colors can be good and simple indicators of star formation activity in galaxies. Therefore, in this section, we compare our previous results with some typical colors. We compute a color–magnitude diagram (SDSS $u - r$ color versus R magnitude) of galaxies for which we have SDSS data (79 E and 68 S0). In Figure 11, elliptical and lenticular galaxies are represented by red and green dots, respectively, and as expected, most galaxies (∼73%) in our sample reside in the red sequence (Strateva et al. 2001; Mignoli et al. 2009). Among the remaining galaxies, 22% (18 E and 15 S0) reside in the green valley and 5% (2 E and 5 S0) in the blue cloud (Strateva et al. 2001). The

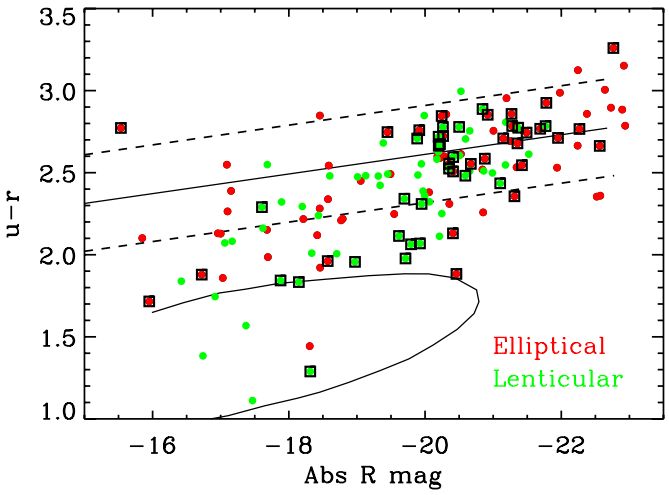

Figure 11. Optical color ($u-r$) vs. the absolute R magnitude computed using SDSS data of the 147 sources in our sample for which such data exist. Elliptical and lenticular galaxies are represented by red and green dots, respectively. Sources with a 160 μm MIPS detection have been outlined with a black square. The solid straight line represents the red sequence and the two dashed lines delimit the 3σ confidence interval. The solid curved line marks the position of the blue cloud. These areas were taken from Temi et al. (2009b) and are not derived from the data points.

(A color version of this figure is available in the online journal.)

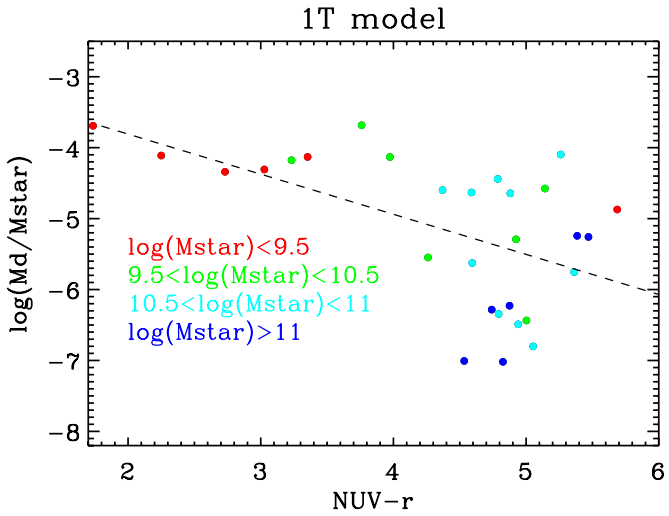

Figure 12. $M_{\rm dust}/M_{\rm star}$ vs. (NUV $-$ r) color. The dashed line corresponds to the best linear fit for all sources detected in NUV and with a relative error on $M_{\rm dust}$ < 50%. The red dots correspond to the least massive galaxies (in terms of stellar mass) of the sample (log ($M_{\rm star}$) < 9.5) and the most massive sources are represented by the blue dots.

(A color version of this figure is available in the online journal.)

color–magnitude distribution of ETGs does not seem to depend on the galaxy morphology apart from a statistically poor hint of dominance of S0 in the blue clouds.

In Figure 11, black squares outline a 160 μm MIPS detection, which indicates the presence of cold dust in galaxies. The 160 μm detections (92) are bound to brighter galaxies (R < −19.5) (74) or to galaxies in the green valley (14); this distribution is explained by a larger specific dust mass and sSFR in galaxies from the green valley.

Figure 12 shows the evolution of the dust-to-stellar mass ratio in logarithmic scale versus the (NUV − r) color. The dashed line corresponds to the best fit for our 29 sources with a secure SED fit and detected in the NUV. We find the same trend than (e.g., Smith et al. 2012; Agius et al. 2013), i.e., a decreasing $M_{\rm dust}$/

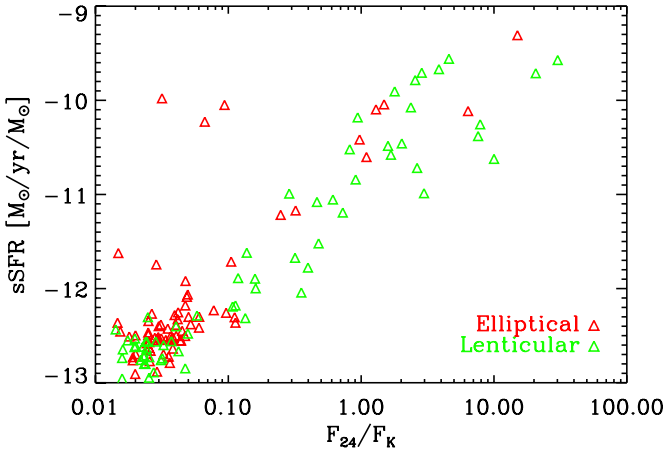

Figure 13. Specific SFR estimated with the SED fitting vs. the ratio F_{24}/F_K for our elliptical (red) and lenticular (green) galaxies. The sSFR estimate correlates well with the 24 μm color.

(A color version of this figure is available in the online journal.)

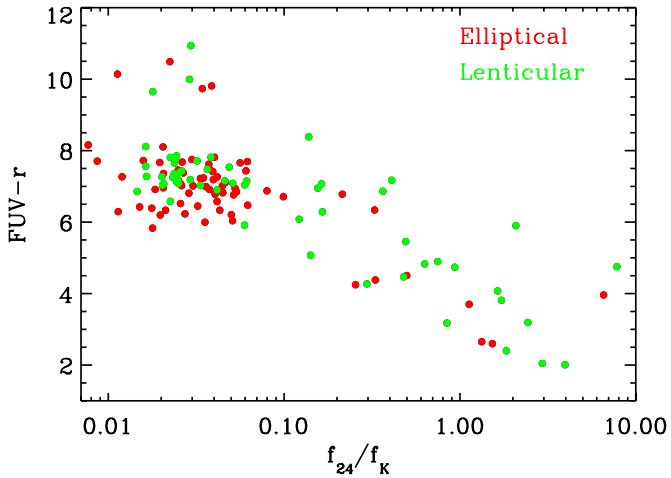

Figure 14. FUV $-$ r color calculated from *GALEX* and SDSS data as a function of the infrared color F_{24}/f_K, obtained from MIPS and 2MASS data. Elliptical and lenticular galaxies are represented by red and green dots, respectively.

(A color version of this figure is available in the online journal.)

$M_{\rm star}$ ratio with an increasing (NUV$-r$) color. We color code the stellar mass on each point of this plot with red ($\log(M_{\rm star}) < 9.5$), green ($9.5 < \log(M_{\rm star}) < 10.5$), cyan ($10.5 < \log(M_{\rm star}) < 11$), and blue dots ($\log(M_{\rm star}) > 11$). We see that the most massive galaxies (in stellar mass), i.e., galaxies with $\log(M_{\rm star}) > 10.5$ (cyan and blue dots), are very red($(\mathrm{NUV} - r) > 4$). The most massive sources (blue dots) present a very low $M_{\rm dust}/M_{\rm star}$ ratio, which corresponds most preferentially to galaxies with low $M_{\rm dust}$ and massive elliptical galaxies, as seen on Figure 7. The NUV $-$ r color seems to correlate with the dust mass only for bluer galaxies (NUV$-r < 4.5$); this result is consistent with the relation between sSFR and M_d/M_*, and the slope (-0.57 ± 0.17) is compatible with our slope in Figure 7, and results from Rowlands et al. (2012) assuming a linear relation between sSFR and NUV$-r$. The correlation is clearer for the lower mass range of our sample ($\log(M_*/M_\odot) < 10$.

We test our sSFR estimated using CIGALEMC with the ratio F_{24}/F_K, which is, in general, a good indicator of specific star formation when its value is larger than 0.1 (Temi et al. 2009b). Figure 13 shows a linear relation between the sSFR versus and the 24 μm color. Most of the galaxies with a large sSFR and 24 μm are S0 ($\sim$80%). This confirms our previous finding that S0 are more active in forming stars than E galaxies.

Three elliptical galaxies occupy a peculiar location in Figure 13, at $\log(\mathrm{sSFR}) \sim -10$ and $F_{24}/F_K \sim 0.05$. These galaxies are IC3370, NGC 4494, and NGC 5077. They all host an AGN according to the Veron catalog[16] (Véron-Cetty & Véron 2010). According to our SED fitting, their age$_{D4000}$, determined with the 4000 Å break, is also very low (age$_{D4000} < 1.5$ Gyr), which would imply they had a recent episode of star formation.

IC3370 geometry has been found to be triaxial (Samurović & Danziger 2005) and Jarvis (1987) classified it as a peculiar S0pec with a box shape, and found some large isophotal twisting (ΔP.A. $\simeq 25^\circ$) in its bulge. Jarvis (1987) also argue its peculiar shape could be due to the slow merger of two massive disk galaxies following Binney & Petrou (1985) model.

NGC 4494 has been found to have an unusually low X-ray flux compared to its B-band flux (O'Sullivan et al. 2001a), and this low ratio could be a hint for a recent merger (O'Sullivan & Ponman 2004) since, in general, it is found to be low for young, ETGs (Mackie & Fabbiano 1997; Sansom et al. 2000; O'Sullivan et al. 2001b). We also found earlier that NGC 4494 had an unusually low dust content for such a high SFR.

NGC 5077 is a LINER, with a Hα bright gaseous disk in its central area (Bertola et al. 1991; Pizzella et al. 1997). We have a hint that two out of the three outliers could be mergers, which could explain their unusual 24 μm color. However, there is also the possibility that our fit converges to a wrong solution for these three galaxies, since we do not have UV (*GALEX*) nor optical data (SDSS) for these galaxies.

Using *GALEX* and SDSS data, we compute the UV–optical color FUV $-$ r on our sample where data were available (72 E and 65 S0). Galaxies with IR color F_{24}/F_K less than 0.1 are clustered around a FUV $-$ r color of 7 and F_{24}/F_K of 0.03 on Figure 14. Galaxies with larger IR colors are also bluer spreading in FUV $-$ r from 6 to 2. Above a 0.1 F_{24}/F_K color, the logarithm of the IR color linearly decreases as the FUV $-$ r color increases. Bluer galaxies with FUV$-r < 6$ and $F_{24}/F_K > 0.1$ are composed of 7 elliptical and 16 lenticular galaxies. It is another indication that S0 galaxies are, in proportion, more active than ellipticals and show a clear agreement between IR and UV star formation estimators.

7. CONCLUSIONS

This paper analyzed a sample of 221 local ETGs to measure their star formation activity and emphasize differences between elliptical and lenticular galaxies. Indeed, most ETGs are red galaxies but studies from past decades (e.g., Faber et al. 2007; Schawinski et al. 2007b) implied an evolution from blue galaxies to red ones through a green phase possibly powered by an AGN. 52% of our sample are ellipticals and 48% are S0. We performed SED-fittings on our galaxies which produced constraints on their physical parameters; we concentrated on their SFR, dust luminosity, stellar and dust mass, and dust temperature. Using these parameters, we derived the following conclusions.

1. S0 have a larger sSFRs and larger dust luminosities than elliptical galaxies when renormalized by their stellar mass.
2. The average dust temperature of the sample is about 32.3 K fitting with a single-temperature model, but it decreases to 22.4 K when using a two-temperature model. This

[16] http://heasarc.gsfc.nasa.gov/W3Browse/all/veroncat.html

difference most likely comes from the fact that our two-temperature model requires at least one *Herschel*-SPIRE detection, and thus biases the selection towards colder galaxies. We did not find any difference between elliptical and lenticular galaxy dust temperature.

3. The dust-to-stellar mass ratio is decreasing with the stellar mass for both elliptical and lenticular galaxies, and these relations are statistically indistinguishable.
4. The sSFR does not evolve with the dust-to-stellar mass ratio for $\log(M_d/M_*)<-5$ but steeply increases at higher dust-to-stellar mass ratio. Elliptical galaxies are mainly located at $\log(M_d/M_*)<-5$ with no correlation between their sSFR and dust-to-stellar mass ratio, while SO galaxies are located at a higher $\log(M_d/M_*)$, which correlated well with the sSFR.
5. According to our BPT and NIR diagrams, a larger fraction (∼12%–19%) of S0 galaxies show signs of AGN activity when compared to elliptical galaxies (∼0%–1%). This observation is consistent with a scenario where blue SFGs evolve to a red elliptical passing through a S0 AGN active phase (Schawinski et al. 2007b).
6. FIR and UV colors are both in good agreement with our multi-frequency analysis and with each other. All indicators point towards S0 being more active at forming stars on average than ellipticals.

These results emphasize the differences between elliptical and lenticular galaxies to possibly explain the transition phase between blue and red galaxies through the green valley. In the near future we will focus on the green and blue early-type galaxies identified in this paper to have a better understanding of the star formation transition phase, using *GALEX*, IRAC, and MIPS data.

We would like to thank our anonymous referee for his/her useful comments which helped improve the original manuscript. This publication makes use of data products from the Two Micron All Sky Survey, which is a joint project of the University of Massachusetts and the Infrared Processing and Analysis Center/California Institute of Technology, funded by the National Aeronautics and Space Administration and the National Science Foundation. This publication makes use of data from SDSS-III. Funding for SDSS-III has been provided by the Alfred P. Sloan Foundation, the Participating Institutions, the National Science Foundation, and the US Department of Energy Office of Science. The SDSS-III Web site is http://www.sdss3.org/. SDSS-III is managed by the Astrophysical Research Consortium for the Participating Institutions of the SDSS-III Collaboration including the University of Arizona, the Brazilian Participation Group, Brookhaven National Laboratory, University of Cambridge, Carnegie Mellon University, University of Florida, the French Participation Group, the German Participation Group, Harvard University, the Instituto de Astrofisica de Canarias, the Michigan State/Notre Dame/JINA Participation Group, Johns Hopkins University, Lawrence Berkeley National Laboratory, Max Planck Institute for Astrophysics, Max Planck Institute for Extraterrestrial Physics, New Mexico State University, New York University, Ohio State University, Pennsylvania State University, University of Portsmouth, Princeton University, the Spanish Participation Group, University of Tokyo, University of Utah, Vanderbilt University, University of Virginia, University of Washington, and Yale University. This work is based in part on observations made with the *Spitzer Space Telescope*, which is operated by the Jet Propulsion Laboratory, California Institute of Technology under a contract with NASA. This work is based in part on observations made with the NASA *Galaxy Evolution Explorer*. *GALEX* is operated for NASA by the California Institute of Technology under NASA contract NAS5-98034.

REFERENCES

Agius, N. K., Sansom, A. E., Popescu, C. C., et al. 2013, MNRAS, 431, 1929
Agladze, N. I., Sievers, A. J., Jones, S. A., Burlitch, J. M., & Beckwith, S. V. W. 1996, ApJ, 462, 1026
Amblard, A., Cooray, A., Serra, P., et al. 2010, A&A, 518, L9
Assef, R. J., Stern, D., Kochanek, C. S., et al. 2013, ApJ, 772, 26
Auger, M. W., Treu, T., Gavazzi, R., et al. 2010, ApJL, 721, L163
Bacon, R., Copin, Y., Monnet, G., et al. 2001, MNRAS, 326, 23
Baldwin, J. A., Phillips, M. M., & Terlevich, R. 1981, PASP, 93, 5
Barway, S., Wadadekar, Y., Vaghmare, K., & Kembhavi, A. K. 2013, MNRAS, 432, 430
Bertola, F., Bettoni, D., Danziger, J., et al. 1991, ApJ, 373, 369
Binette, L., Magris, C. G., Stasińska, G., & Bruzual, A. G. 1994, A&A, 292, 13
Binney, J., & Petrou, M. 1985, MNRAS, 214, 449
Boulanger, F., Abergel, A., Bernard, J.-P., et al. 1996, A&A, 312, 256
Calzetti, D. 1997, in AIP Conf. Ser. 408, The Ultraviolet Universe at Low and High Redshift, ed. W. H. Waller (Melville, NY: AIP), 403
Calzetti, D., Kennicutt, R. C., Engelbracht, C. W., et al. 2007, ApJ, 666, 870
Calzetti, D., Kinney, A. L., & Storchi-Bergmann, T. 1994, ApJ, 429, 582
Cappellari, M., Emsellem, E., Bacon, R., et al. 2007, MNRAS, 379, 418
Cappellari, M., Emsellem, E., Krajnović, D., et al. 2011a, MNRAS, 413, 813
Cappellari, M., Emsellem, E., Krajnović, D., et al. 2011b, MNRAS, 416, 1680
Cardelli, J. A., Clayton, G. C., & Mathis, J. S. 1989, ApJ, 345, 245
Cimatti, A., Daddi, E., Renzini, A., et al. 2004, Natur, 430, 184
Cortese, L., Ciesla, L., Boselli, A., et al. 2012, A&A, 540, A52
da Cunha, E., Charlot, S., & Elbaz, D. 2008, MNRAS, 388, 1595
Dale, D. A., & Helou, G. 2002, ApJ, 576, 159
Desert, F.-X., Boulanger, F., & Puget, J. L. 1990, A&A, 237, 215
de Zeeuw, P. T., Bureau, M., Emsellem, E., et al. 2002, MNRAS, 329, 513
di Serego Alighieri, S., Bianchi, S., Pappalardo, C., et al. 2013, A&A, 552, A8
Draine, B. T., & Lee, H. M. 1984, ApJ, 285, 89
Driver, S. P., Allen, P. D., Graham, A. W., et al. 2006, MNRAS, 368, 414
Dunne, L., & Eales, S. A. 2001, MNRAS, 327, 697
Dunne, L., Eales, S., Edmunds, M., et al. 2000, MNRAS, 315, 115
Elbaz, D., Hwang, H. S., Magnelli, B., et al. 2010, A&A, 518, L29
Emsellem, E., Cappellari, M., Krajnović, D., et al. 2007, MNRAS, 379, 401
Emsellem, E., Cappellari, M., Krajnović, D., et al. 2011, MNRAS, 414, 888
Faber, S. M., Willmer, C. N. A., Wolf, C., et al. 2007, ApJ, 665, 265
Fang, J. J., Faber, S. M., Salim, S., Graves, G. J., & Rich, R. M. 2012, ApJ, 761, 23
Giovannoli, E., Buat, V., Noll, S., Burgarella, D., & Magnelli, B. 2011, A&A, 525, A150
Griffin, M. J., Abergel, A., Abreu, A., et al. 2010, A&A, 518, L3
Grillo, C., Gobat, R., Lombardi, M., & Rosati, P. 2009, A&A, 501, 461
Hildebrand, R. H. 1983, QJRAS, 24, 267
Hughes, D. H., Robson, E. I., Dunlop, J. S., & Gear, W. K. 1993, MNRAS, 263, 607
Hughes, T. M., & Cortese, L. 2009, MNRAS, 396, L41
Ilbert, O., Capak, P., Salvato, M., et al. 2009, ApJ, 690, 1236
Ilbert, O., Salvato, M., Le Floc'h, E., et al. 2010, ApJ, 709, 644
Jarvis, B. 1987, AJ, 94, 30
Kaviraj, S. 2010, MNRAS, 408, 170
Kaviraj, S., Khochfar, S., Schawinski, K., et al. 2008, MNRAS, 388, 67
Kaviraj, S., Schawinski, K., Devriendt, J. E. G., et al. 2007, ApJS, 173, 619
Kewley, L. J., Dopita, M. A., Sutherland, R. S., Heisler, C. A., & Trevena, J. 2001, ApJ, 556, 121
Kewley, L. J., Groves, B., Kauffmann, G., & Heckman, T. 2006, MNRAS, 372, 961
Lacy, M., Storrie-Lombardi, L. J., Sajina, A., et al. 2004, ApJS, 154, 166
Le Floc'h, E., Aussel, H., Ilbert, O., et al. 2009, ApJ, 703, 222
Mackie, G., & Fabbiano, G. 1997, in ASP Conf. Ser. 116, The Nature of Elliptical Galaxies; 2nd Stromlo Symposium, ed. M. Arnaboldi, G. S. Da Costa, & P. Saha (Melville, NY: AIP), 401
Maraston, C. 2005, MNRAS, 362, 799
Maraston, C., Daddi, E., Renzini, A., et al. 2006, ApJ, 652, 85
Marino, A., Rampazzo, R., Bianchi, L., et al. 2011, MNRAS, 411, 311

Mennella, V., Brucato, J. R., Colangeli, L., et al. 1998, ApJ, 496, 1058
Mignoli, M., Zamorani, G., Scodeggio, M., et al. 2009, A&A, 493, 39
Morrissey, P., Conrow, T., Barlow, T. A., et al. 2007, ApJS, 173, 682
Noll, S., Burgarella, D., Giovannoli, E., et al. 2009, A&A, 507, 1793
O'Sullivan, E., Forbes, D. A., & Ponman, T. J. 2001a, MNRAS, 328, 461
O'Sullivan, E., Forbes, D. A., & Ponman, T. J. 2001b, MNRAS, 324, 420
O'Sullivan, E., & Ponman, T. J. 2004, MNRAS, 349, 535
Paturel, G., Petit, C., Prugniel, P., et al. 2003, A&A, 412, 45
Pizzella, A., Amico, P., Bertola, F., et al. 1997, A&A, 323, 349
Reach, W. T., Dwek, E., Fixsen, D. J., et al. 1995, ApJ, 451, 188
Rieke, G. H., Young, E. T., Engelbracht, C. W., et al. 2004, ApJS, 154, 25
Rowlands, K., Dunne, L., Maddox, S., et al. 2012, MNRAS, 419, 2545
Salim, S., Fang, J. J., Rich, R. M., Faber, S. M., & Thilker, D. A. 2012, ApJ, 755, 105
Salpeter, E. E. 1955, ApJ, 121, 161
Samurović, S., & Danziger, I. J. 2005, MNRAS, 363, 769
Sansom, A. E., Hibbard, J. E., & Schweizer, F. 2000, AJ, 120, 1946
Sarzi, M., Shields, J. C., Schawinski, K., et al. 2010, MNRAS, 402, 2187
Schawinski, K., Kaviraj, S., Khochfar, S., et al. 2007a, ApJS, 173, 512
Schawinski, K., Thomas, D., Sarzi, M., et al. 2007b, MNRAS, 382, 1415
Scoville, N., Aussel, H., Brusa, M., et al. 2007, ApJS, 172, 1
Serra, P., Amblard, A., Temi, P., et al. 2011, ApJ, 740, 22
Siebenmorgen, R., Freudling, W., Krügel, E., & Haas, M. 2004a, A&A, 421, 129
Siebenmorgen, R., Krügel, E., & Spoon, H. W. W. 2004b, A&A, 414, 123
Skibba, R. A., Engelbracht, C. W., Dale, D., et al. 2011, ApJ, 738, 89
Smith, M. W. L., Gomez, H. L., Eales, S. A., et al. 2012, ApJ, 748, 123
Spiniello, C., Koopmans, L. V. E., Trager, S. C., Czoske, O., & Treu, T. 2011, MNRAS, 417, 3000
Stern, D., Assef, R. J., Benford, D. J., et al. 2012, ApJ, 753, 30
Stern, D., Eisenhardt, P., Gorjian, V., et al. 2005, ApJ, 631, 163
Strateva, I., Ivezić, Ž., Knapp, G. R., et al. 2001, AJ, 122, 1861
Tasca, L. A. M., Kneib, J.-P., Iovino, A., et al. 2009, A&A, 503, 379
Temi, P., Brighenti, F., & Mathews, W. G. 2005a, ApJL, 635, L25
Temi, P., Brighenti, F., & Mathews, W. G. 2007a, ApJ, 660, 1215
Temi, P., Brighenti, F., & Mathews, W. G. 2007b, ApJ, 666, 222
Temi, P., Brighenti, F., & Mathews, W. G. 2009a, ApJ, 695, 1
Temi, P., Brighenti, F., & Mathews, W. G. 2009b, ApJ, 707, 890
Temi, P., Mathews, W. G., & Brighenti, F. 2005b, ApJ, 622, 235
Thomas, D., Maraston, C., Bender, R., & Mendes de Oliveira, C. 2005, ApJ, 621, 673
Trager, S. C., Faber, S. M., Worthey, G., & González, J. J. 2000, AJ, 120, 165
Treu, T., Auger, M. W., Koopmans, L. V. E., et al. 2010, ApJ, 709, 1195
Véron-Cetty, M.-P., & Véron, P. 2010, A&A, 518, A10
Yan, R., & Blanton, M. R. 2012, ApJ, 747, 61
Yi, S. K., Yoon, S.-J., Kaviraj, S., et al. 2005, ApJL, 619, L111
Young, L. M., Bureau, M., Davis, T. A., et al. 2011, MNRAS, 414, 940